

Armin Schaffer, BSc

Evaluation of the Soil Moisture-Precipitation Feedback in Austria

MASTERARBEIT

zur Erlangung des akademischen Grades

Master of Science

Masterstudium

Environmental System Sciences /

Climate Change and Environmental Technology

eingereicht an der

Technischen Universität Graz

Betreuer

Mag. Dr. rer. nat. Heimo Truhetz

Wegener Center für Klima und Globalen Wandel

Umwelt-, Regional- und Bildungswissenschaftlichen Fakultät der
Universität Graz

Graz, Februar 2021

EIDESSTATTLICHE ERKLÄRUNG

Ich erkläre an Eides statt, dass ich die vorliegende Arbeit selbstständig verfasst, andere als die angegebenen Quellen/Hilfsmittel nicht benutzt und die den benutzten Quellen wörtlich und inhaltlich entnommenen Stellen als solche kenntlich gemacht habe. Das in TUGRAZonline hochgeladene Textdokument ist mit der vorliegenden Masterarbeit identisch.

04.02.2021



Datum, Unterschrift

Abstract

The influence of soil moisture on the formation of precipitation has been observed by several studies. The so-called soil moisture-precipitation feedback (SMPF) can either be positive, characterized by an increased probability of rain over more humid land surfaces, or negative, describing the effect of soil moisture on surface energy fluxes, and thus increasing the occurrence of convective precipitation.

In this thesis the SMPF in Austria is evaluated by adapting a method utilized in several studies. Due to the lack of comprehensive observational soil moisture data, the High-Resolution Land Data Assimilation System (HRLDAS) is employed and run with atmospheric observational data, to produce high resolution land surface data. The results were compared to in-situ measurements and used to assess the land surface conditions in Austria. Besides these datasets, the SMPF is analyzed for two convection permitting regional climate models (RCMs), i.e. CCLM and WRF, to evaluate their performance.

The soil moisture of the data assimilation system, as well as of the RCMs, have significant errors compared to observations. This may be due to the coarse resolution of land and soil parameters as well as precipitation biases within the RCMs. The analysis of the soil conditions indicated that the conditions required for a climatological dominant SMPF to arise, are not present in Austria. The feedback diagnostics of the observational and RCM data likewise suggest that soil moisture conditions have no systematic and significant influence on the occurrence of precipitation. However, rising temperatures and the expansion of the semi-arid climate of southern Europe towards the Alps may favor conditions for a dominant SMPF in the future.

Zusammenfassung

Der Einfluss von Bodenfeuchte auf Niederschlagsmuster konnte bereits von mehreren Studien nachgewiesen werden. Dieser sogenannte Bodenfeuchte-Niederschlag-Feedback (SMPF) kann sowohl positiv als auch negativ ausgeprägt sein. Der positive Fall ist gekennzeichnet durch erhöhte Niederschlagswahrscheinlichkeit über Gebieten mit erhöhter Feuchtigkeit. Im Falle des negativen Feedbacks hingegen beeinflusst die Trockenheit des Bodens die Wärmeenergieflüsse der Erdoberflächen und erhöht dadurch den konvektiven Auftrieb und folglich die Wahrscheinlichkeit für Niederschlag.

Diese Arbeit versucht das SMPF mittels einer Methode, die in mehreren Studien angewendet wurde, für Österreich zu ermitteln. Wegen des Mangels an flächendeckenden Bodenfeuchte Messungen, wurde das Datenassimilierungssystem HRLDAS herangezogen und mit atmosphärischen Beobachtungsdaten betrieben, um hochaufgelöste Boden Daten zu erhalten. Diese Daten wurden mit Vorortmessungen verglichen und genutzt, um die Bodengegebenheiten in Österreich zu ermitteln. Weiters wurde das Feedback auch für zwei hochaufgelöste regionale Klimamodelle (RCMs), CCLM und WRF, ermittelt, um ihre Leistungsfähigkeit zu beurteilen.

Die Bodenfeuchte Daten des Assimilierungssystems, sowie der RCMs, wiesen signifikante Abweichungen zu den Beobachtungen auf. Sowohl die geringe Auflösung der Bodenparameter der Modelle als auch Fehler in der Simulation des Niederschlags könnten hierfür verantwortlich sein. Weiters ergab die Analyse der Bodengegebenheiten, dass die Bedingungen in Österreich nicht für einen Einfluss der Bodenfeuchte auf den Niederschlag geeignet sind. Diese Erkenntnis deckt sich mit den Ergebnissen der Analyse des SMPF, wo kein systematischer Einfluss ermittelt werden konnte. Die Ergebnisse der RCMs stimmten hiermit überein. Jedoch könnte die Bodenfeuchte durch das Ansteigen der globalen Temperatur und der Ausdehnung des südeuropäischen, trockenen Klimas in den Alpenraum in der Zukunft verstärkt Einfluss auf den Niederschlag haben.

Acknowledgement

First of all, I would like to thank my supervisor Heimo Truhetz for introducing me to the Wegener Center for Climate and Global Change and for always supporting me throughout this thesis. Further I want to thank all members of the Regional Climate Research Group for the interesting discussions and the feedback I got in our weekly meetings. A special thanks goes to the head of the group Douglas Maraun and the vice-head Albert Osso. I am looking forward to working with you in my upcoming PhD study. Moreover, I am very grateful for the financial support from the reclip:convex project (project ID: B769999), which is funded by the Austrian Climate Research Program. Lastly, I want to thank Guillermo Martinez Cabalga, Gerhard Schaffer, Elisabeth Suppik, Matthias Wintersteller and Heimo Truhetz for taking the time to proofread this thesis and giving me feedback.

Contents

Abstract	ii
Zusammenfassung	iii
Acknowledgement.....	iv
Contents.....	v
1. Introduction.....	1
2. Climate system.....	4
2.1. Description of the climate system	4
2.2. Land surface-atmosphere interaction.....	9
2.3. Soil moisture-atmosphere feedbacks	13
3. Data	20
3.1. INCA	20
3.2. ERA5 and ERA-Interim	22
3.3. WegenerNet.....	22
3.4. Noah LSM and HRLDAS.....	24
3.5. WRF - Weather Research and Forecasting Model	27
3.6. CCLM - COSMO Model in Climate Mode.....	29
4. Methodology and Statistics.....	31
4.1. HRLDAS forcing data preprocessing.....	31
4.2. Data postprocessing.....	34
4.3. Statistics.....	36
4.4. Soil moisture precipitation feedback diagnostics	38
5. Results and Discussion	43
5.1. HRLDAS soil moisture evaluation.....	43
5.2. Land surface conditions.....	54
5.3. Soil moisture precipitation feedback	60

6. Conclusions.....	71
Bibliography.....	74
List of Figures	83
Appendix	85
A. Event size and precipitation limit tests	85
B. Seasonal land surface conditions	86

1. Introduction

Climate change is one of the biggest challenges humanity has to face in the current century. To better assess the consequences, we need to improve our understanding of the climate system, in particular, it is essential to further our knowledge of the internal processes and involved feedbacks (IPCC, 2001). Many of these processes, like deep and shallow convection, although are not resolved by general circulation models (GCMs) or state-of-the-art regional climate models (RCMs) and thus depend on parameterizations, which are a major source of model uncertainties (e.g. Awan et al., 2011; Suklitsch et al., 2008). Shortcomings in the representation of dynamical synoptic processes in the coarsely resolved RCM driving boundary data are further handed down, additionally increasing biases (e.g. Shepherd, 2014). All of this consequently leads to deep uncertainties in current climate projections, especially for summertime extreme precipitation in the Alpine region (Gobiet et al., 2014; Jacob et al., 2014; Maraun, 2013). These challenges are increasingly faced by employing convection permitting RCMs, which have the capacity to resolve many dynamical processes in limited domains (e.g. CORDEX-FPS (Coppola et al., 2020)), making the investigation into regional feedbacks possible.

These feedbacks often occur between the components of the climate system and can have a major impact on its condition. Feedbacks concerned with the change of greenhouse gas concentration in the atmosphere for instance are important to understand and predict future temperature changes. Changes in the land surface conditions, through land use and climate change may also have severe impacts, notably on a regional scale (IPCC, 2013). Land surface-atmosphere interaction is a field of considerable research, but due to the complexity of the processes and the strong heterogeneity of the land surface, there are still considerable uncertainties (Seneviratne et al., 2010). Especially interactions and feedbacks of the soil moisture with the atmosphere show ambiguities. They have been shown to affect climate variability (Seneviratne and Stöckli, 2008), the duration and severity of droughts and heatwaves (Fischer et al., 2007; Whan et al., 2015) and precipitation patterns in some regions (Hohenegger and Stevens, 2018; Taylor et al., 2013). The lack of comprehensive observational soil moisture data further increases the difficulty of analyzing and evaluating these interactions.

The soil moist-precipitation feedback (SMPF) in particular differs substantially, depending on the prevailing climate and soil conditions (Seneviratne et al., 2010). There are strong indications that the underlying mechanism influences precipitation patterns in many global regions. Based on observational data a study showed that precipitation in the Sahel zone is more likely to occur when there were drier conditions (using one day prior rainfall as proxy). However, this negative feedback is merely captured by convection-permitting climate simulations. Climate models which parametrize convection and RCM showed a positive feedback, meaning precipitation is more likely when there are wetter soil conditions (Taylor et al., 2013). Other studies evaluated the SMPF globally and quantified it using parameters representing the spatial relationship (Taylor et al., 2012), as well as temporal and soil moisture heterogeneity links of soil moisture and precipitation events (Guillod et al., 2015; Moon et al., 2019). All of them conclude that the SMPF is negative in many parts of the world, especially in semi-arid regions. Areas with considerable topographic height variation, like the Alpine region, are excluded from these analyses. This is due to orographic effects, which tend to be the dominating factor on precipitation patterns (Imamovic et al., 2017).

This study adopts the method presented by Taylor et al. (2012), Guillod et al. (2015) and Moon et al. (2019) to assess the SMPF in Austria on a regional scale. The feedback parameters are calculated based on data of two convection-permitting RCMs, the Consortium for Small Scale Modelling (COSMO) model in Climate Mode (CCLM) (Böhm et al., 2006) and the Weather Research and Forecasting model (WRF) (Skamarock et al., 2008), stemming from the CORDEX-FPS (Coppola et al., 2020) and compared to results from observational data. Due to the lack of soil moisture observations, the High-Resolution Land Data Assimilation System (HRLDAS) (Chen et al., 2007) is employed to generate soil moisture data with high temporal and spatial resolution. The system is run with observational weather data from the INCA system (Haiden et al., 2011). A focus of this thesis is the evaluation of the results obtained by this model. For this purpose, the WegenerNet dataset (Fuchsberger et al., 2020), consisting of in-situ measurements from a climate station network located in south-eastern Styria, is used.

The goal of this thesis is to answer the following questions:

1. How do land surface model soil moisture data, derived from atmospheric observations, and RCM soil moisture data perform compared to in-situ measurements data? What consequences might shortcomings have for climatologic studies?
2. Is there a noticeable effect of soil moisture conditions on the distribution of precipitation on a regional scale in Austria? How do convection-permitting RCMs perform in this regard?
3. Is the method presented by Taylor et al. (2013), Guillod et al. (2015) and Moon et al. (2019) applicable in regions of complex topography on a regional scale?

This thesis is structured in six chapters. The following chapter gives an introduction to the climate system, as well as into the soil moisture-temperature and -precipitation feedback. Chapter 3 presents the HRLDAS, the two RCMs, i.e. CCLM and WRF, and the datasets used in this study, whereas chapter 4 explains the adapted SMPF diagnostic method, the data processing and statistical essentials. The last two chapters are concerned with the results of the soil moisture comparison, land surface condition analysis and the SMPF analysis, which are presented in detail and the conclusions, where the findings of the thesis are outlined, and the research questions are addressed.

2. Climate system

Climate is described in terms of mean and variability of temperature, precipitation, windspeed and other climatological variables over different periods of time (classically 30-year period). While weather describes the short term atmospheric conditions, climate can be seen as an aggregate of these conditions, also expressing seasonal variability and extremes, like heatwaves and storms (Goosse, 2015). The climate system consists of the entirety of all components which influence the state of the climate. It is not static, but changes with time due to external forces, like solar and human activity (IPCC, 2007). To be able to predict these changes, it is necessary to obtain an understanding of the processes within the system and their physical, chemical and biological mechanisms. In the following chapter the components of the climate system are introduced, with the focus on the interface between the atmosphere and land surface, as well as their conditions in the Alpine Region. For these components the most important processes involved in the interaction of soil moisture and the atmosphere are described. These interactions and their mechanisms are then studied in more depth, looking in particular at the soil moisture-precipitation feedback.

2.1. Description of the climate system

The climate system describes the processes and dynamic nature of the climate and weather. Its five main components are the atmosphere and the land surface, which are the most important ones for this thesis, as well as the hydrosphere, the cryosphere and biosphere. These spheres are linked to each other on many different spatial and temporal scales, making the system highly complex. These interactions manifest in form of fluxes of mass (e.g. water, carbon), heat or momentum. The system is further affected by different external forces. The Sun, providing energy via radiation, is the most important. Likewise, human activity on this planet, such as greenhouse gas emission and land use change, is referred to as an external influence (IPCC, 2001).

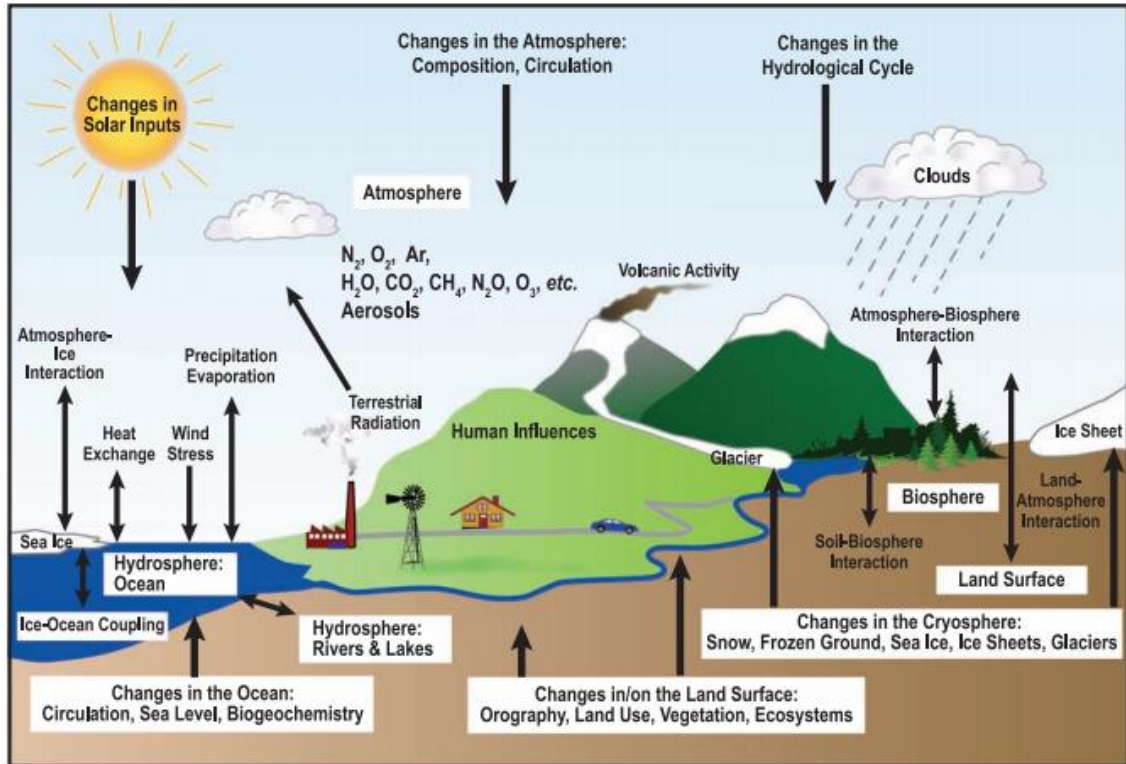


Figure 1 Schematic of the components of the climate system, their interactions (two sided arrows) and internal processes (arrows) (IPCC, 2007).

Atmosphere

The state of the climate system is generally described in terms of the atmospheric conditions. It is the most dynamic and fastest changing component of the system. Its spectrum ranges broadly in space and time, from turbulent motion with the size of centimeters and sub-second timescales to large scale circulation, encompassing the whole globe, which can vary on yearly scales. The most important parameters are temperature, wind speed and humidity. Water vapor content is highly variable in the atmosphere. Nearly all the atmospheric water is located in the troposphere, which is the lowest level of the atmosphere, but even in this level the amount of water varies greatly. In average the atmosphere holds $13 \cdot 10^3 \text{ km}^3$ of water, corresponding to 25 mm of precipitation over the entire earth, which is very small compared to the volume of the oceans ($1.338 \cdot 10^9 \text{ km}^3$) (Oki and Kanae, 2006). The atmosphere gains water by evaporation from the oceans and the land surface, as well as transpiration from plants. The amount of water evaporated from the oceans ($436.5 \cdot 10^3 \text{ km}^3 \text{ y}^{-1}$) is about 6.6 times higher than the flux of water into the atmosphere from land ($65.5 \cdot 10^3 \text{ km}^3 \text{ y}^{-1}$). The combined effect over land is

called evapotranspiration (ET). Although differences of these processes are important, like diurnal changes and active soil depth, in practice it is difficult to separate them (Hartmann, 2016). The ET depends on several factors, such as temperature, humidity, soil moisture content and land cover. The evaporated water may be transported within the atmosphere and returns to the surface via precipitation. Precipitation over land is stored in different reservoirs or transported via surface fluxes, e.g. rivers, closing the hydrological cycle.

Atmospheric water forms clouds when water droplets condense due to the moisture surpassing the saturation point and the presents of condensation nuclei, e.g. dust and aerosol particles. If these droplets reach a certain mass, they fall down as precipitation. The saturation point, and thus the water holding capacity of air, is defined by the Clausius-Clapeyron equation and depends on air pressure and temperature (see chapter 4.1). If an air parcel has a humidity close to the saturation point and is cooled, the saturation point sinks and excess water will condensate. The cooling is generally achieved through lifting of the parcel and subsequent adiabatic cooling. There are two main reasons for vertical movement in the atmosphere: buoyancy forces, due to differences in density within the atmosphere, and orographic effects. The first mechanism refers to temperature differences and hence the resulting atmospheric instability. This effect can be seen in fronts, where cold air masses move into regions of warm air, forcing it upwards (cold front) or warm air masses move on top of cold air (warm fronts). On a smaller scale and primarily in summer there is thermal convection, where differences in radiation or energy fluxes lead to near surface air temperature rise, destabilizing the lower atmosphere. If the air holds enough moisture, the resulting strong updraft causes clouds to form. The released latent heat of the condensation further powers the upward movement and thunderstorms may form. Orographic effects refer to forced upward movement due to the land surface topography (Malberg, 2007). These effects have a major influence on precipitation patterns in mountain areas like the Alpine Region.

Hénin et al. (2019) estimate that 30 % to 40 % of precipitation in central Europe is related to frontal activity. Local maxima of frontal precipitation were found in the Alps in summer months, agreeing with observations showing that front frequency in the region is roughly 15 times higher in summer than in winter (Jenkner et al., 2009). A regional

climate study suggests that the fraction is even higher for Austria with 40 % to 70 % in winter months and 50 % to 70 % in summer months (Piazza et al., 2019).

Land surface

Within the hydrological cycle the land surface serves as an important storage. The main storage is within aquifers as groundwater accounting for $23.4 \cdot 10^6 \text{ km}^3$ of water. The stored moisture within the unsaturated soil matrix is called soil moisture ($17 \cdot 10^3 \text{ km}^3$). The water volume amounts to approximately 10 % of the volume of all lakes. Another major storage of water of the earth's surface is permafrost, which accounts for $300 \cdot 10^3 \text{ km}^3$ of water. Soil moisture is an important source of water for not only the atmosphere, but also the biosphere, greatly influencing the biosphere and continental ET (Oki and Kanae, 2006). Vegetation coverage and type in turn influences transpiration. Depending on the depth of the root-zone, water from deeper soil layers can be taken up by the plants and transpire to the atmosphere. The land water balance can be expressed as:

$$\frac{dS}{dt} = P - ET - \Delta f \quad (1)$$

where $\frac{dS}{dt}$ is the change of stored water in time, which equals the difference of precipitation (P) and the sum of evapotranspiration (ET) and runoff at the surface or percolation to deeper soil layers (Δf). The change of stored water not only describes soil moisture, but also snow and ice coverage, ground water and surface water changes (Hartmann, 2016). As already mentioned, ET greatly depends on the soil moisture. This is due to the binding strength of the water to the soil matrix, resisting evaporation and absorption by plants, which depends on the water content. This metric is called the soil moisture potential or soil matric suction. From this potential three important soil moisture parameters can be defined. First, the saturation moisture (Θ_{SAT}) is the maximal amount of water that can be absorbed by the soil. At this level all pores of the soil matrix (volume of voids) are filled with water. It is only reached after strong precipitation events. Additional water cannot be absorbed by the soil and produces runoff instead. At this level the matric potential is lower than the gravitational force, thus water is transported downwards over time. At the

point where the soil can hold on to the water against the gravitational pull, the field capacity (Θ_{FC}) is reached. Further drying the soil and thus increasing the matric potential, water becomes less available to evaporation and plants. At the point where most plants cannot absorb water from the soil, due to the retention strength, the wilting point (Θ_{WILT}) is reached (Figure 2).

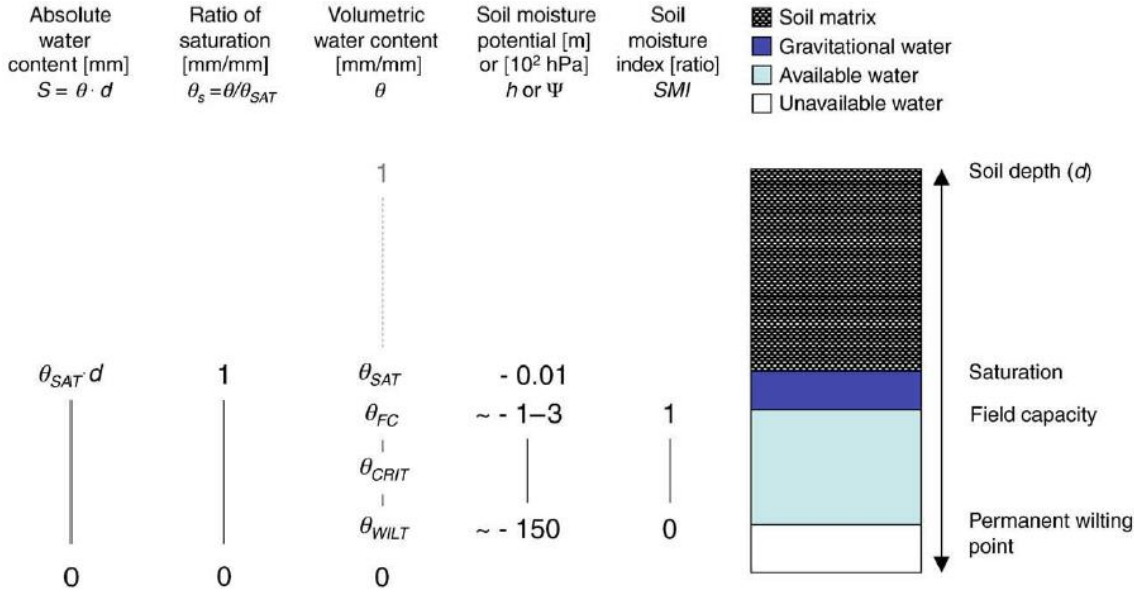


Figure 2 Characteristic soil moisture levels and units. The schematic represents a soil sample of depth d with indicated characteristic soil water levels: saturation soil moisture (Θ_{SAT}), field capacity (Θ_{FC}), critical soil moisture (Θ_{Crit}) and wilting point (Θ_{WILT}) is. In this thesis the volumetric water content in $m^3 m^{-3}$ is used to describe the soil moisture (Seneviratne et al., 2010).

2.2. Land surface-atmosphere interaction

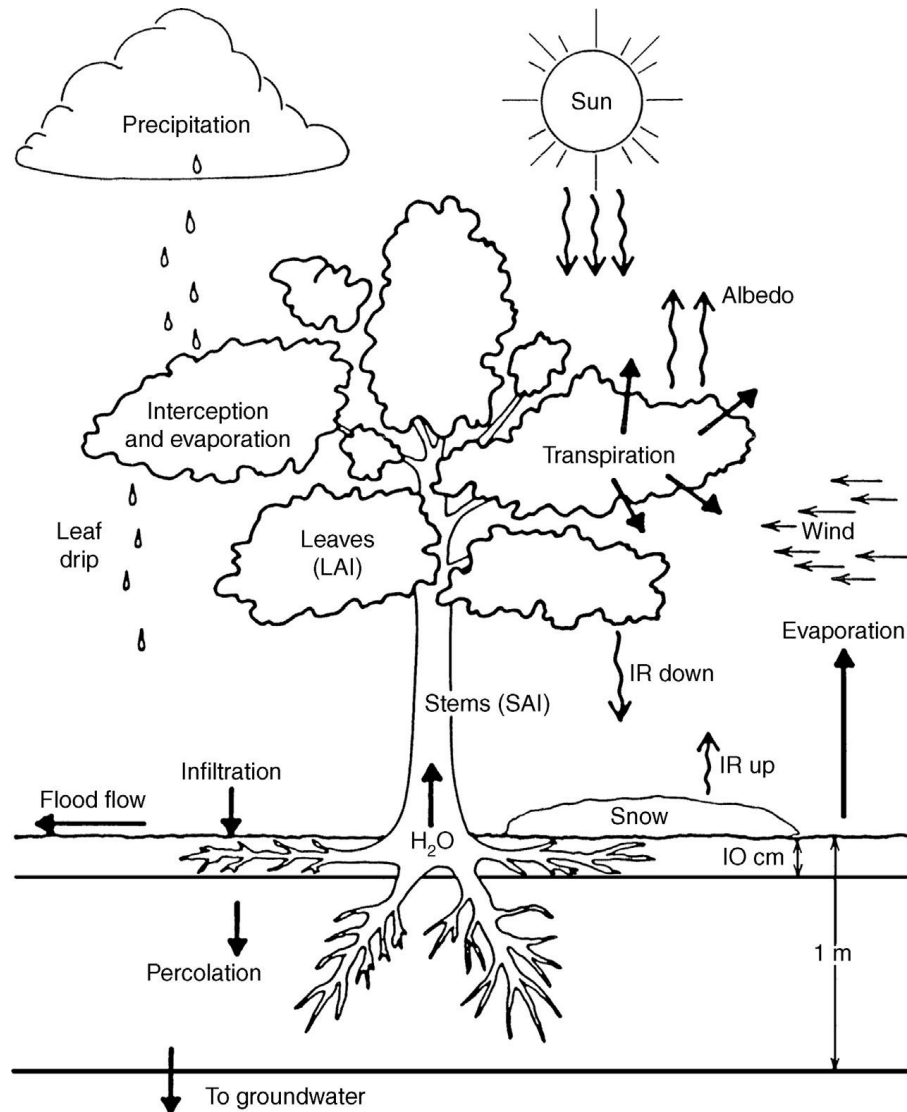


Figure 3 Schematic of land surface-atmosphere interactions with the contributing hydrological and energy fluxes (Hartmann, 2016).

The land surface and the atmosphere are connected via the hydrological cycle by ET and precipitation and further via surface energy fluxes. ET can be approximated and modeled using the Penman-Monteith equation, which was developed by John L. Monteith based on the equation from Howard L. Penman, which describes evaporation from an open water surface:

$$\lambda E = \frac{\Delta R_n + \rho c_p (e_s(T) - e) r_H^{-1}}{\Delta + \gamma(1 + r_s/r_H)} \quad (2)$$

Here λ is the latent heat of vaporization of water [J kg^{-1}], E the evaporation rate [$\text{kg s}^{-1} \text{m}^{-2}$], Δ the rate of change of saturation vapor pressure with temperature [K^{-1}], R_n the net radiation flux density [W m^{-2}], ρ the air density [kg m^{-3}], c_p the specific heat capacity [$\text{J kg}^{-1} \text{K}^{-1}$], $e_s(T)$ the temperature dependent saturation vapor pressure [Pa], e the prevailing vapor pressure [Pa], r_H the resistance for heat transfer by convection [s m^{-1}], γ the psychrometric constant [Pa K^{-1}] and r_s the resistance of a set of stomata (leafpores) [s m^{-1}]. The equation thus relates radiative energy fluxes, the water vapor deficit of the air and conductivity of heat through air and plant leaves to the amount of evaporation (in chase of (2) to the evaporative energy per time and area) (Monteith and Unsworth, 2013).

The surface conditions further influence the earth's radiative budget and consequently atmospheric temperatures. Due to the atmospheric transparency to solar short-wave radiation, most of it reaches the earth's surface and is either absorbed or reflected. The earth's reflectivity, the albedo, greatly depends on the surface and vegetation conditions. Bare soil, for instance reflects between 5 to 40 % of solar radiation, while coniferous forest only reflect 5 to 15 % (Goosse, 2015). The surface in turn heats up and emits energy in form of infrared radiation (long-wave radiation) and heat energy fluxes, heating up the atmosphere from below. Similar to the hydrological balance, the energy balance at the land surface can be expressed as:

$$\frac{dE_s}{dt} = R_n - SH - LH - \Delta F \quad (3)$$

where $\frac{dE_s}{dt}$ is the change of stored energy in the surface soil or water in time, R_n is the net radiation, equal to the difference of incoming radiation and outgoing radiation, SH and LH are the sensible and latent heat fluxes to the atmosphere and ΔF the energy flux within the land surface. The net radiation energy at the surface is balanced on longer time scales by the energy fluxes. These fluxes of thermal energy are either in form of sensible heat, directly increasing the temperature of the system, or latent heat, converted to change the

phase of water by evaporation or sublimation. The latent heat flux is thus directly linked to the ET rate and precipitation. About 68 % of the absorbed solar radiation is balanced by latent (55 %) and sensible heat (13 %). Only the remaining 32 % are balanced by the net flux of thermal radiation. These heat fluxes thus play an important role in cooling the surface and heating the atmosphere. Hence, the atmosphere is in a so-called radiative-convective equilibrium (Hartmann, 2016).

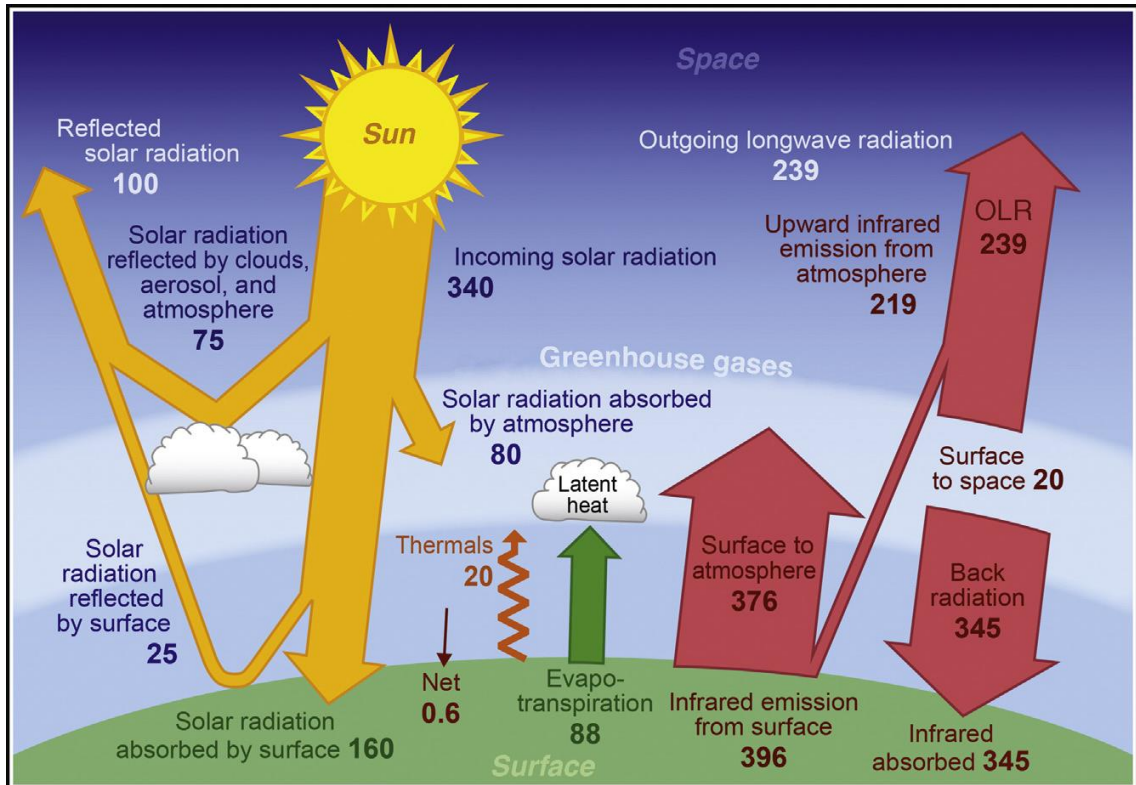


Figure 4 Global and annual average energy fluxes in $W m^{-2}$ (Hartmann, 2016).

The partitioning into these energy fluxes depends greatly on the land surface conditions and the prevailing climate. In wet regions ET is limited by the energy supply, therefore latent heat is the dominant flux. In contrast, dry and semi-arid regions have limited water supply, increasing the sensible heat flux (Seneviratne & Stöckli, 2008). Therefore, surface soil moisture not only has a huge impact on the continental water cycle, but also on the land energy budget. The ratio of latent heat to sensible heat, called the Bowen ratio, thus is an important variable to describe regional differences in the soil moisture and ET regime (Hartmann, 2016; Seneviratne et al., 2010). A Bowen ratio higher than 1 indicates less humid conditions, higher values denote semi-arid to arid land surface conditions,

whilst regions with values lower than 1 are characterized by temperate forests and grasslands. Lowest values are reached in tropical regions and over water bodies. The soil moisture value at which the transition from an energy-limited to an soil moisture-limited climate is located, is called the critical soil moisture value (Figure 5).

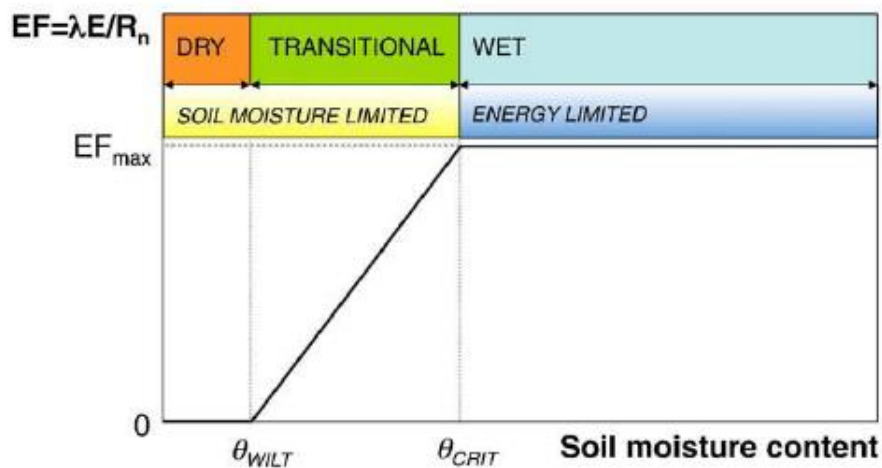


Figure 5 Definition of the soil moisture regimes and the corresponding ET regimes. The evaporation fraction (EF) is depicted on the ordinate. From Seneviratne et al. (2010) based on Budyko (1974).

The transitional zone from a wet to a dry climate is defined as the soil moisture between the critical soil moisture and the wilting point. It is expected to be in regions of saturation ratio values between 0.2 and 0.35. In these regions ET tends to strongly depend on soil moisture and is large enough to influence the local climate., both conditions are required for soil moisture-climate coupling (Koster et al., 2004). Teuling et al. (2009) investigated the global correlation between yearly ET and radiation, and precipitation respectively. The multi-model analysis shows regions of energy-limited ET, characterized by high correlation between radiation and ET, and of soil moisture-limited ET, characterized by high correlation between ET and precipitation, which is utilized as a proxy for soil moisture. Especially interesting for this thesis are the conditions in the Alpine region. It can be seen that this region has high ET dependencies on radiation and low or negligible dependences on precipitation. However, the conditions change to the east and southeast with increasing influence of precipitation, indicating a transition zone from a wet to a dry climate (Figure 6). In a changing climate the Alpine Region could also become part of

the European transition zone, which could influence soil moisture-atmosphere interactions and thus regional circulation patterns (Seneviratne et al., 2006).

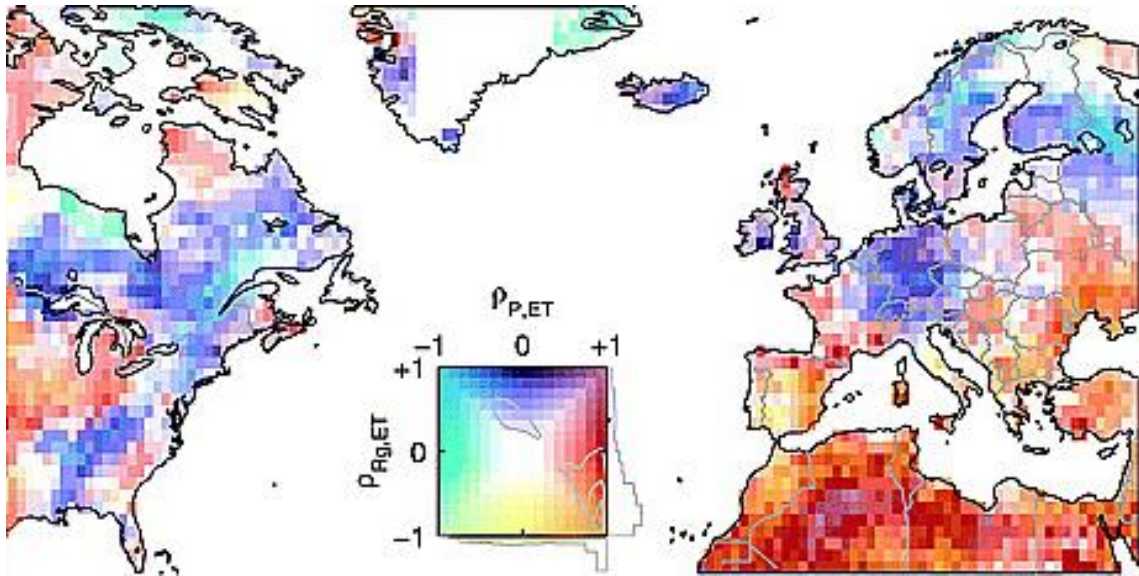


Figure 6 Multi-model analysis of the correlation of ET with radiation ($\rho_{Ag,ET}$) and ET with precipitation ($\rho_{P,ET}$) for the period of 1986 to 1995. Colors indicate the combination of both values. The grey lines at the color bar represent the global frequency distribution. Central Europe is dominated by radiation dependent ET, with transition zones in eastern, southeastern Europe and the Mediterranean Region (Teuling et al., 2009).

2.3. Soil moisture-atmosphere feedbacks

The terms “feedback”, “coupling” and “interaction” are often used interchangeably in scientific literature. In this thesis, based on Seneviratne et al. (2010), “Coupling” is defined as the influence one variable has on another variable, considering all processes. When talking about “feedbacks”, the cause-and-effect chain, connecting one variable with itself, considering intermediate variables, is meant. In contrast, “interaction” is used in a more general sense, describing the relationship of two variables within a system, without indicating the direction of causality.

Feedback mechanisms increase the complexity of a system and can change its behavior. Many different feedback loops act on the climate system, varying greatly in strength and

sign. Positive feedbacks increase the magnitude of the response and tend to destabilize the system, whilst negative feedbacks decrease the response, therefore having a stabilizing effect. Understanding feedbacks is essential to improve our knowledge about climate variability and the dynamic properties of the climate system (IPCC, 2001). There are two main influences soil moisture has on the variability of atmospheric conditions: the soil moisture-temperature and the soil moisture-precipitation feedback (Seneviratne & Stöckli, 2008; Seneviratne et al., 2010).

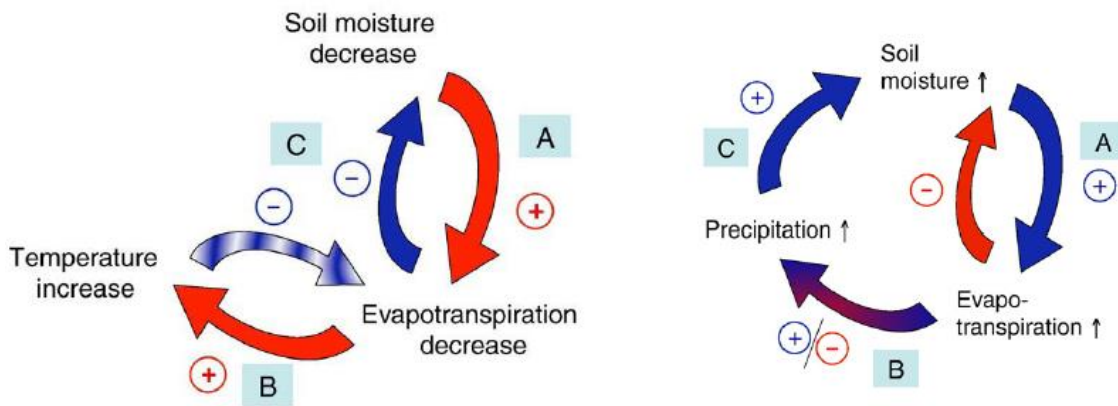


Figure 7 Processes involved in the soil moisture-temperature feedback (left) and the soil moisture-precipitation feedback (right). The coloring and sign show if the coupling is positive or negative. Temperature-ET coupling is colored blue and white indicating a possible positive coupling or no coupling, depending on the regional climate conditions. ET-precipitation coupling similarly is colored red and blue indicating potential negative or positive coupling (Seneviratne et al., 2010).

The soil moisture-temperature feedback describes the interaction of soil moisture with the near surface air temperature. As seen in Figure 7, (A) describes the link of soil water content and evapotranspiration. If soil moisture decreases, the amount of energy needed to remove water from the soil increases, thus decreasing the ET rate. As mentioned before, there are two conditions required for soil moisture to have an influence on the climate. There has to be a considerable amount of ET and it has to strongly depend on the soil water content. For this reason, the coupling is expected to be strongest in dry and transitional regions (Koster et al., 2004; Seneviratne et al., 2010). Reduced ET in turn decreases the loss of water from the soil to the atmosphere, increasing soil moisture.

Relationship (B) shows the link of ET and air temperature. Decreasing ET leads to lower latent heat fluxes and higher sensible heat fluxes, increasing near surface temperatures. The strength of the negative coupling of increasing temperature with decreasing ET depends on the water supply situation. In wet regions the strength is high, though near zero in dry regions. (C) refers to the potential positive feedback (induced by connecting the two negative feedbacks), where further decreasing soil moisture leads to further increase in air temperatures. The coupling of soil moisture and temperature is estimated to be strongly negative in many areas, especially in semi-arid regions. In these regions the feedback can increase the severity and duration of droughts and heat extremes (e.g. Fischer et al., 2007; Whan et al., 2015). Soil moisture is thus an important factor when studying heat extremes in many global regions. Due to climate change, these areas could become even larger and engulf central and south eastern Europe by the late 21st century (Figure 8).

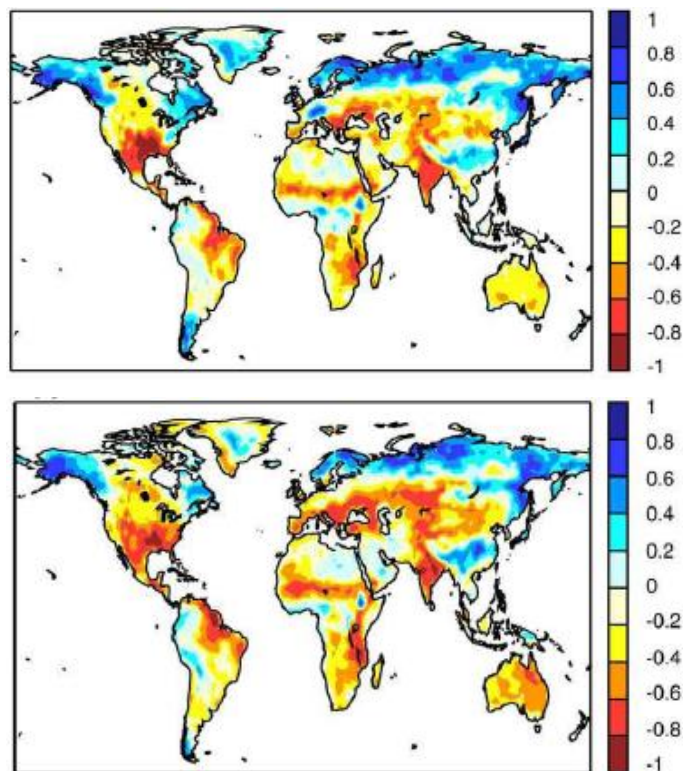


Figure 8 Analysis of soil moisture-temperature coupling for 1970 to 1989 (top) and 2080 to 2099 climate (bottom), based on three IPCC GCMs. Semi-arid regions show strong negative coupling in the 1970 to 1989 period. These regions may increase in size due to rising global temperatures (Seneviratne et al., 2010).

The second soil moisture-atmosphere interaction is with precipitation. This feedback is very complex and depends on many different climatologic conditions. It quantifies the likelihood of encountering precipitation depending on the wetness of the soil. The relationship (A) of soil moisture and ET (Figure 7) is the same as in the temperature feedback, with soil moisture increasing potential ET, which in turn reduces soil water content. This, as mentioned before, holds especially true in semi-arid regions and the transition zones from dry to wet climate. Coupling of ET with precipitation (B) is the most uncertain link, as well as difficult to assess, because of the number of processes involved. The positive link of precipitation on soil moisture (C) can be considered trivial, except for some special cases, e.g. rain in wet regions with saturated soil, increasing runoff instead (Seneviratne et al., 2010).

Thus, the coupling mechanism determining whether the feedback is positive, or negative is the link of ET and precipitation (B). To result in a positive feedback, the coupling has to be positive, meaning more evaporation and transpiration would result in more precipitation. This conjecture can be assumed to be reasonable, because more ET leads to higher water content in the air, making precipitation more likely to occur or stronger. If large areas of land are investigated, this would hold true, but on a regional scale dynamical processes and moisture advection have a huge role on precipitation patterns. The hypothesized mechanism for a negative coupling of ET and precipitation is that less soil moisture increases the amount of sensible heat flux, increasing near surface air temperatures and decreasing atmospheric stability. If atmospheric instability is reached, convection can initiate. Consequent convergence at the surface could be a driver of moisture advection from regions of wetter soils. The advected moisture within the convective system could form clouds and precipitation. A similar effect can be observed at coastlines. Daytime differential heating of the ocean and land surfaces induces a circulation, the so-called sea breeze, which leads to the formation of cumulus clouds at the inland edge of the circulation (Miller et al., 2003).

This mechanism has been observed using convection-permitting simulations over idealized land surfaces. The SMPF is positive at first, drying out areas where no precipitation occurs, increasing the soil moisture heterogeneity. When these areas reach soil moisture levels close to the wilting point, this effect is reversed by the mechanism previously described, resulting in a negative feedback. The mechanism is further

suspected to influence precipitation patterns in the Sahel zone, where the SMPF increases the likelihoods of precipitation over drier soils and the northward extension of the monsoon in drier years (Hohenegger and Stevens, 2018; Taylor et al., 2013, 2011). Moreover, soil moisture and wind patterns in Europe indicate a similar mechanism in areas of convective initiations (Taylor, 2015). An additional important influence on the mechanism is the background flow. Convective clouds may form over drier soils but could be transported towards regions of wetter soils with high convective potential. This leads to the formation of high precipitation amounts and a positive feedback (Froidevaux et al., 2014).

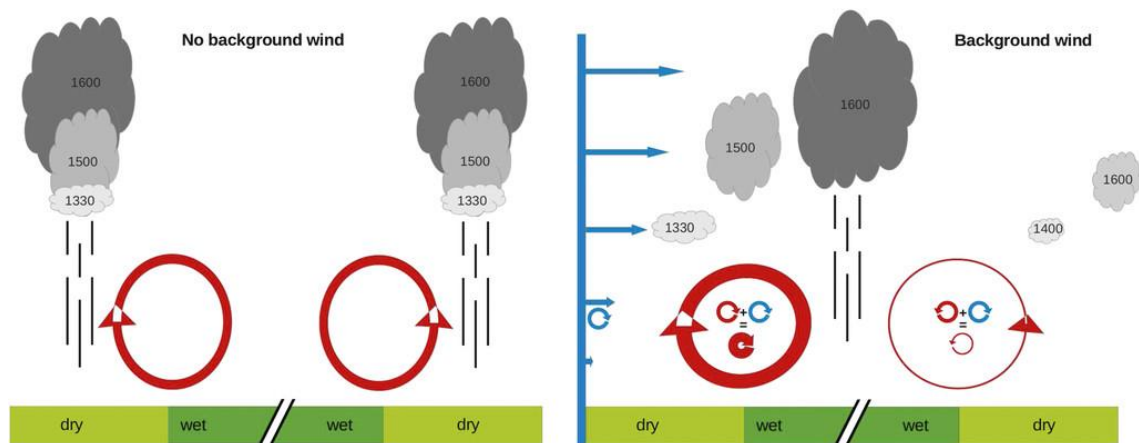


Figure 9 Conceptual scheme of regional circulation (red circular arrows) induced by soil moisture heterogeneity. (left) Without background wind, convection is initiated over drier areas, which leads to moisture advection from wetter areas and subsequent precipitation (negative feedback). (right) With background wind (blue arrows) present, regional circulation on the upwind side of drier areas is increased due to the additional vorticity (blue circular arrows), transporting storms to wetter soil patches (positive feedback). On the downwind side background vorticity decreases the circulation pattern and inhibits cloud formation. The numbers inside the clouds indicate the local standard time of their depicted maturity (Froidevaux et al., 2014).

Taking a closer look into the soil condition preferences for precipitation globally, a negative spatial feedback can be observed in many parts of the world. This means, that precipitation is more likely to occur in heterogenic soil moisture conditions, in the drier

areas (Taylor et al., 2012). When looking into the temporal preferences, there are strong positive feedbacks in most regions. These soil condition metrics (spatial, temporal and heterogeneity) indicate that precipitation is more likely to occur in locally dry areas, but overall wetter soil conditions, with strong moisture heterogeneity and gradients (Figure 10) (Guillod et al., 2015; Moon et al., 2019). This joint coupling perspective cannot be observed in Europe, due to the presence of many interfering effects. Using similar methods and metrics on a more regional level could give a clearer picture about the preferences in Europe. The soil moisture precipitation coupling, as mentioned, strongly depends on the scale of the analysis. Climate models which parameterize convection, like GCMs and coarse resolution RCM, show significant biases towards a positive feedback (Hohenegger et al., 2009; Koster et al., 2004). Very high-resolution analysis on the other hand may be too small to capture the influence of humidity advection from areas of high soil moisture to convective active areas (Holgate et al., 2019).

When investigating the SMPF in the mid-latitudes it is important to focus on precipitation originating from thermal convection. Synoptic regimes, like frontal rain, may also be influenced by land surface conditions, but to a lesser extent (Ford et al., 2015; Keil et al., 2019). Further, mountainous regions have to be excluded from the analysis. Even small changes of orographic height have the potential to dominate the formation of precipitation, making an investigation into soil moisture effects impossible (Imamovic et al., 2017).

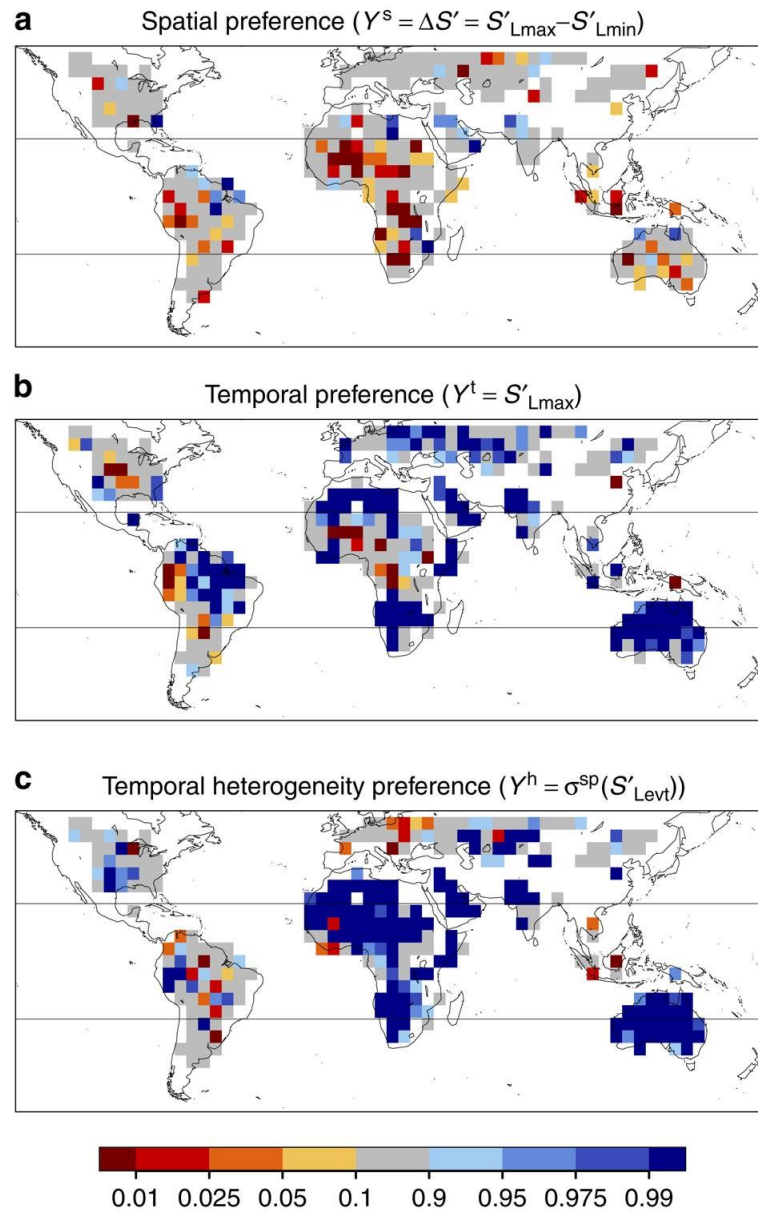


Figure 10 Afternoon precipitation preference over soil moisture anomalies for the period of 2002 to 2011. (a) spatial, (b) temporal and (c) heterogeneity preference. Red indicates strong negative feedbacks and blue strong positive feedbacks. Strong negative spatial and positive temporal preferences are found in semi-arid regions. Areas in Europe do not show spatial preferences or were excluded from the analysis due to the proximity to large water bodies or mountains (Guilod et al., 2015).

3. Data

Because of the lack of soil moisture data, the decision was made to use the High-Resolution Land Data Assimilation System (HRLDAS) and run it with observational data from the Integrated Nowcasting through Comprehensive Analysis (INCA) system, as well as atmospheric pressure data from the ERA5 reanalysis. To validate the output data from this model, the station network WegenerNet is employed. In addition to soil moisture from this model and precipitation from the INCA observations, outputs of two RCMs are used to analyze the SMPF. They are the WRF and the CCLM. They utilize boundary conditions from the ERA-Interim reanalysis and run on high spatial resolution, thus explicitly resolving and calculating convective processes, which, as demonstrated in the previous chapter, is essential to investigate soil moisture-atmosphere interactions. Both are included in the CORDEX-FPS model ensemble, a study investigating convective phenomena over Europe. In the following section the HRLDAS, WRF and CCLM, as well as the ERA reanalysis data (ERA5 and ERA-Interim) and the observational datasets INCA and WegenerNet, are presented in detail.

3.1. INCA

The INCA system (Haiden et al., 2011) is a meteorological observation system operated by the Austrian weather service Zentralanstalt für Meteorologie und Geodynamik (ZAMG). It derives high-resolution data from surface station observations, interpolated to a nominal 1 km mesh grid, using the spatial structure of remote sensing data. The recorded data contains several meteorological variables (Tab. 1) from 2004 to the present day. The Austrian INCA domain covers an area of 600 km west to east and 350 km south to north, centered over the eastern Alps.

Table 1 List of variable fields of the INCA system with respective units and their temporal resolution. Asterisks indicate variables which were used in this thesis.

Variable	Unit	Temporal resolution [min]
Near surface temperature *	°C	60
Near surface relative humidity *	%	60
Near surface windspeed *	m s ⁻¹	60
Precipitation *	mm	15
Precipitation type	-	15
Cloudiness	%	15
Global radiation *	W m ⁻²	60
Snowfall line	m	60
Ground temperature	°C	60

It is important to note that, depending on the variable, the data has varying amounts of uncertainties. Haiden et al. (2011) quantify the bias and error of temperature, wind and precipitation compared to observational station data. Temperature mean absolute error (MAE) for the validation month of July 2009 is 0.9 °C and root mean square error (RMSE) is 1.3 °C. Larger errors are encountered in winter months and mountain valleys, where inversion is more frequent. Because the focus of this analysis lies on summertime and less mountainous regions, these are not as relevant as the aforementioned errors. Wind data shows a MAE of about 1 m s⁻¹ and a RMSE of about 1.4 m s⁻¹, with slightly higher errors in July than in January. Precipitation values, which are essential for the SMPF analysis, have larger errors attached. Short-duration analysis (15 min) for point values show relative errors of up to 50 % in summer, and more than 100 % in winter. However areal averages are significantly more reliable.

Due to missing timesteps in the INCA dataset, it has to be preprocessed. Because values are missing only for short consecutive time frames, bilinear interpolation is sufficient. Nevertheless, it is important to mention, because this leads to large errors in some timeframes, especially in precipitation data.

3.2. ERA5 and ERA-Interim

The ERA5 and ERA-Interim are global atmospheric reanalysis projects of the European Centre for Medium-Range Weather Forecasts (ECMWF). Reanalysis data provide coherent and spatially complete data of the atmospheric conditions over the past decades. They combine observations and numerical weather models to reconstruct the state of the climate system. They are produced with a single version of an assimilation system, assimilating observations of different parameters from different sources to a spatial and temporal coherent dataset. Therefore, changes in the method do not affect the output. The ERA-Interim reanalysis was started in 2006 and includes gridded data of a variety of land and ocean surface parameters and atmospheric parameters, covering the troposphere and stratosphere. Vertical integrated flux data and monthly averages of several parameters are also produced. It covers the period from 1979 to 31st August 2019 with a horizontal resolution of approximately 80 km (Dee et al., 2011). The ERA5 is the new generation of reanalysis products from the ECMWF, replacing the ERA-Interim. It operates similar to its predecessor, but on enhanced spatial resolution of 31 km. It further covers an even longer period from 1950 to the present day (Hersbach et al., 2020).

In this study the ERA reanalysis data are used in two ways. First, ERA-Interim provides the atmospheric boundary conditions for the CCLM and WRF, thus dynamically downscaling the data onto a high-resolution domain and consequentially resolving convective processes. Further, it is used to prescribe the starting conditions of the HRLDAS simulation. Secondly, atmospheric pressure from ERA5 is utilized to run the HRLDAS generating high resolution soil and surface parameters. For this purpose, mean sea level pressure was remapped onto the 1 km INCA grid and extrapolated to the surface pressure of the INCA surface height, using the barometric formula (chapter 4.1).

3.3. WegenerNet

The WegenerNet (Fuchsberger et al., 2020) is a climate station network in southeastern Austria operated by the Wegener Center for Climate and Global Change of the University of Graz. It provides measurements with high temporal and spatial resolution since 2007 for two regions in Styria. The Feldbach Region in the vicinity of the town of Feldbach in southeastern Styria, comprised of 155 stations (Figure 11) and the smaller observation

site in the Johnsbachtal in the mountainous region of upper Styria with 14 stations. They provide measurements for multiple hydrometeorological variables, including air pressure, air temperature, relative humidity, precipitation, wind speed and direction, global radiation, soil temperature and moisture.

Of the 155 stations in the Feldbach Region, 12 record soil moisture by two different metrics. The method first used measures the soil moisture matric potential by quantifying the energy that is required to remove water from the soil pores, called the pF-Value, in 0.3 m depth. From this value the soil moisture can be calculated via a soil type characteristic function (Fuchsberger and Kirchengast, 2013). Starting in 2013 some of the stations were reequipped with a time-domain reflectometry (TDR) sensor, measuring soil water content in 0.2 m depth. Here only the more recent TDR soil moisture records are used to validate the soil moisture output of the models. This data has significantly higher quality, than the soil moisture derived from the matric soil potential but is only available since autumn 2013. This reduces the overlapping time period with the model data, making the soil moisture evaluation less informative.

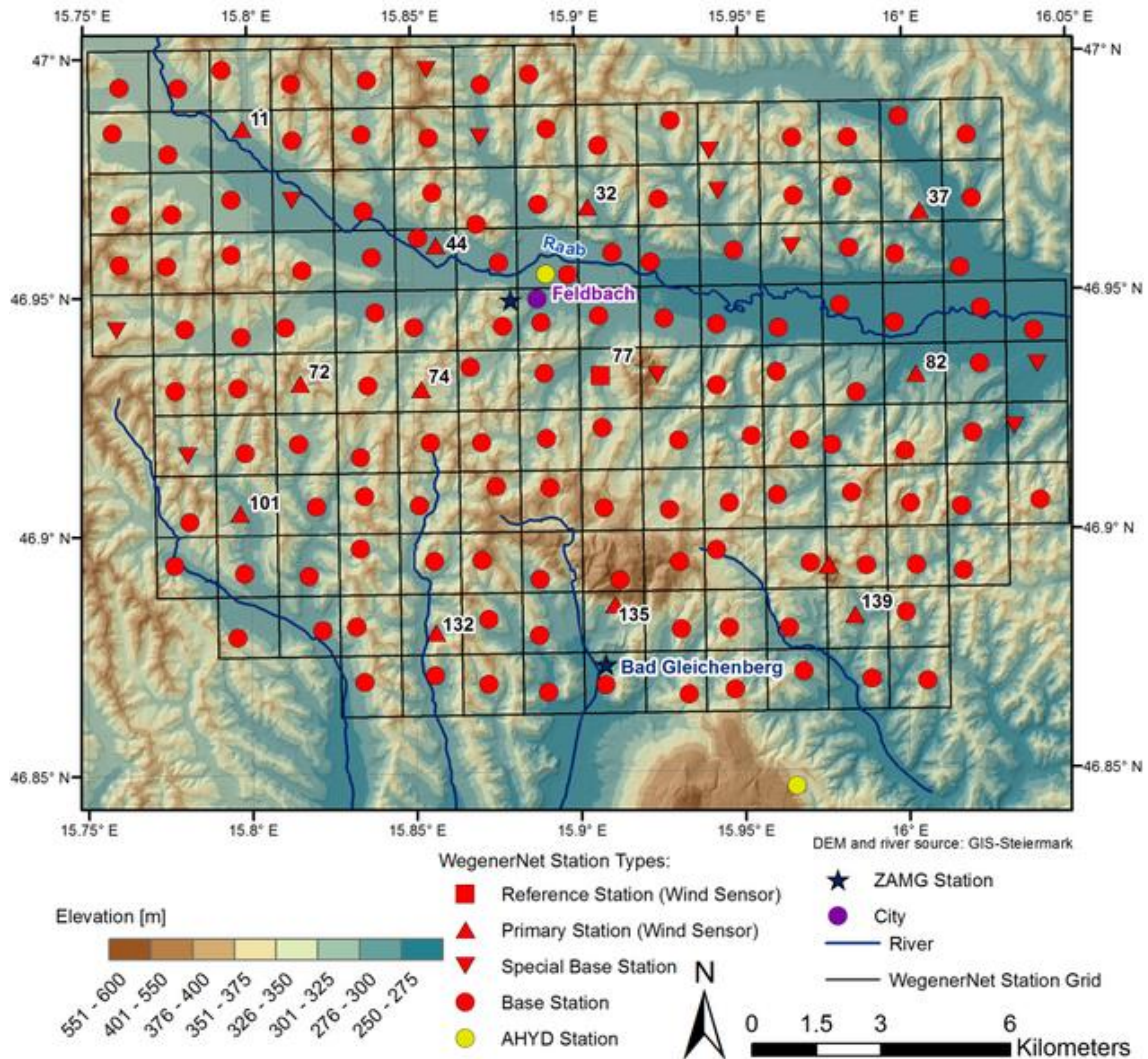


Figure 11 The WegenerNet Feldbach region, consisting of 155 ground stations (red dots, squares and triangles), of which 12 record soil parameters (Fuchsberger et al., 2020).

3.4. Noah LSM and HRLDAS

As described in chapter 2.1, the land surface is of vital importance for the climate system. Land surface models (LSM) simulate a wide range of processes happening at the Earth surface and the interactions with other parts of the climate system, like the exchange of energy, water and other substances, like carbon and nitrogen, with the atmosphere. The first LSMs consisted of simple schemes to describe the boundary conditions and surface energy fluxes of GCMs. Over the past decades, they have been improved and increased

in complexity by including many physical, chemical and biological processes, as well as anthropogenic forcing (Fisher and Koven, 2020).

One such model is the Noah-Multiparameterization Land Surface Model (Noah-MP LSM) (Niu et al., 2011), which is based on the Noah LSM (Chen et al., 1997, 1996; Chen and Dudhia, 2001; Ek et al., 2003), which is also known as Oregon State University LSM (OSU LSM). It was developed by the National Oceanic and Atmospheric Administration (NOAA) of the US Government as an effort to improve the Noah LSM. The Noah-MP LSM structure consists of several soil and aquifer layers, with the possibility of snow layers, as well as a vegetation canopy layer. It includes several parameterization schemes of hydrological, chemical and vegetative processes, like runoff and groundwater, dynamic vegetation and radiative transfer. It is implemented in the coupled WRF model (Skamarock et al., 2008) and also in the High Resolution Land Data Assimilation System (HRLDAS), developed by the National Center of Atmospheric Research (NCAR) (Chen et al., 2007). This system was developed to initialize land surface variables of climate models for high resolution applications. Since coherent land surface data observations do not as of yet exist on required high horizontal resolution, the HRLDAS can be used to generate these data from observations of atmospheric variables. This type of data assimilation system is often referred to as an uncoupled or offline LSM. Using the HRLDAS makes it possible to compute climatologic surface variables. Land surface fluxes like evaporation from the soil and the canopy layer, transpiration rate, as well as latent and sensible heat fluxes are generated on a two-dimensional grid. In this study this data is used to evaluate the prevailing surface conditions, such as the soil moisture and ET regimes in the studied region. The soil variable output, including soil moisture and soil temperature, is available in a third spatial dimension, consisting of four soil layers. The default thicknesses of these layers are 0.1 m, 0.3 m, 0.6 m and 1.0 m, summing up to 2 m (Figure 12).

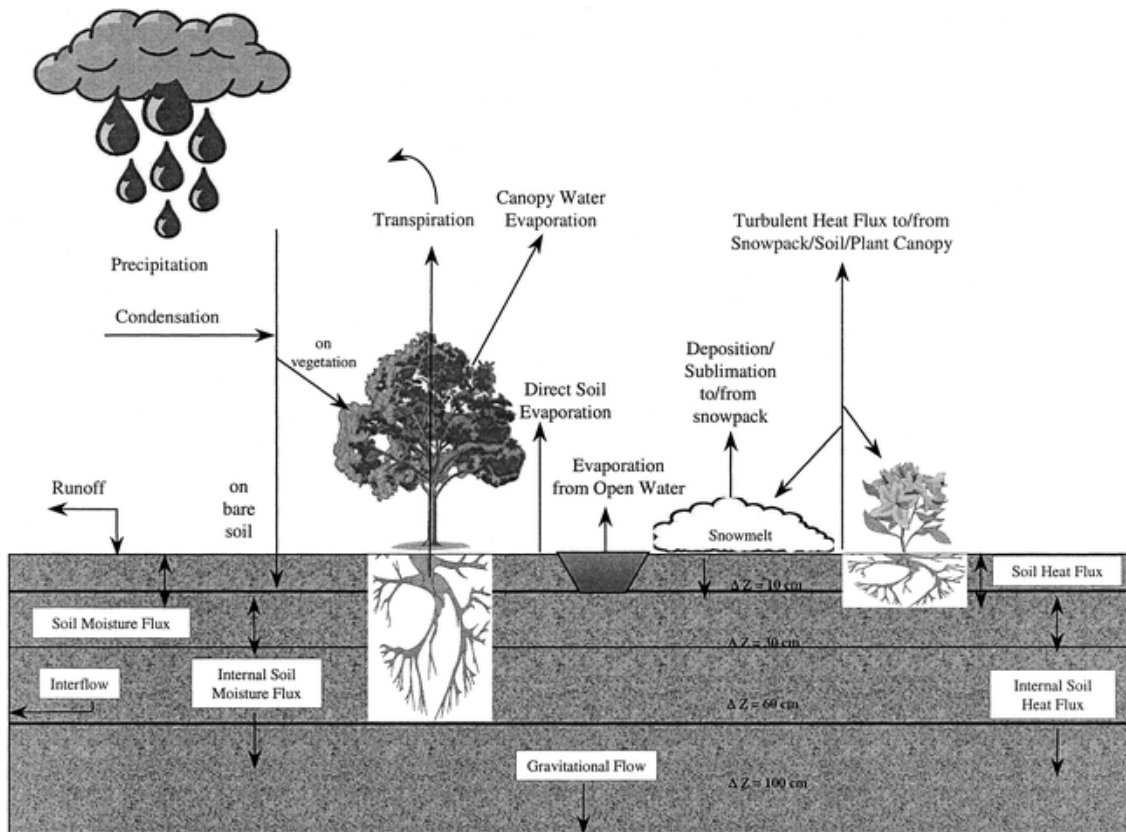


Figure 12 Schematic representation of the Noah LSM in coupled mode (e.g. WRF). The structure is similar to the Noah-MP LSM (Chen and Dudhia, 2001).

For this study the HRLDAS v4.1 is used. All parameterization options were set to the default option, with exception of the runoff scheme, for which different options were tested (chapter 5.1). The forcing variables needed to run the system are temperature, precipitation, windspeed, specific humidity, downwelling shortwave radiation, downwelling longwave radiation and surface pressure. Here all of these are either directly taken from the INCA dataset, or are calculated from the INCA data (downwelling longwave radiation from temperature, relative humidity and shortwave radiation using a parameterization scheme and specific humidity from relative humidity, see chapter 4.1), with the exception of surface pressure. The pressure data, as mentioned before, is computed from ERA5 reanalysis by projecting the mean sea level pressure onto the high-resolution surface height, using the barometric formula (chapter 4.1). The data to initialize the simulation were taken from ERA-Interim. To setup the model environment, additional input data, like terrain and land use parameters and soil texture type, is needed. These data are obtained from the Noah-LSM and originate from different sources, e.g. the soil

map from the Food and Agriculture Organization (FAO) of the United Nations (Dy and Fung, 2016; FAO, 1978) and vegetational parameters from satellite data (Chen and Dudhia, 2001). The initialization data and the land surface parameters need to have the same grid configurations as the forcing data. Thus, the surface information and ERA-Interim data were bilinearly remapped onto the 1 km x 1 km INCA grid. The HRLDAS simulation was conducted with forcing data from the 01.01.2004 to the 30.04.2019. Because model evaluations showed that it takes 8 to 10 months to reach quasi equilibrium soil moisture and temperature in the deep soil layers, with strong dependence on the soil texture type (Chen et al., 2007), the data of the first year (2004) is not used in the analysis to ensure coherent conditions.

3.5. WRF - Weather Research and Forecasting Model

WRF (Skamarock et al., 2008) is a mesoscale numerical weather prediction (NWP) system developed and maintained by the NCAR, the NOAA and others. It was first released in 2000 and has since become one of the most used NWP models (Powers et al., 2017). It is suitable across different climate research fields, such as applications in data assimilation and parameterized-physics research, downscaling simulations and idealized simulations (e.g. convection-permitting simulations). Similar to the HRLDAS, it relies on the Noah-MP LSM to prescribe the surface boundary conditions.

The data used in this study are obtained from a WRF-ARW (Advanced Research WRF) v3.8.1 simulation conducted by Klaus Goergen (Institute of Bio- and Geosciences, Research Centre Jülich, Jülich, Germany), which was featured in an investigation of convection permitting simulations by Truhetz and Goergen (2019). From here on, this simulation is denoted as WRF. The model configuration follows the Coordinated Regional Downscaling Experiments Flagship Pilot Studies (CORDEX-FPS) (Coppola et al., 2020) protocol for evaluation simulations, with ERA-Interim providing the initial and lateral boundary conditions. In a first nesting step the resolution of the reanalysis data is increased to 15 km grid spacing and 3 h time intervals over Europe. This region corresponds to the EURO-CORDEX (Jacob et al., 2014) domain. The second nesting step increases the resolution further to 3 km spatial and 1 h temporal, in the Alpine WRF domain, covering the greater Alpine region (Figure 13). The CORDEX-FPS initiative investigates present and future convective processes and

extreme events over Europe, using ensembles of high-resolution RCMs. This simulation uses the GRIMS (Global/Regional Integrated Model System) (Hong and Jang, 2018) shallow convection scheme, which has been shown to improve precipitation, especially in mountainous areas (Truhetz and Goergen, 2019). Precipitation and soil moisture data are available on the 3 km grid, with a temporal resolution of 1 hour for the period of 2004 to 2014. The soil dimension structure is similar to HRLDAS, because both models utilize related LSMs (Noah LSM and Noah-MP LSM), with four layers of 0.1, 0.3, 0.6 and 1.0 m soil thickness respectively.

Although conducting the model simulations on convection permitting scales improves the representation of precipitation, there are still substantial biases. WRF has been shown to produce more intense precipitation over smaller areas than observations, especially in lowlands (Truhetz and Goergen, 2019). This may impact the soil moisture of the model, as well as the SMPF analysis (Figure 14).

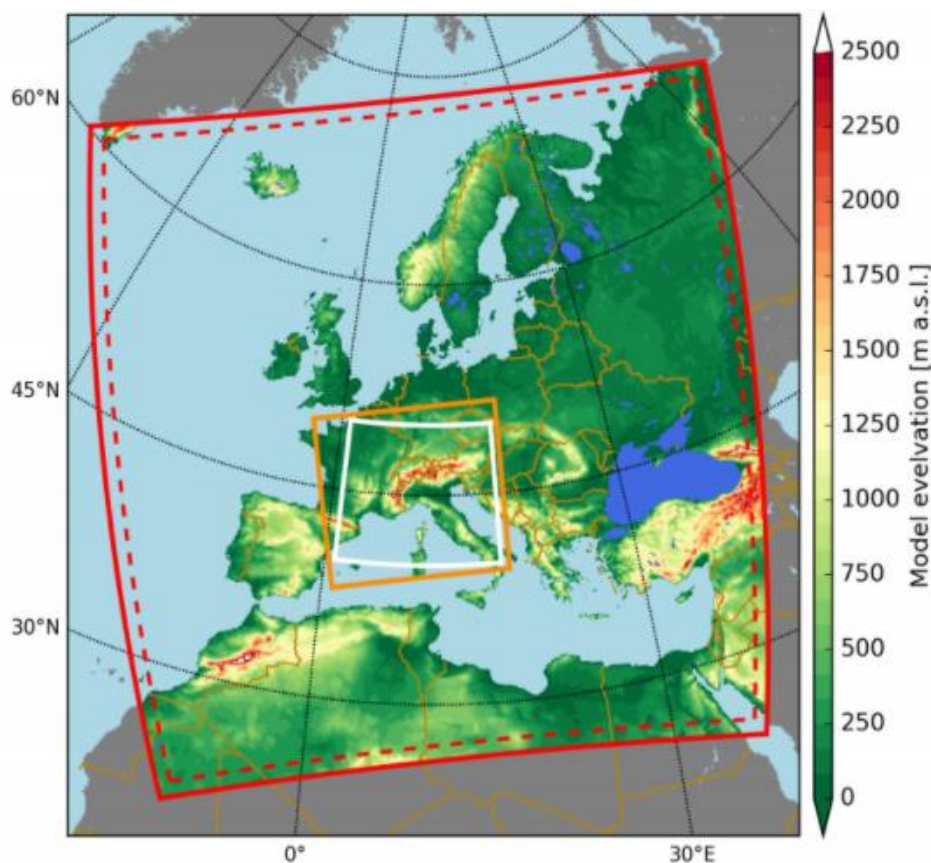


Figure 13 Orography for the 15 km pan-European WRF domain (red), the EURO-CORDEX domain (red dashed), the 3 km Alpine WRF domain (orange) and the CORDEX-FPS focus domain (white) (Truhetz and Goergen, 2019).

3.6. CCLM - COSMO Model in Climate Mode

The second RCM whose performance is evaluated in the form of the SMPF is the CCLM (Böhm et al., 2006). It was developed by the German Weather service (DWD) and COSMO. The coupled LSM is the multi-layer version of the TERRA soil model (TERRA-ML) (Doms et al., 2018). An important property of this LSM is that energy and hydrological fluxes are calculated based on the mean soil moisture of the active soil layer. The depth of this active soil layer can be chosen accordingly. To account for seasonal variability in these fluxes, the vegetational root depth changes depending on the season, mobilizing soil water of a deeper or shallower layer accordingly.

CCLM is also featured in the CORDEX-FPS and part of the convection-permitting model ensembles. The data used in this study are obtained from a CCLM v5.0 simulation, conducted by the Karlsruhe Institute of Technology (Coppola et al., 2020). From here on, this simulation is denoted as CCLM. Similar to WRF, CCLM is nested twice, with ERA-Interim providing the boundary conditions. The first nesting step although is performed over a 12.5 km grid (EURO-CORDEX domain). The second step is performed over the Alpine WRF domain with 3 km spatial resolution. The active soil layer depth is 3.82 m, meaning that the ET and surface energy fluxes depend on the soil moisture down to a large depth. Consequently, the annual cycle of active soil layer moisture is dampened due to the low fluctuations in the deep soil. The data is available on the 3 km grid, with a temporal resolution of 1 hour for precipitation and 6 hours for soil moisture for the period of 2000 to 2015. Soil moisture data is only available in the five top layers in cubic meter water per square meter area ($\text{m}^3 \text{m}^{-2}$). In contrast, the HRLDAS and WRF output soil moisture in cubic meter water per cubic meter soil (m^3m^{-3}). The thickness of the five layers are 0.01 m, 0.03 m, 0.06 m, 0.12 m and 0.24 m, amounting to 0.46 m. Therefore, the data of only a small part of the active soil layer depth (3.82 m, soil layer 1 to 7) is available. It further is the upper section of the soil matrix, that shows the strongest variations over time. The soil moisture data of the CCLM in this thesis thus have to be treated with caution.

Similar to WRF, CCLM has significant precipitation biases. The average afternoon precipitation intensity is twice as high as for observational data. This is compensated by smaller precipitated areas (Piazza et al., 2019). As for the WRF biases, this may impact

the representation of the soil moisture by this model, as well as the results of the SMPF analysis (Figure 14).

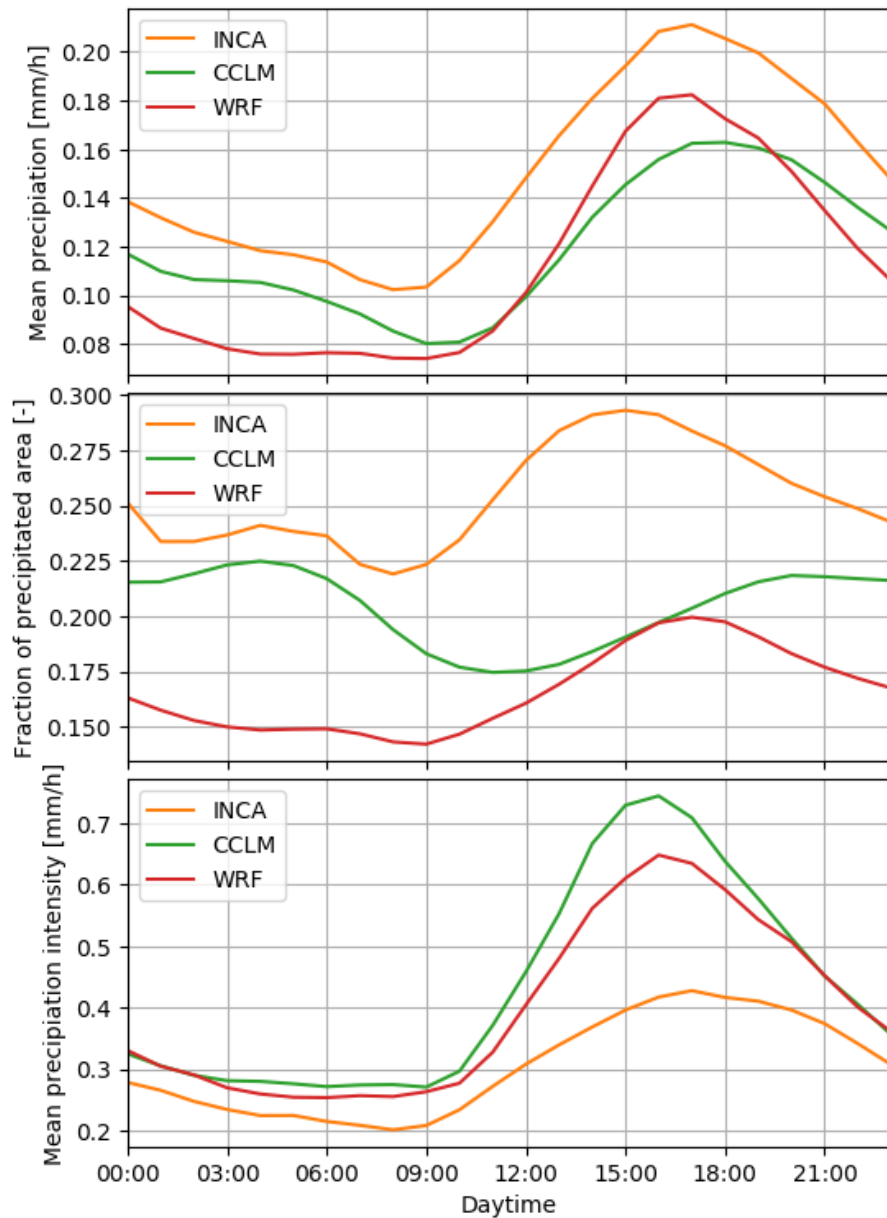


Figure 14 Hourly mean precipitation (top), fraction of precipitated areas (middle) and precipitation intensity (bottom) of the INCA (orange), CCLM (green) and WRF (red) data within the study region, computed for the months of May to September from the period of 2005 to 2014. Only areas of orographic height lower than 1000 m are used (based on Piazza et al. (2019) and Truhetz and Goergen (2019)).

4. Methodology and Statistics

In this chapter, the method to analyze the SMPF is explained in detail. The SMPF in Austria is quantified using three metrics based on the previously mentioned studies of Taylor et al. (2012), Guillod et al. (2015) and Moon et al. (2019). Taylor et al. (2012) demonstrated the feedback diagnostic with one resulting metric, which Guillod et al. (2015) adopted and expanded to three metrics, to present a clearer picture of the soil moisture precipitation coupling mechanisms. This method was chosen because it can be easily downscaled on a regional level and has the potential to reduce interfering effects, like frontal precipitation and orographic effects (see chapter 2.3). Furthermore, the preprocessing of the forcing data for the HRLDAS, the simulation data postprocessing and all further statistical analyses used in the thesis will also be described.

4.1. HRLDAS forcing data preprocessing

As previously mentioned, some of the data used to drive the HRLDAS had to be processed. In this section the parameterization scheme applied to calculate the long-wave radiation is explained in detail. Further, the calculation of specific humidity from relative humidity and surface pressure from mean sea level pressure are described.

Long-wave radiation parameterization

The HRLDAS needs incoming short and longwave radiation forcing data. However, the INCA observations only contain short-wave radiation. Longwave radiation has to be calculated utilizing other variables via a parameterization scheme. In this study the scheme of Gabathuler et al. (2001) is employed. It is a function of air temperature, relative humidity and global radiation (short-wave). This scheme was calibrated on observational data, including high-mountain observations. Thus, it is especially suited for mountainous regions, like the Alps. Besides the atmospheric variables mentioned, the function includes the Stefan-Boltzmann constant σ ($5.67 \cdot 10^{-8} \text{ W m}^{-2} \text{ K}^{-4}$) and the dimensionless clearness index k_0 . This index describes the atmospheric transmissivity to short-wave radiation. It is calculated using formula (4), dividing the amount of measured global radiation (SW) from INCA [W m^{-2}], by the theoretically possible irradiation for any given date and time

(I_0) [W h m^{-2}] (SW is multiplied with 1 hour to convert it from the solar power at a certain point in time to the approximate energy received within 1 h [W h m^{-2}]).

$$k_0 = \frac{SW}{I_0} \quad (4)$$

I_0 for one hour can in turn be calculated using the normal solar irradiance at the top of the atmosphere $S_{0,n}$ and the angle of the sun at the given date and time. The angle is described by the latitude φ , the declination δ and the hour angles ω_1 and ω_2 , which are the hour angles of the INCA time minus and plus half an hour respectively (Kalogirou, 2014).

$$I_0 = \frac{12}{\pi} S_{0,n} \left(\frac{\pi}{180^\circ} (\omega_2 - \omega_1) \sin(\varphi) \sin(\delta) + \cos(\varphi) \cos(\delta) (\sin(\omega_2) - \sin(\omega_1)) \right) \quad (5)$$

The declination and $S_{0,n}$ for any given day can be assessed using equation (6) and (7) respectively, where S_0 is the solar constant (1361 Wm^{-2}) and N is the day of the year.

$$\delta = -23.45^\circ \frac{\pi}{180^\circ} \sin \left(\frac{\pi}{180^\circ} \frac{360^\circ}{365} (N + 284) \right) \quad (6)$$

$$S_{0,n} = S_0 \left(1 + 0.33 \cos \left(\frac{\pi}{180^\circ} N \frac{360^\circ}{365} \right) \right) \quad (7)$$

Using all these formulas, the clearness index can be put into the long-wave radiation (LW) equation (8). Gabathuler et al. (2001) derive it from the Stefan-Boltzmann Law, estimating the emission temperature of the atmosphere using a function of the clearness index and surface air temperature (T_a), in addition to a linear regression model of LW and relative humidity RH obtained from observational data:

$$LW = (-21 K_0 + T_a)^4 \sigma + 0.84 RH - 57 \quad (8)$$

Conversion of relative to specific humidity

Besides radiation, HRLDAS also needs a humidity variable as part of the forcing data. The INCA dataset contains relative humidity observations, but specific humidity is needed. Specific humidity (QH) is defined as the ratio of water vapor mass and moist air mass (9) (which is the sum of vapor mass plus dry air mass), whilst relative humidity (RH) is defined as the ratio of water vapor pressure to saturation vapor pressure (10) (or mass of water vapor divided by maximal possible vapor content at a specific temperature). To convert relative humidity to specific humidity, the air pressure p , molecular mass ratio of water (M_v) to dry air (M_d) ($M_v/M_d = 0.622$), vapor pressure e and the saturation vapor pressure e_s are required.

$$QH = \frac{m_v}{m_v + m_d} = \frac{M_v}{M_d} \frac{e}{\left(p - \left(1 - \frac{M_v}{M_d}\right) e\right)} \quad (9)$$

$$RH = \frac{e}{e_s} 100 \% \quad (10)$$

By rearranging the relative humidity equation (10), the vapor pressure can be derived, if the saturation vapor pressure for the given temperature is known. Using the Clausius-Clapeyron relation, the saturation vapor pressure can be calculated. Formula (11) shows the equation derived from the Clausius-Clapeyron relation, as well as an approximation for usual air temperatures. Here e_{s0} is the saturation vapor pressure at 273.15 K (611.2 Pa), L_v is the specific latent evaporation heat of water at the given temperature (T), R_v is the specific gas constant of water vapor ($461.5 \text{ J kg}^{-1} \text{ K}^{-1}$) and T_0 is the reference temperature of 273.15 K.

$$e_s(T) = e_{s0} \exp\left(\frac{L_v(T)}{R_v} \left(\frac{1}{T_0} - \frac{1}{T}\right)\right) \approx 611.2 \exp\left(17.67 \frac{T - T_0}{T - 29.65}\right) \quad (11)$$

The temperature and the surface pressure values are taken from the HRLDAS forcing data, originating from the INCA dataset and ERA-Interim reanalysis respectively. Thus, the specific humidity could be calculated using the equations above (Malberg, 2007).

Conversion of mean sea level to surface pressure

An important meteorological parameter not included in the INCA dataset is the atmospheric pressure. The HRLDAS needs prescribed surface pressure as part of the forcing data. From the ERA5 data the mean sea level pressure can be obtained. This data has to be remapped onto the high-resolution HRLDAS grid, which is done bilinearly, and projected onto the surface height. Atmospheric pressure decreases exponentially with height. This relationship is described by the barometric formula for an isothermal atmosphere:

$$p_z = p_o \exp\left(\frac{-g * z}{R_A * \bar{T}_v}\right) \quad (12)$$

where p_z is the pressure at the height z , p_o is the pressure at mean sea level, g is the gravitational acceleration (9.81 m s^{-2}), R_A is the specific gas constant of air ($287.1 \text{ J kg}^{-1} \text{ K}^{-1}$) and \bar{T}_v is the mean virtual temperature of the air parcel (Malberg, 2007). The mean sea level pressure is taken from the ERA5 data and the surface height is taken from the orographic field of INCA. The mean virtual temperature was approximated with the INCA near surface temperature, which is sufficient for this study.

4.2. Data postprocessing

Before the start of the analysis, all simulation data have to be remapped onto the same mesh grid and have the same temporal resolution and the same units. First, the 3 km x 3 km WRF grid is chosen. The reasoning is that the WRF and CCLM data already are on the desired grid and that the 3 km grid is more likely to capture the processes of interest than the 1 km grid of INCA. That is because the processes involved in the SMPF (e.g. ET, convective plumes) have larger horizontal scales than 1 km (Atkinson and Wu Zhang, 1996) and larger scales also increase the computing speed. The 3 km grid thus may provide a clearer picture. Therefore, INCA precipitation and HRLDAS soil moisture data is bilinearly remapped onto the 3 km grid. Moreover, the temporal resolution of soil moisture and precipitation data varies between the models. To be as consistent as possible, the 6-hour resolution of CCLM for soil moisture is chosen for the analysis, meaning that only every sixth value of the HRLDAS and WRF data was

utilized. Furthermore, the INCA 15 minutes precipitation is converted to hourly precipitation, to match the other models. Lastly, the soil moisture data had to be adjusted to the same unit.

The precipitation data of all models had to be converted to mm h^{-1} . INCA and CCLM data have to be multiplied by 3600 to convert their fluxes per second (mm s^{-1}) to hourly fluxes. In WRF accumulated convective and non-convective precipitation is stored. Because over long simulation periods a lot of precipitation can be accumulated, a bucket system is also included, where if a certain limit is reached the precipitation variables are set to zero and the bucket count is raised by one. Thus, the flux within a time interval can be calculated by computing the difference of precipitation sum (convective + non-convective + bucket-limit * bucket-counts) of two timeframes. If the timeframes are separated by an hour, the resulting flux equals mm h^{-1} . Further, to convert CCLM soil moisture to $\text{m}^3 \text{m}^{-3}$, the layer thickness has to be accounted for. Dividing the soil moisture ($\text{m}^3 \text{m}^{-2}$) by the individual thickness results in the desired values in cubic meters water per cubic meter of soil ($\text{m}^3 \text{m}^{-3}$).

For the SMPF analysis of the HRLDAS and WRF data the top soil layer is investigated. Consequently, the soil moisture of the layer from 0 to 0.1 m of HRLDAS and WRF are used. As already mentioned, the CCLM computes land surface fluxes based on the moisture of the active soil layer, which is not available. Therefore, the soil moisture of the entire available soil matrix (soil layer 1 to 5) is evaluated and used for the analysis.

Table 2 List of soil moisture and precipitation resolutions and units of the simulation data and of the target for the SMPF analysis. WRF stores precipitation data as accumulated amounts.

	Soil moisture			Precipitation		
	Resolution		Unit	Resolution		Unit
	Spatial	Temp.		Spatial	Temp.	
Target	3 km x 3 km	6 h	$\text{m}^3 \text{m}^{-3}$	3 km x 3 km	1 h	mm h^{-1}
HRLDAS/ INCA	1 km x 1 km	1 h	$\text{m}^3 \text{m}^{-3}$	1 km x 1 km	15 min	mm s^{-1}
CCLM	3 km x 3 km	6 h	$\text{m}^3 \text{m}^{-2}$	3 km x 3 km	1 h	mm s^{-1}
WRF	3 km x 3 km	1 h	$\text{m}^3 \text{m}^{-3}$	3 km x 3 km	1 h	mm

4.3. Statistics

Statistical parameters are calculated to better assess the results of this thesis. Besides the arithmetic mean and the standard deviation, the coefficient of correlation is used to compare soil moisture time series to observational data and significance tests are used to evaluate the event distribution of feedback parameters.

Arithmetic mean and standard deviation

The arithmetic mean is a commonly used measure of central tendency and is calculated by the sum of all values of a series divided by the number of values:

$$\bar{x} = \frac{1}{n} \sum_{i=0}^n x_i \quad (13)$$

where x_i are the datapoints of the series and n the number of datapoints.

The standard deviation is also a commonly used statistical metric for the measure of dispersion of a data series. It is calculated by taking the square root of the sum of the squared differences of all data points and the mean divided by the number of data in the series:

$$\sigma = \sqrt{\frac{1}{n} \sum_{i=0}^n (x_i - \bar{x})^2} \quad (14)$$

where x_i are the datapoints, \bar{x} is the arithmetic mean and n the number of values within the data series.

Correlation coefficient

The correlation coefficient r , after Bravais and Pearson, is a statistical measure for how well two datasets (x_1, x_2, \dots, x_n) and (y_1, y_2, \dots, y_n) fit a linear approximation. It has a value

between -1 (perfectly negatively correlated) and 1 (perfectly positively correlated). If the value is close to 0, the datasets do not correlate. The coefficient is calculated with the following equation:

$$r_{x,y} = \frac{\sum_{i=0}^n (x_i - \bar{x})(y_i - \bar{y})}{\sqrt{\sum_{i=0}^n (x_i - \bar{x})^2} \sqrt{\sum_{i=0}^n (y_i - \bar{y})^2}} \quad (15)$$

where x_i, y_i are the datapoints and \bar{x}, \bar{y} are the means of the two series (Weigand, 2019).

Significance test and p-value

Statistical significance tests are used to test the reliability of the null hypothesis. In this thesis the Welch's t-test is used to evaluate significant differences of the precipitation event characteristics compared to the control events. This significance test examines the differences of the population averages and requires normal distributed data but does not assume equal variances of the two populations. The t-value is calculated using equation (16), from which the p-value can be derived:

$$t = \frac{\bar{x}_A - \bar{x}_B}{\sqrt{\frac{\sigma_A^2}{n_A} - \frac{\sigma_B^2}{n_B}}} \quad (16)$$

Here \bar{x}_A and \bar{x}_B are the averages, σ_A^2 and σ_B^2 the variances and n_A and n_B the sizes of the two populations A and B . The p-value provides information about the statistical significance. If the p-value is below a chosen limit (here 0.05), the null hypothesis has to be rejected or in other words, the sample distribution differs significantly from the reference distribution (Weigand, 2019).

4.4. Soil moisture precipitation feedback diagnostics

The soil moisture-precipitation coupling influence convective precipitation events, which happen most dominantly in the warmer seasons. For that reason, the analysis is limited to the months of May to September. To reduce orographic influences, the mountainous western part of Austria (Tyrol and Vorarlberg) is excluded from the analysis. Therefore, the analysis region is constrained to central and eastern Austria. The resulting domain is divided into four equally sized subregions. For each of the regions the SMPF metrics are calculated separately to evaluate potential geographic differences. The location of these subregions roughly corresponds to Austrian federal states and are subsequently named after them: the Carinthian (southwest), Upper Austrian (northwest), Styrian (southeast) and Lower Austrian/Viennese (northeast) region (Figure 11).

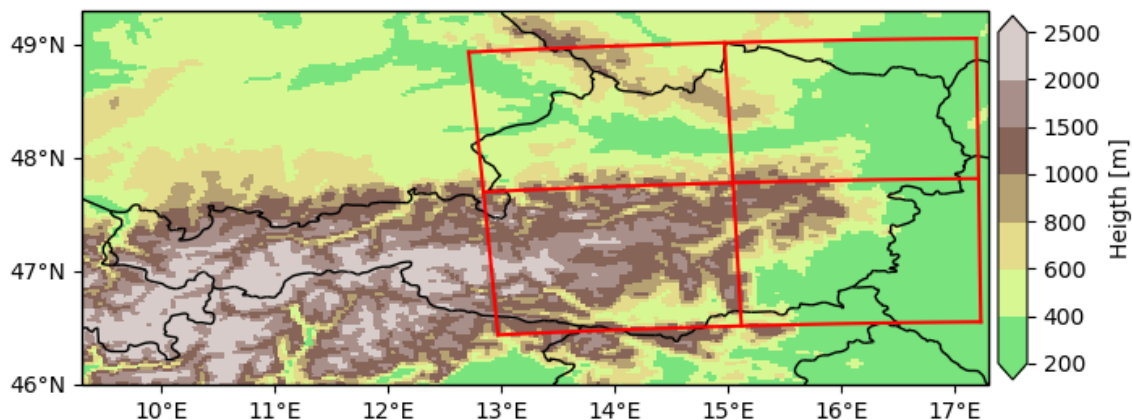


Figure 15 Orographic height in meters at 3 km resolution and borders of the study domain (324 km x 276 km) with the four subregions (red lines). The mountainous western part of Austria is excluded to reduce the influence of orographic effects on the analysis.

The next step is to define the precipitation event domain. Here a square of 45 km side length, equal to 15 grid cells, is chosen. In the reference studies these event domains were, with $1.25^\circ \times 1.25^\circ$ (at 50° latitude roughly 90 km) twice as larger. There are several reasons why a much smaller domain is defined. First, the reference studies investigate the SMPF globally. This study in contrast tries to evaluate regional effect in an area with complex terrain. Secondly, tests showed that 45 km is the largest domain size with an

exactable number of events being detected (Appendix A, Figure A.1). The issue with a small event area is that the driving mechanisms for the SMPF could act on larger scales, thus not capturing the effects of interest. A precipitation event is registered if a grid cell displays at least 4 mm accumulated afternoon precipitation (12:00 to 21:00 UTC). Afternoon precipitation is chosen, because the sensitivity of convection to the land surface conditions are expected to be highest at this time. This grid cell is the center of an event domain. If any grid cell of the event domain shows higher accumulated afternoon precipitation than the central cell or more than 1 mm of preceding accumulated morning precipitation (6:00 to 12:00 UTC), the event is declassified. This is done to reduce the strong impact of synoptic weather effects in the region, like frontal rainfall. To further reduce other interferences, the event domains are limited to regions of heights lower than 1000 m (orographic effects) and areas without large water bodies (e.g. Lake Neusiedl). If an event is registered, the central grid cell with the maxima in afternoon precipitation is denoted as L_{max} and the event domain as $Levt$. Similarly, the grid cell or cells with minimal precipitation in $Levt$ are denoted as L_{min} . Figure 16 depicts an exemplary classification of events as described above.

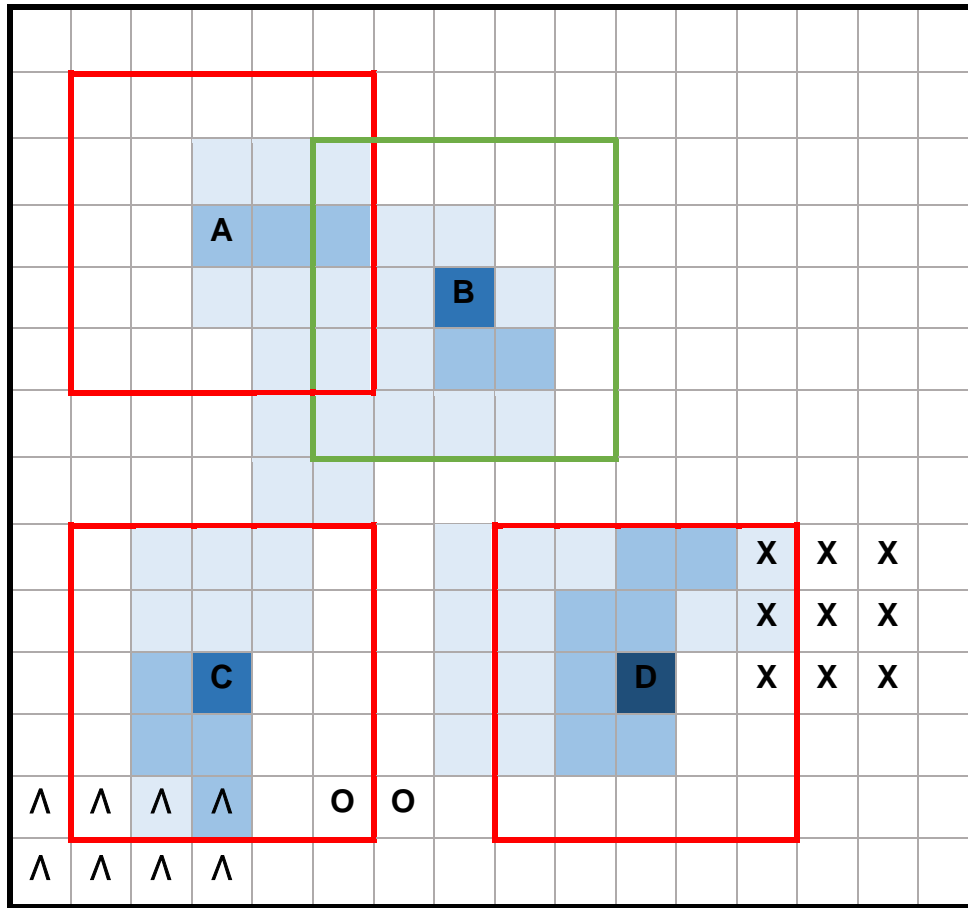


Figure 16 Exemplary classification of precipitation events in the SMPF analysis. Here 5 x 5 grid cell event areas are chosen for the illustration. The green square depicts a classified event, while red squares are events that have not been included. Blue shading indicates accumulated afternoon precipitation, with saturation depicting increased amounts. “X” indicates accumulated morning precipitation exceeding 1 mm, “^” indicates regions of orographic height exceeding 1000 m and “O” depicts water bodies. The capital letters indicate the location of maximal precipitation within the event region, which are chosen to be the central grid point. Event “A” is not included because it overlaps with event “B”, which has a higher maximal precipitation value. Event “C” is declassified because of mountains and water bodies within its area and event “D” because at least one grid cell displays an exceedance of morning precipitation.

To account for regional differences in soil moisture, the anomaly (S') is calculated by subtracting a multi-year mean 31-day moving average from the absolute soil moisture values. The moving average is calculated for each day by averaging daily mean data from the 15 preceding days, the day of interest and the 15 following days. If the data for the preceding or following day is not available (at the start and the end of the study time frame), the size of the moving average is reduced (minimal size to calculate the mean is 16 days at 01.01.2005 and 31.12.2014). These moving means are then averaged for every calendar day over the study time frame, resulting in the 365 mean 31-day moving averages. On leap year's days, the average of the 28.02. is subtracted. For every event the morning (06:00 to 12:00 UTC) soil moisture anomalies are analyzed.

The SMPF is evaluated by three parameters, representing the spatial (Y^s), the temporal (Y^t) and heterogeneity component (Y^h) of the feedback mechanism. Y^s is defined as the difference of S' at L_{max} and S' at L_{min} or the mean of $S'_{L_{min}}$ if there are multiple L_{min} locations, comparing the soil moisture differences within the event domain (17). Y^t is defined as S' at L_{max} , comparing the soil moisture at the location of maximal precipitation in different points in time (18). Lastly, Y^h is defined as the spatial standard deviation of all soil moisture values within an event domain, giving information about the distribution of soil moisture (19).

$$Y^s = S'_{L_{max}} - S'_{L_{min}} \quad (17)$$

$$Y^t = S'_{L_{max}} \quad (18)$$

$$Y^h = \sigma^{sp}(S'_{Levt}) \quad (19)$$

The parameters are calculated for all events and denoted Y_e . For every precipitation event, control events are classified. Control events have the same domain as precipitation events but are limited to days of the same month in different years. If an event is registered in the control event domain, the control event is declassified. For all control events the three parameters are also evaluated. These results are denoted as Y_c . All events and control events are then allocated to the subregions of the study domain.

Following the method by Taylor et al., Guillod et al. and Moon et al., all events and control events are pooled together, and bootstrapping is performed. 1000 bootstrap samples are taken per subregion, with the same size as the number of events found. From

the mean of these samples, the mean of all the control events is subtracted. This serves as the base of the climatologic distribution of the feedback parameters. By comparing the mean of all events, likewise subtracted by the mean of the control events (20), with this distribution, the feedback strength can be assessed.

$$\delta_e = \text{mean}(Y_e) - \text{mean}(Y_c) \quad (20)$$

In this study a more detailed look is taken into the parameter distribution of events and control events for each subregion. They are compared to each other and significant preferences of precipitation for the spatial, temporal and heterogeneity metric are investigated. Furthermore, the locations of the precipitation events are analyzed to study possible subregional influences and interferences on the SMPF diagnostics.

5. Results and Discussion

The findings of this thesis are split into three parts. First the results of the evaluation of the HRLDAS soil moisture data, using in-situ measurements from the WegenerNet, are presented in section 5.1. The soil moisture of the two RCMs is also evaluated and any deficits that may influence the SMPF analysis are discussed. The second part (chapter 5.2) is concerned with the land surface conditions in Austria, derived from HRLDAS output data, and the analysis of their implications on land surface-atmospheric interaction. The results of the main analysis of the SMPF and the comparison of the models to the observations are presented and discussed in section 5.3.

5.1. HRLDAS soil moisture evaluation

Before performing the main HRLDAS simulation the influence of the soil texture type (ISLTYP) and of the runoff parameterization scheme were analyzed. The results of these tests inform the decision, which soil type data and which runoff option should be employed for the main simulation.

Different soil textures have different physical properties, e.g. water holding capacity, wilting point and permeability. Thus, they have a major influence on the absolute soil moisture values. To evaluate if the soil texture type classification could have a significant impact on the SMPF analysis, simulations with a simple model setup were performed. From the HRLDAS initiation and forcing data one 1 km x 1 km grid point was chosen. This grid point was chosen to be near the WegenerNet station 85. The HRLDAS was subsequently run multiple times for this single grid point with forcing data from 2013 to 2015. For each model run the soil texture type (ISLTYP) was changed. Eight soil types were tested (sandy loam, silt loam, silt, loam, sandy clay loam, silty clay loam, clay loam, sandy clay, silty clay and clay) and their resulting soil moisture output compared to each other and to the soil moisture data from the WegenerNet station. Moreover, by subtracting the multi-year mean 31-day moving average (2014 to 2015) from the soil moisture, the soil moisture anomaly was computed. Three soil texture types have been plotted to give an impression of the influence on the soil moisture data generated by HRLDAS for the period of 2014 to 2015 (data of 2013 is not used to ensure quasi equilibrium conditions of the LSM). Soil type 3 sandy loam, as an example for a soil with low water capacity,

6 loam, which is the classification for the entire WegenerNet Feldbach region taken from the WRF input data, and 12 clay, as an example for soil with high water holding capacity. It can be seen that clay very closely resembles the observational data, while sandy loam shows even lower values than the default type of loam (Figure 17). Despite this, the correlation of all three are almost equivalent with values between 0.64 and 0.66. This can also be seen in the anomaly plots, where the three soil types have very similar values, relatively close to the observations. The agreement with the observational data is highest in the summer months and lowest in winter. Consequently, it can be concluded that the soil texture type has only a small impact on soil moisture anomaly. The SMPF can thus be evaluated with reasonable confidence. The low spatial variability of the model data although may affect the spatial feedback metric.

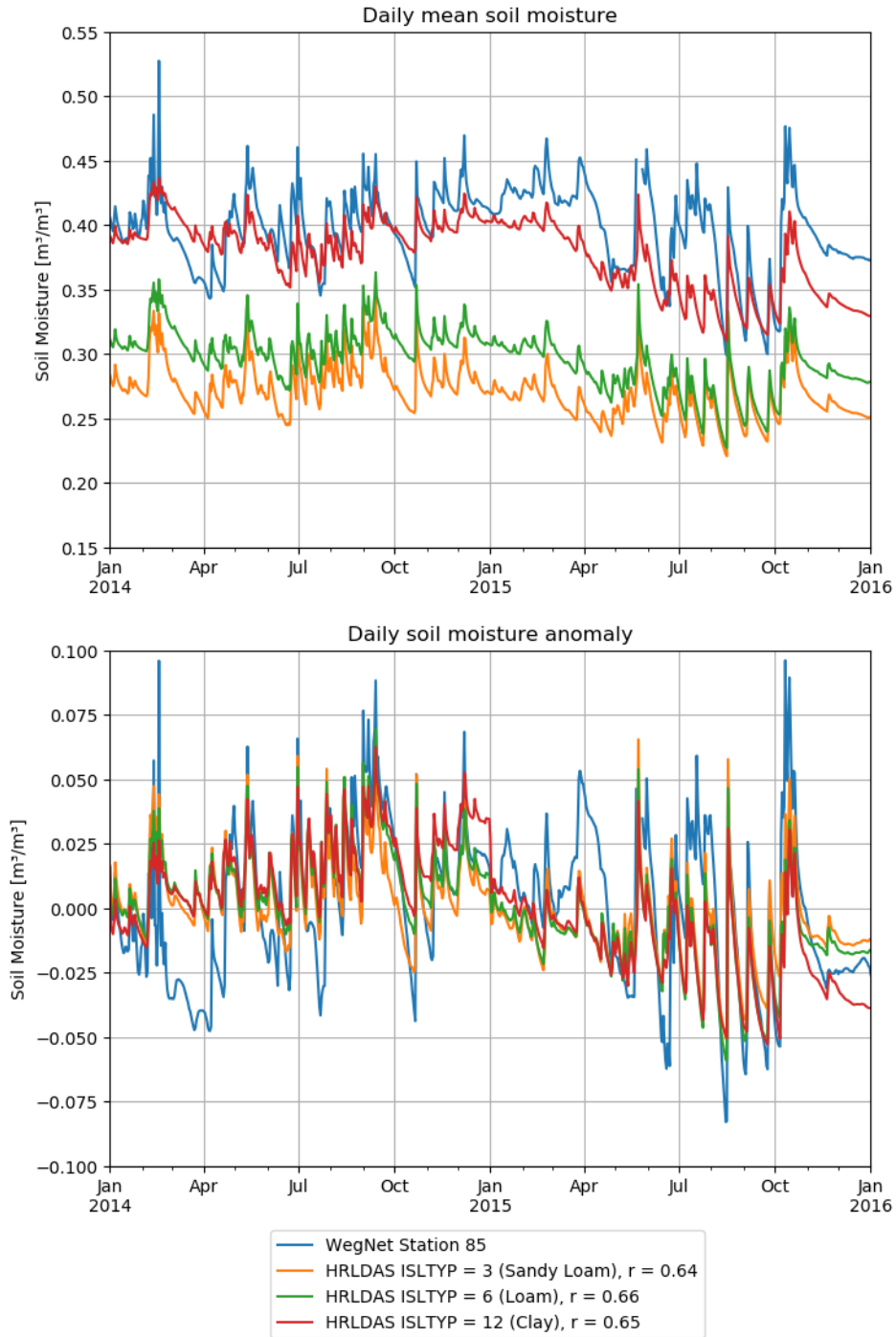


Figure 17 Daily mean absolute soil moisture (top) and anomalies (bottom) for the period of 2014 to 2015 of WegenerNet station number 85 (blue) and HRLDAS in 0.1 to 0.4 m depth (second soil layer) run with identical model conditions with three different soil types: 3 (sandy loam, orange), 6 (loam, blue) and 12 (clay, red). The correlation coefficient (r) is evaluated for the daily mean soil moisture data of the three model runs and the observations for the plotted period.

To analyze the different runoff parameterization schemes of HRLDAS, a similar approach to the previously presented analysis of the soil type influence was chosen. The same model setup, of one 1 km x 1 km grid point from the model initiation and forcing data from 2013 to 2015 close to the WegenerNet station number 85, is used to evaluate the impact of four different runoff schemes (1: topmodel with groundwater, 2: topmodel with equilibrium water table, 3: original surface and subsurface runoff (default option), 4: Biosphere-Atmosphere Transfer Scheme (BATS) surface and subsurface runoff). Because the soil texture type also influences the runoff, again eight soil types were tested for each runoff option per model run. The soil moisture output of three soil types (3 sandy loam, 6 loam and 12 clay) was again compared to each other and to the observations from the WegenerNet station for the period of 2014 to 2015 (data of 2013 is not used to ensure quasi equilibrium conditions of the LSM). Again, also the soil moisture anomaly is computed and plotted (Figure 18).

It can be seen, that for the two soil texture types with lower water holding capacities (sandy loam and loam) all three tested runoff schemes lead to a lower soil water amount compared to the default option. Soil type 12 (clay) an increase in soil moisture for runoff scheme 1 and 2 in some months and a decrease for option 4, compared to the default runoff option 3. In summer all runoff options show similar values for this soil type. Evaluating the results of the soil moisture anomalies, neither the soil type nor the runoff parameterization scheme greatly impacts the model output. The agreement with the observational data is again highest in summer and lowest in winter. No option performed significantly better than the others. Thus, the default runoff option was chosen for the main simulation run.

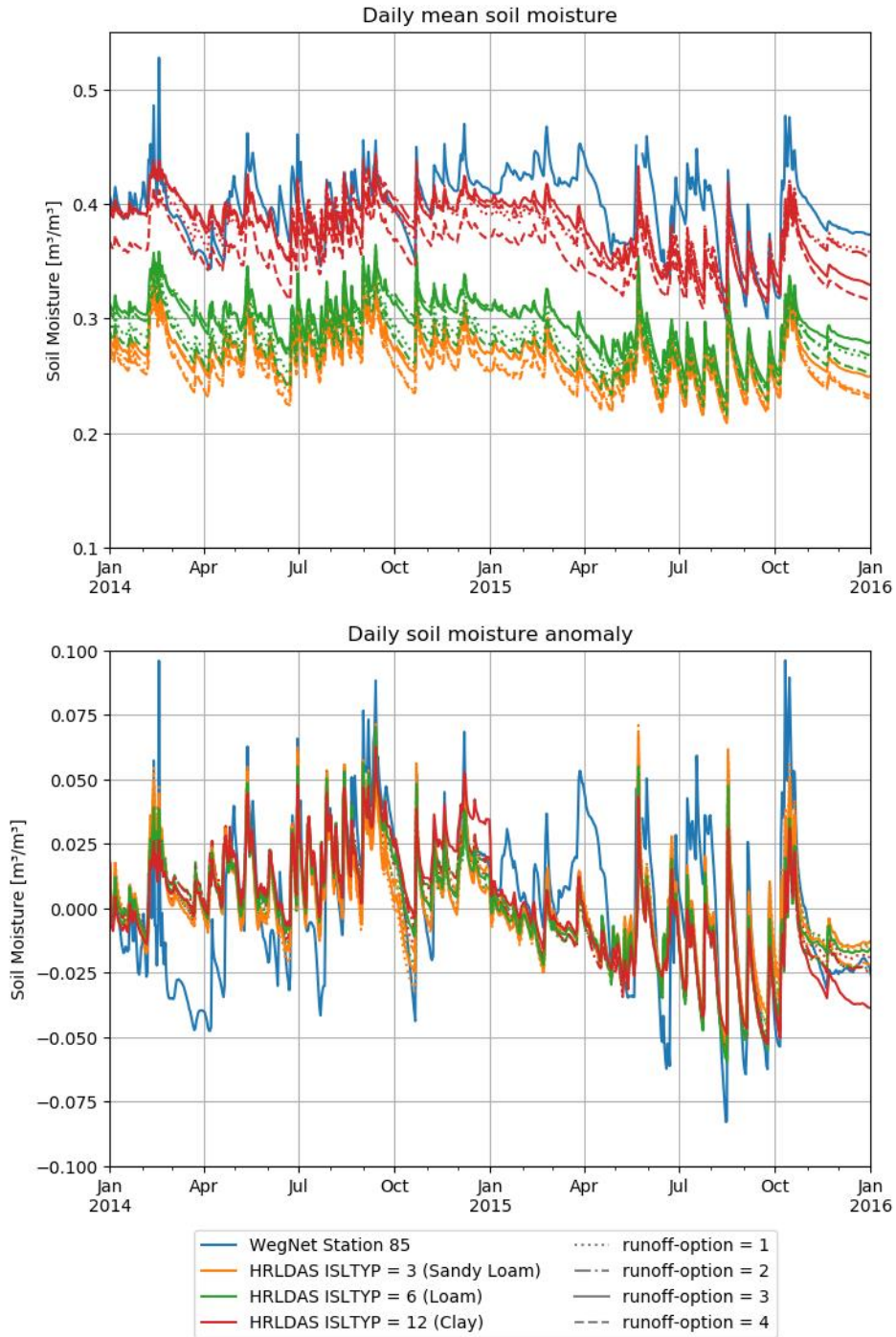


Figure 18 Daily mean absolute soil moisture (top) and anomalies (bottom) for the period of 2014 to 2015 of WegenerNet station number 85 (blue) and HRLDAS in 0.1 to 0.4 m depth (second soil layer) run with identical model conditions with four runoff parametrization schemes (1, dotted; 2, dotdashed; 3, soil; 4, dashed) for three different soil types: 3 (sandy loam, orange), 6 (loam, blue) and 12 (clay, red).

The main HRLDAS simulation is run from 01.01.2004 to 30.04.2019. In Figure 19 an exemplary daily mean soil moisture field of the upper most soil layer for the 21.06.2009 is shown. This date was chosen, because it preceded a major 3-day precipitation event in Austria, caused by a stationary cut-off low over Italy (Haiden, 2009). It can be seen that the soil moisture values range from 0.2 to 0.4 $\text{m}^3 \text{m}^{-3}$ with little spatial variability. Lowest moisture in Austria can be found in the eastern Alpine foreland. Further to southeast (Hungary, Slovenia and Croatia) soil moisture reaches values lower than 0.15 $\text{m}^3 \text{m}^{-3}$, indicating the semi-arid Mediterranean climate conditions. The east-west soil moisture gradient illustrates the increasing continental climate to the east. Further, sharp edges in the field can be observed. These are results of the different soil types properties.

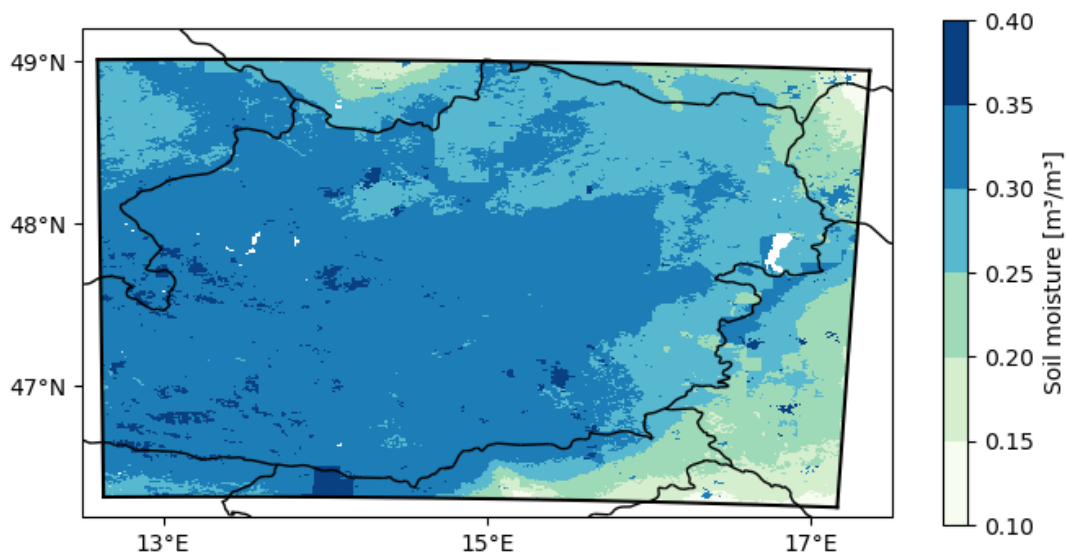


Figure 19 Exemplary soil moisture 1 km x 1 km field output in 0 to 0.1 m depth from HRLDAS. Daily averaged soil moisture for the 21.06.2009, one day before a major three-day precipitation event. Artificial patterns arise from the soil types, which have different physical properties.

In Figure 20 the Noah-LSM soil types of WRF, which are used to initiate the HRLDAS model, are shown. Due to their coarse resolution, regional soil type differences from e.g. rivers, mountains and valleys are not represented. This may be a reason for the low spatial variability in the soil moisture field. The most common soil type in Austria is loam, which has a saturation soil moisture of 0.439 $\text{m}^3 \text{m}^{-3}$ and a wilting point of 0.066 $\text{m}^3 \text{m}^{-3}$

(Dy and Fung, 2016), meaning that the absolute soil moisture in these regions is capped at this value.

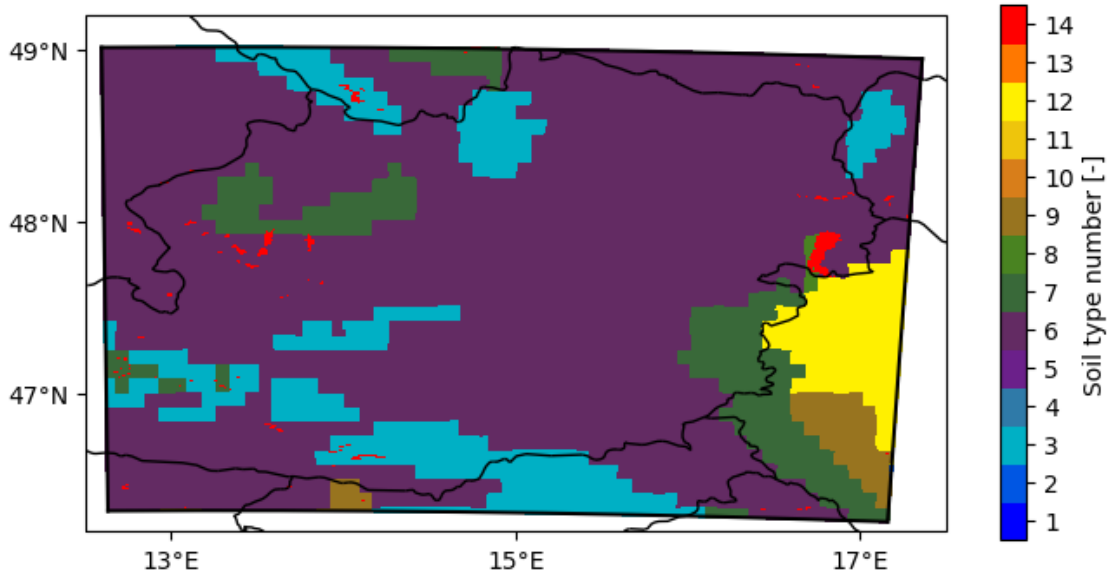


Figure 20 WRF soil types used in the HRLDAS model, in the study domain. Soil type numbers refer to: 1 sand, 2 loamy sand, 3 sandy loam, 4 silt loam, 5 silt, 6 loam, 7 sandy clay loam, 8 sandy clay, 9 clay loam, 10 sandy clay, 11 silt clay, 12 clay, 13 organic material, 14 water (Dy and Fung, 2016).

These strong dependences on the soil type may be the source of biases within the absolute soil moisture field. Concerning the SMPF analysis the soil moisture anomaly is the key metric for the soil water content. When subtracting the multi-year mean 31-day moving average (2005 to 2014) from the soil moisture field in Figure 19 the soil moisture anomaly field is derived (Figure 21). On the bases of these fields the SMPF metrics are calculated. By looking at the anomalies instead of the absolute values, the influence the soil types might have is greatly diminished. This can be seen in the absence of sharp edges in the moisture anomaly field in Figure 21. The anomalies for the 21.09.2009 range from -0.05 to $0.05 \text{ m}^3\text{m}^{-3}$ in the study area, showing little regional variability as well. This may already be an indication for the absence of a negative spatial soil moisture-precipitation coupling, which had been shown to arise only in strong heterogenic soil moisture conditions (Hohenegger and Stevens, 2018).

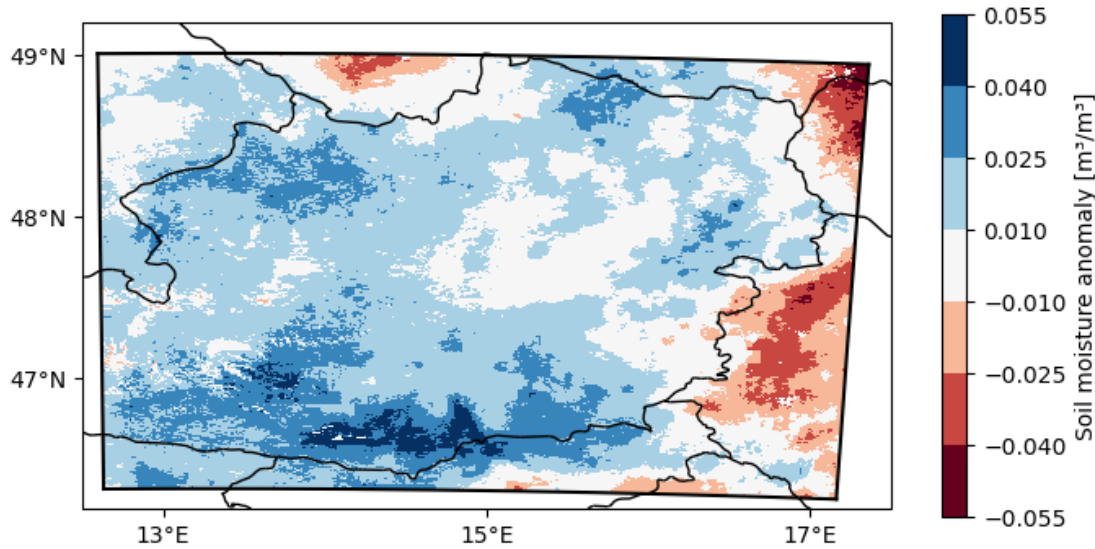


Figure 21 Daily average soil moisture anomaly 1 km x 1 km field in 0 to 0.1 m depth for the 21.06.2009. The anomaly was calculated with the method mentioned in chapter 4.4.

When comparing the soil moisture output, from the soil layers representing 0.2 m depth of the HRLDAS, as well as the output of the two RCMs (HRLDAS and WRF layer 2, CCLM layer 3), with observational data from the WegenerNet, significant differences can be seen (Figure 23). For this purpose, the soil moisture of the three models at the 12 measurement locations of the WegenerNet, that record soil parameters, are determined. The average and standard deviation are computed and plotted from 2013 to 2016. First, the HRLDAS data has good correlation with the observational data ($r = 0.83$), but an error of $0.15 \text{ m}^3 \text{ m}^{-3}$ (or roughly 50 %) in the winter months, where the observational soil moisture reaches values of $0.45 \text{ m}^3 \text{ m}^{-3}$, and an error of at least $0.05 \text{ m}^3 \text{ m}^{-3}$ (17 %) in summer. The observational soil moisture reaches values of $0.47 \text{ m}^3 \text{ m}^{-3}$, which is higher than the saturation soil moisture of loam in the Noah-LSM. This is an indication that the soil texture type is wrongly classified in the WRF initiation data, or that its coarse resolution does not resolve the soil type structure. Further, the variability of the 12 datapoints is much larger in the observational data. This may partially be explained again by the coarse soil type classification in the LSM initiation data, as well as by too uniform precipitation in the forcing data. The high resolution soil type databank eBOD (electronic soil map), provided by the Bundesforschungszentrum für Wald (BFW), shows that the soil types at the location of the measurements in the WegenerNet region vary substantially

(BFW, 2016) (Figure 22). The soil moisture output of the CCLM has even larger errors compared to the observations. In summer the moisture values drop from $0.2 \text{ m}^3 \text{ m}^{-3}$ to below $0.1 \text{ m}^3 \text{ m}^{-3}$, which is close to the wilting point. However, it is important to remember that CCLM does not distinguish between different soil layers when computing fluxes from the land surface to the atmosphere, but used the accumulated hydrologically active layers to the depth of 3.82 m. These significant dry periods may thus have only minor effects on the regional circulation of the model. Despite the large error, the correlation with the observational data of 0.7 is acceptable. Data from WRF look similar, with wetter soil in winter, close to the values of the HRLDAS ($\sim 0.3 \text{ m}^3 \text{ m}^{-3}$), and significant drying in the summer, but not as pronounced as CCLM. Furthermore, WRF shows very low correlation with the WegenerNet data ($r = 0.13$). Since both RCMs show similar behavior in summer, it can be assumed that biases of the driving boundary conditions or decoupling from the ERA-Interim data due to the double nested nature of the RCMs are responsible. In the latter case, internal variability of the first nested region leads to deviations in the model dynamics from the lateral boundary conditions and thus to biases for the second nesting step (Kida et al., 1991).

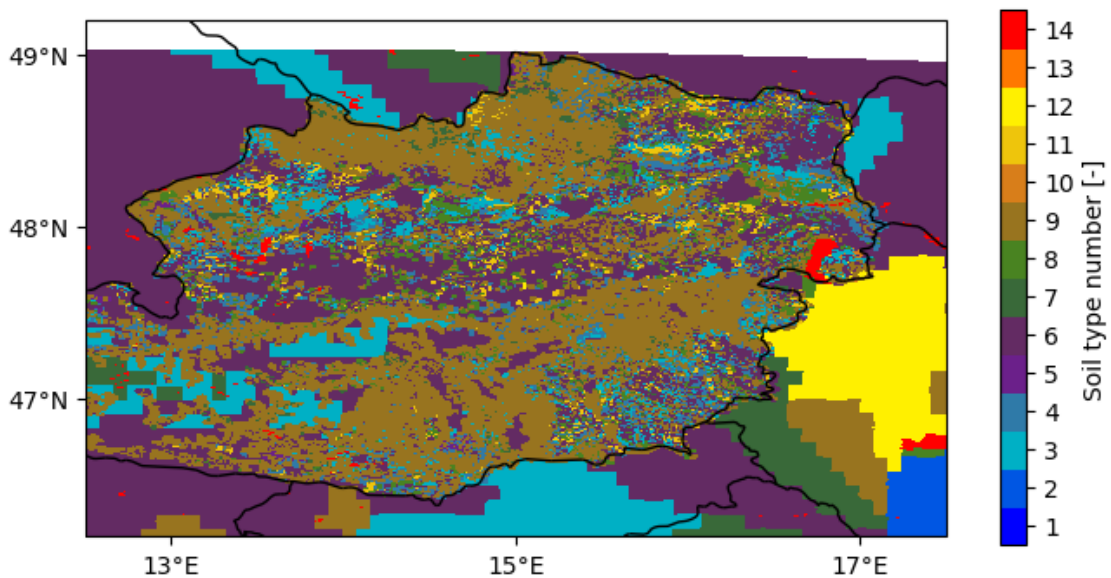


Figure 22 High resolution soil texture type map over Austria (BFW, 2016). Outside of Austria and at locations where the eBOD contained no classification, the Noah-LSM soil types are plotted. The numbers correspond to the same soil types as in Figure 20.

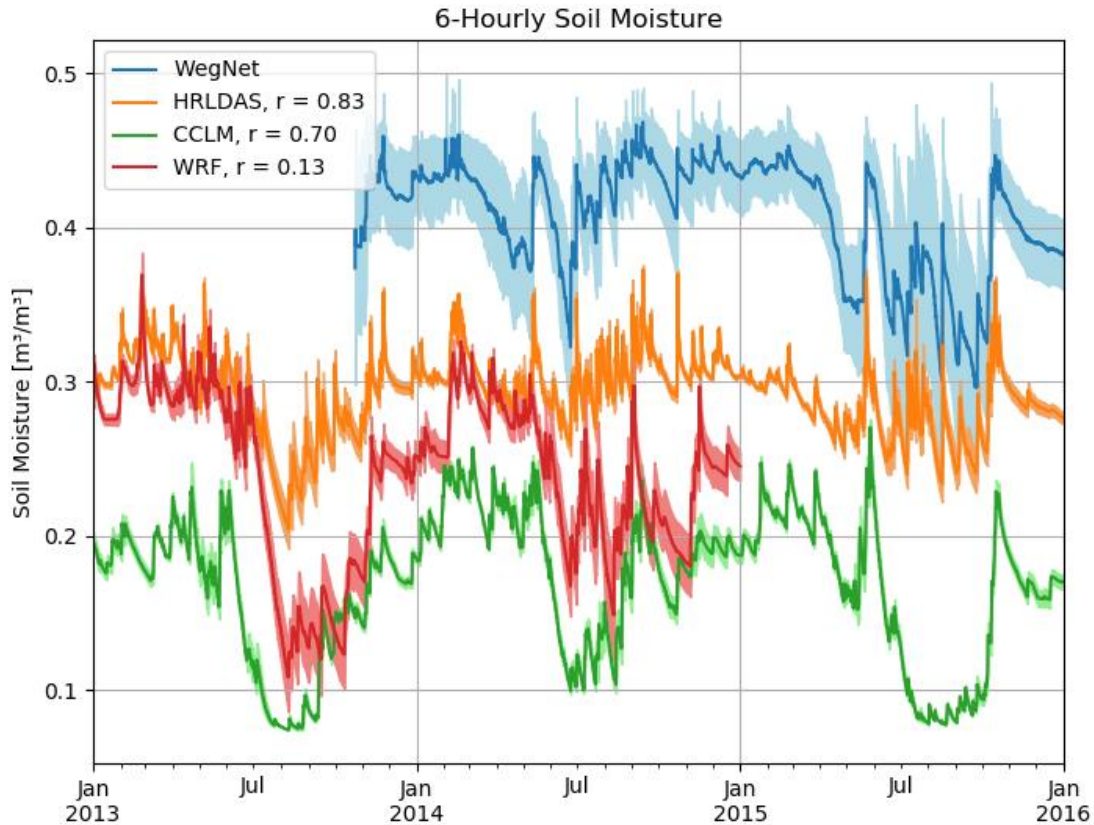


Figure 23 Mean soil moisture of 12 observation sites in the WegenerNet network (WegNet, blue), and the three models at the same locations (HRLDAS, orange; CCLM, green; WRF, red) from 2013 to the end of 2015. The soil layers closest to the depth of the measurement (0.2 m) were chosen for each model. The shaded areas indicate the standard deviation. The correlation coefficient (r) is calculated for each model and the WegenerNet data for the period of October 2013 to December of 2015.

An analysis of the monthly mean precipitation bias in the study region and the studied period shows that both RCMs overestimate precipitation in the months of December to April and underestimate precipitation in the summer months and September (Figure 24). The overestimation in winter and spring in the CCLM amounts to an average of 30% and in WRF even to an average of 40%. WRF also shows similar overestimation of precipitation in November (44%). On the other hand, in summer the precipitation deficit compared to the INCA data amounts to 22% in CCLM and 27% in WRF. The highest deficit in the RCMs of 30% can be seen in August and early September. Thus, the RCMs have less seasonal variability in precipitation than the observations. The deficit of rain

combined with increased ET in the summer months could be one reason for the drastic soil drying in July, August and September, observed in the model data.



Figure 24 Daily mean precipitation in mm, averaged over a 30 day running mean (smaller averaging window at the start and the end of the timeseries) of the INCA (orange), CCLM (green) and WRF (red) data within the study region, computed from the period of 2005 to 2014. Only areas of orographic height lower than 1000 m are used (based on Piazza et al., 2019).

Because the absolute error of the soil moisture is almost constant for HRLDAS and CCLM, the anomalies show a good agreement with the observational data (Figure 25). Also, the WRF data has similar anomalies as the WegenerNet data. However, the correlation of 0.14 is still low (correlation might change compared to the previous figure, because the subtracted mean is not constant over time). The highest anomalies are recorded in the summer during prolonged dry spells (negative anomalies) and after strong precipitation events (positive anomalies). The temporal fluctuations of all data have a similar amplitude. The spatial variability of the models is significantly lower than of the observations. The low regional variance in soil moisture anomaly may have effects on the spatial feedback metric by dampening the moisture gradients within the precipitation events.

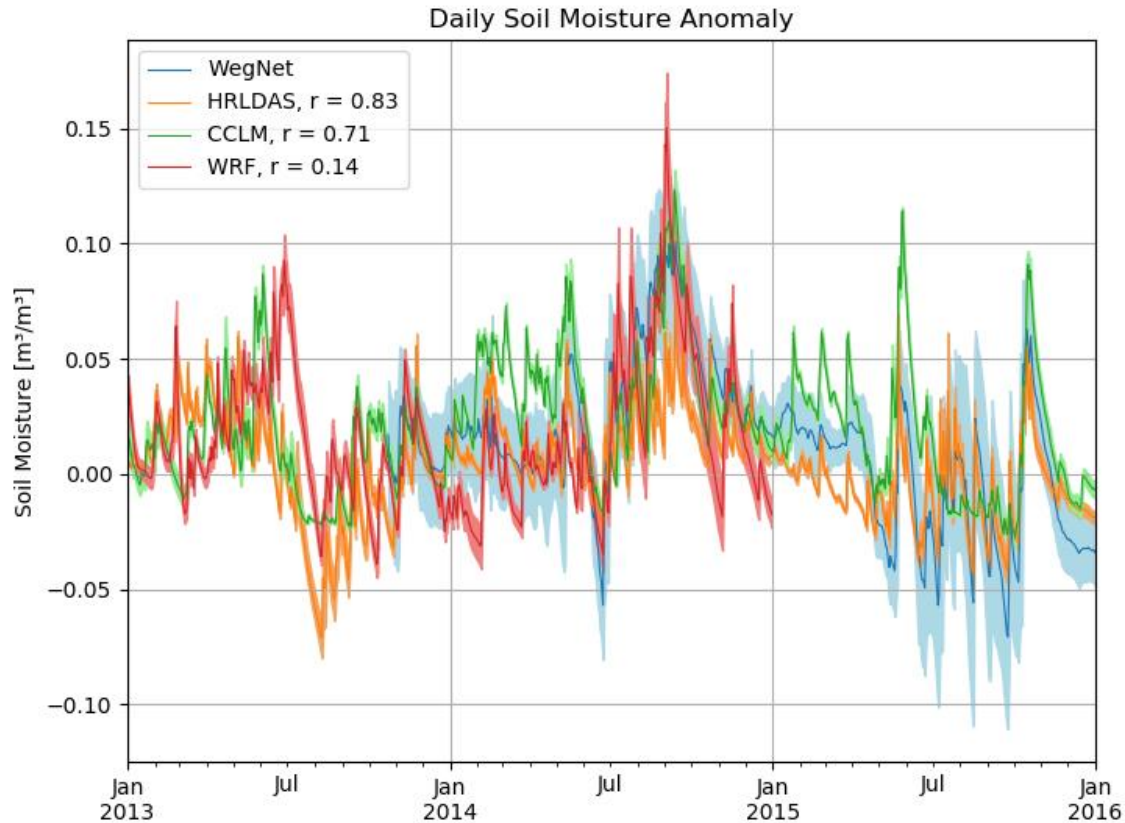


Figure 25 Daily mean soil moisture anomaly of the same data as in Figure 23 (WegenerNet, blue; HRLDAS, orange; CCLM, green; WRF, red). The shaded areas indicate the standard deviation of the 12 locations. The correlation coefficient (r) is calculated for each model and the WegenerNet data for the period of October 2013 to December of 2015.

Although, the absolute soil moisture data of the models have significant errors compared to the observations, the soil moisture anomalies show good agreement with the observations. Therefore, the SMPF analysis is supposed to give realistic results.

5.2. Land surface conditions

Before looking into the results of the SMPF, HRLDAS and INCA data are analyzed to evaluate the land surface conditions of the study region. The conditions may already give information if and where the feedback may arise. For this purpose, the Bowen ratio, calculated from the ratio of sensible and latent heat flux, quantifying the soil moisture

regime, as well as the correlation of soil moisture and radiation with ET rates are computed.

Because it is suggested, that soil moisture atmospheric coupling emerges predominantly in semi-arid regions (Koster et al., 2004; Seneviratne et al., 2006), the soil moisture regime is evaluated. The mean Bowen ratio, describing the regime (chapter 2.2), is derived from daily mean accumulated sensible heat flux and latent heat flux data of the HRLDAS. The ratio is calculated for every day and subsequently temporally averaged. The Bowen ratio is not constant but has considerable seasonal variability. While in summer high radiation and precipitation increase ET and thus latent heat, in winter the ratio is above 1 in the entire region, indicating drier conditions. In spring and autumn the conditions are between those extremes, with dominating sensible heat in most regions (Appendix B, Figure B.1). In Figure 26 the Bowen ratio for the study region can be seen, evaluated for the months of May to September of the 10-year period of 2005 to 2014. In the lowlands, close to rivers (e.g. along the Danube) and lakes (e.g. Lake Neusiedl), the Bowen ratio is 0.4 to 0.8, meaning about twice as much energy is transferred to the atmosphere via latent heat than by sensible heat. This is due to the readily availability of water and riparian vegetation. The Bowen ratio of water bodies like Lake Neusiedl could not be evaluated, because their heat fluxes are not computed in HRLDAS. Stronger influence of sensible heat flux can be found in the mountainous areas (e.g. Central Alps and Bohemian Massif), probably partly affected by the lesser vegetative coverage. Here valleys (e.g. Enns valley) can clearly be distinguished, due to the lower ratio close to rivers. Also, to the southeast the drier Mediterranean climate of Croatia and Hungary are characterized by higher ratios (2.5 to 10). The highest values of well above 15 are located in urban regions. Here sealing of large areas of the soil surface lead to increased albedo on one side and thus increased amount of absorbed solar radiation, and on the other side less water absorption by the soil and increased runoff. Sensible heat in these areas are 100 to 1000 times higher than latent heat. In conclusion, the areas of highest interest for this study (Alpine foreland plains) are, as expected, predominantly of wet or neutral soil moisture regime.

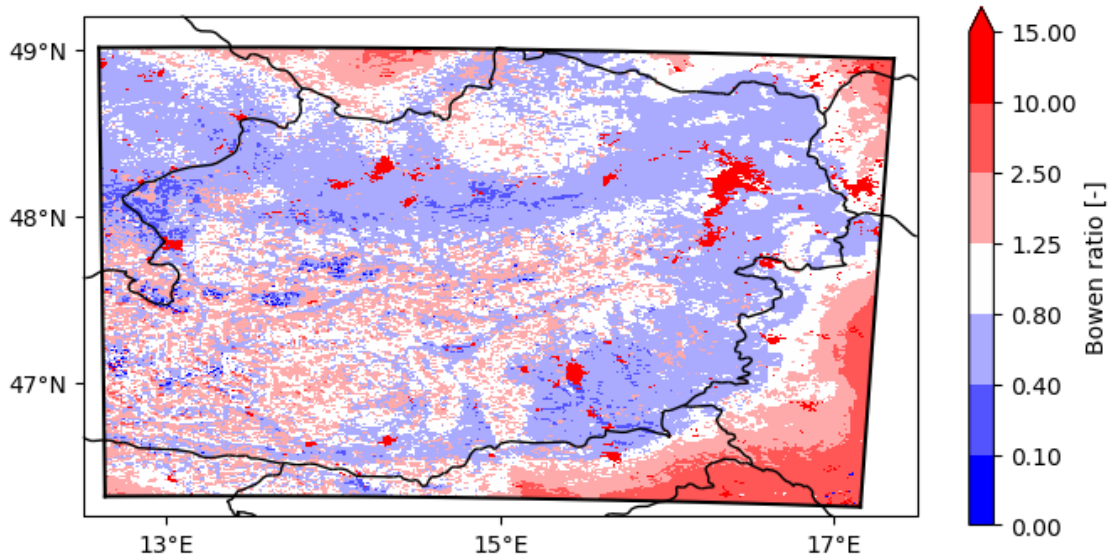


Figure 26 The mean Bowen ratio characterizing the soil moisture regime on the 1 km INCA grid in the study region for the months of May to September, calculated for the years of 2005 to 2014. Blue color indicates more humid soil conditions, with higher latent than sensible heat flux, and red color indicating drier conditions, with dominating sensible heat flux.

Secondly, the correlation of incoming radiation and ET, as well as of soil moisture and ET is computed. This analysis is similar to that conducted by Teuling et al. (Figure 6), with the focus on Austria and the difference that soil moisture instead of precipitation, as proxy for surface soil moisture, is used. The goal is to evaluate if ET rates are limited by the availability of water or energy. Especially important for the SMPF is the relationship of ET and soil moisture. A strong dependence of ET on the soil moisture conditions is required to systematically impact regional climate and circulation (Koster et al., 2004). First the daily mean accumulated evaporation from the soil and from the canopy layer, as well as transpiration rates are evaluated and added together, resulting in the daily mean ET. Similarly, the daily mean incoming short-wave radiation and long-wave radiation are used to obtain the daily mean total incoming radiation. The correlation of ET with total radiation, and average morning (6:00 to 12:00 UTC) soil moisture at 0 to 0.1 m depth respectively, is computed for every day of the analysis period. Average morning soil moisture was used to be in accordance with the SMPF analysis, as well as to reduce the influence of severe afternoon rainfalls. The mean correlations are then calculated and plotted (Figure 27). In accordance with the SMPF analysis and the evaluation of the

Bowen ratio, only the months of May to September for the timeframe of 2005 to 2014 are evaluated. The correlation of ET with radiation is very strong in most parts of the study region. A coefficient of 0.8 to 1 in the Alpine foreland suggests a very strong dependence of the evaporation of water on the received radiative energy. Lower correlation can be found in the central Alps, probably due to the lesser availability of water and the drier conditions (see Bowen ratio). Similarly, to the soil moisture regime, the correlation decreases towards the southeast, meaning that ET is not limited by energy. The opposite is the case for the dependence on soil moisture. Whilst no or insignificant correlation can be located at the Alpine forelands, negative dependences can be found in the mountainous and urban areas. Thus, increased soil moisture leads to a decrease in ET. This can have several causes. One explanation may be that soil moisture is highest during and after strong precipitation events, when conditions are cloudier and thus insolation is lower, reducing the amount of evaporative available energy. Therefore, negative correlation would be a result of the prevailing weather conditions coinciding with higher soil water content. A study investigating the impact of monthly mean soil moisture on latent heat flux came to the same conclusions about the negative dependence of evaporation in very humid soil conditions (Vargas Zeppetello et al., 2019). Remarkable are further the positive correlations found in the Bohemian massif and to the southeast in Hungary and Croatia of up to 0.8. This shows a high dependence of ET on the availability of water. Together with the results from the Bowen ratio, it can be seen that the southeast of the study region has semi-arid land surface conditions. These are the characteristics of the transitional climate zone, between dry and wet climate of the Mediterranean and eastern European region (Seneviratne et al., 2006). In Austria although, the ET regime is of energy-limited character and increased influence of latent heat flux compared to sensible heat, classifying as a humid region. These findings strongly agree with the findings of Teuling et al. (Figure 6). This has significant implications for land surface-atmosphere interactions. Because of the missing soil moisture-evaporation coupling the feedback mechanism (soil moisture-precipitation and -temperature), as conceptualized, cannot develop (Figure 7) (Koster et al., 2004). Thus, a systematic and significant influence of soil moisture on precipitation patterns is not expected for the further analysis of the HRLDAS and INCA data. Individual events, however, may be affected by the land surface conditions.

Looking into the seasonal variation of the ET regime (Appendix B, Figure B.2 and B.3) it can be seen that the strongest correlation of ET and incoming radiation is in autumn and summer. Due to the precipitation peak in summer, water availability is high during the months of June to August. In Autumn high soil water carryovers from summer, relatively high precipitation rates in September, paired with reduced radiation leads to a strong dependence on evaporative available energy. In winter, when there are low amounts of precipitation and the lowest radiation fluxes, the dependence decreases. In the period of March to Mai precipitation and radiation are similar to Autumn, but due to prior dry conditions in winter the effect is reduced. The correlation of ET and soil moisture depicts the lowest values in spring and summer, possibly related to more humid soil coinciding with cloudy conditions, reducing insulation. In autumn there is no positive nor negative dependence found, except for previously discussed southeastern edge of the study region. In winter the dependence on soil moisture increases slightly but is still insignificant. This further illustrates the mostly radiation dependent ET regime in Austria and that a soil moisture-atmospheric coupling via evaporative effects is not expected in this region.

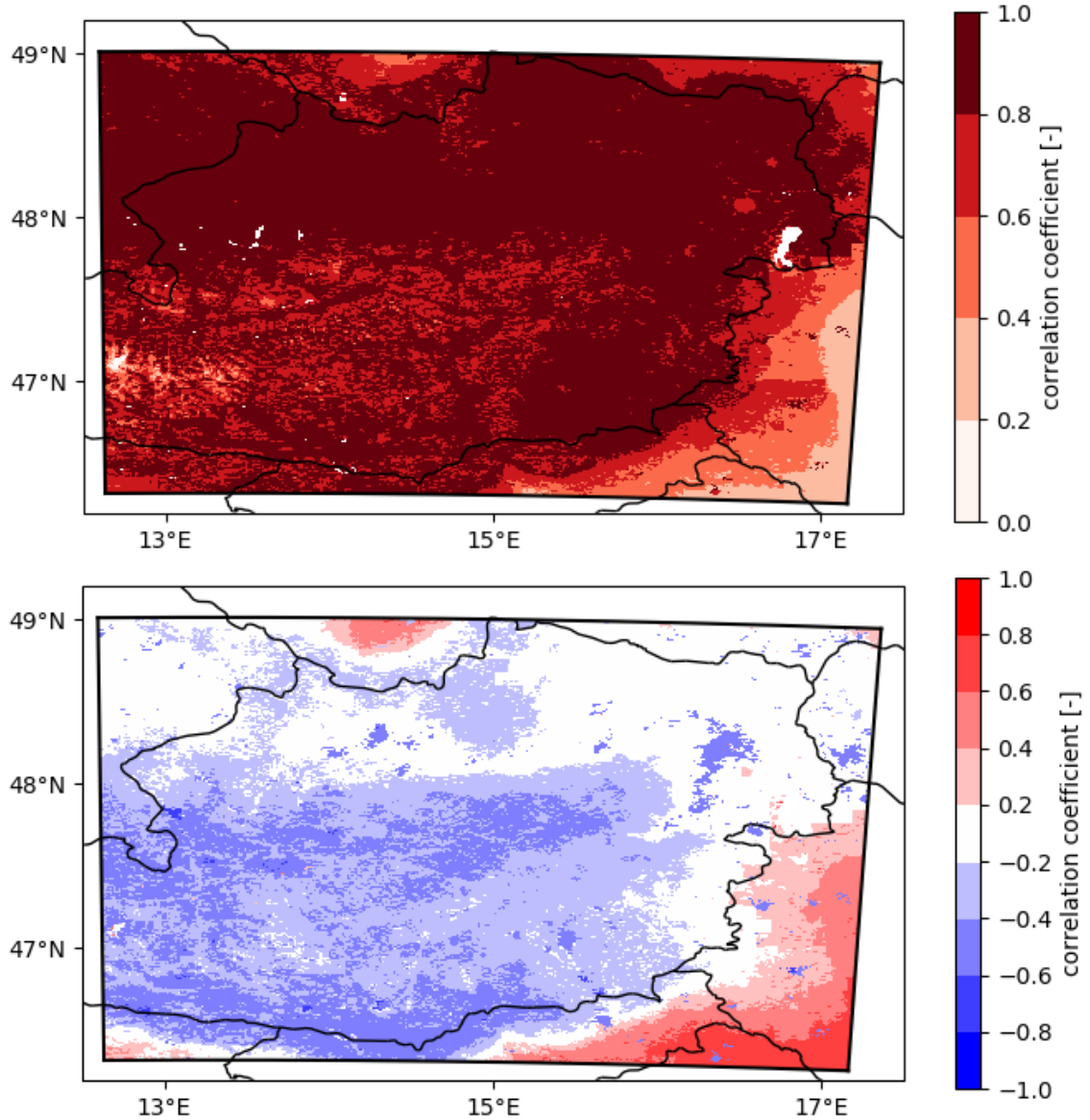


Figure 27 Mean correlation coefficient of (top) daily mean incoming radiation and daily mean accumulated ET and (bottom) daily mean average morning (6:00 to 12:00 UTC) soil moisture and daily mean accumulated ET, with 1 km resolution, for the months of May to September, for the period of 2005 to 2014. All of Austria shows a high correlation of incoming radiation and ET, while the correlation of soil moisture and ET is negligible or negative, indicating a wet, energy-limited ET regime. To the southeast the conditions are reversed, indicating a transitional zone.

5.3. Soil moisture precipitation feedback

The SMPF metrics are calculated for the period of 2005 to 2014 for the HRLDAS soil moisture and INCA precipitation data (from here on HRLDAS) and for the CCLM and WRF RCMs. First, the results are presented in a similar way to Taylor et al. (2012) and Guillod et al. (2015). For that reason, the mean feedback metrics of the precipitation events were compared to the reference distributions, obtained by bootstrapping. The percentile range in which the values are located are displayed for every region in Figure 28. Red coloring indicates that precipitation is more likely over drier, green over wetter soil conditions, either in the spatial or temporal dimension. Concerning the soil moisture heterogeneity metric, red refers to more homogeneous and green coloring to more heterogeneous soil moisture distributions.

It can be seen that no results are shown for the southwestern Carinthian region. That is because no precipitation events are registered in this region for all three datasets. The central Alps take up most of the southwestern study region, therefore it was expected to find no events with the event size of 45 km. The other regions register 80 to 190 events for all models (more detailed in Figure 29).

The quasi observational data (HRLDAS and INCA) it seems that there is a preference for precipitation to occur over spatially wetter soil areas, to a different degree in the region. This is especially the case in the northeastern region of Lower Austria and Vienna, where the spatial feedback metric lies in the top 5th-percentile. In the other two regions the preference is less pronounced, with the Upper Austrian region and Styrian region display mean event values within the 20th-percentile and 30th percentile respectively. The temporal feedback parameter indicates a strong preference of precipitation events happening over negative soil moisture anomalies compared to the control events in the northern regions. The southeastern region shows insignificant preferences. The heterogeneity metric, on the other hand displays no preferences relative to the control events in the northern regions and weak preference for more heterogenic soil moisture conditions in the Styrian region.

The comparison with the results of the RCMs proved difficult, due to strongly varying precipitation preferences in all metrics. The northwestern region shows a strong negative preference in the spatial feedback in CCLM and no preference in WRF. However, the northeastern region shows slight positive soil moisture anomaly preferences in both

models, whilst the Styrian region displays a weak positive feedback in CCLM and a weak negative feedback in WRF. These differences are also present for the other two metrics.

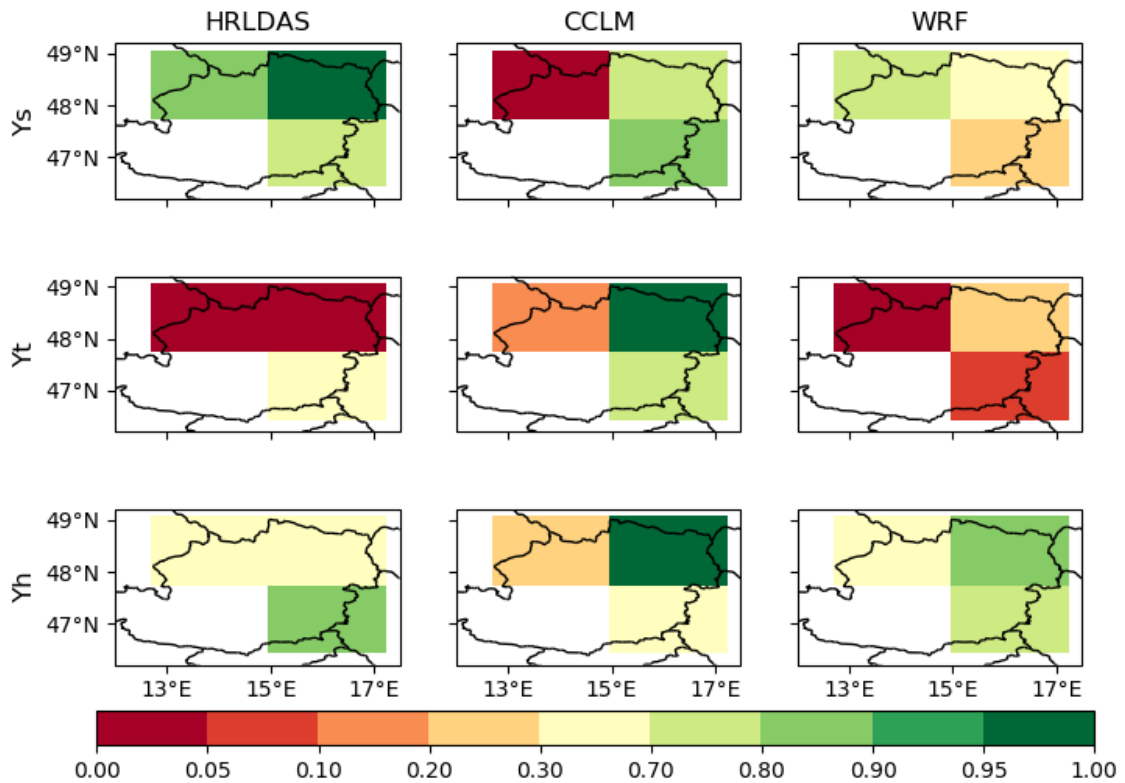


Figure 28 The percentile of the spatial (Y^s , top row), temporal (Y^t , middle row) and heterogeneity (Y^h , lowest row) SMPF metric, compared to the reference distribution, of the analyzed regions, for the HRLDAS (left column), CCLM (middle column) and WRF (right column) for the months of May to September for the timeframe of 2005 to 2015. Red coloring indicates a preference in precipitation over drier or more homogeneous soils and green a preference over wetter or heterogeneous soils.

Because these results only presented the mean soil moisture condition preference of precipitation events, the decision was made to investigate the metric distribution of events and control events in more detail. For this purpose, all events and control events were used to generate a probability density curve for each metric in every region. The advantage of this analysis is that not only the direction of the shift towards a positive or negative preference relative to the control data could be evaluated, but also the strength and the significance. Also, the shape of the curve could give valuable information about

the behavior of precipitation formation depending on the soil conditions. If a significant negative and positive SMPF would be present, a bimodal distribution could be observed. In this case different statistical test would be required for testing the hypothesis. However, the data displays characteristics of a normal distribution. Thus, the significance of the hypothesis, that soil conditions at precipitation events are similar to those at control events, can be evaluated with the Welch's t-test. If the p-value is lower than 0.05, the hypothesis has to be rejected, meaning the conditions differ significantly.

Starting with the northwestern region (Region 1), it can be seen that the event probability distributions are very similar to the control data. Further, only two differ significantly. The spatial metric of the CCLM data is shifted by $0.003 \text{ m}^3 \text{ m}^{-3}$ towards the left, indicating a slight but significant ($p = 0.03$) preference for drier soil conditions. The temporal metric distribution of the HRLDAS ($p = 0.00$) and the WRF data are similarly shifted towards more negative values by $0.007 \text{ m}^3 \text{ m}^{-3}$ and $0.006 \text{ m}^3 \text{ m}^{-3}$ respectively. All other distributions do not significantly differ from the control data. In the Styrian region (Region 2), none of the event probability distributions differ significantly for any model. Consequently, it is very likely that precipitation does not occur favorably over drier or wetter soil conditions. The northeastern region of Lower Austria (Region 3) shows significant deviations in the temporal metric from control data for HRLDAS ($p = 0.00$) data. Again, a very small shift in the mean of $0.006 \text{ m}^3 \text{ m}^{-3}$ indicating a negative temporal soil moisture anomaly preference in the quasi observational data. The CCLM data, as can already be seen in the previous analysis (Figure 28), displays a positive temporal preference ($p = 0.046$, rounded to 0.05 in Figure 29), with a shift of $0.008 \text{ m}^3 \text{ m}^{-3}$. Although the peaks of both distributions match well, the skewness of the event curve is higher, shifting the mean towards more positive values.

Taking all these results into account, it can be argued, that the soil conditions do not have a significant influence on the precipitation preference in observational data, nor in the RCMs. Especially the heterogeneity metric probability distributions almost perfectly resemble the very narrow control data distribution for all three datasets. This means that the soil moisture differences within an event domain are quite stable over time and do not influence the likelihood of precipitation. Here the shortcomings of the model soil moisture output may impact the results. As mentioned before, the soil moisture fields are more homogeneous than observational data of the WegenerNet, thus reducing the spatial

heterogeneity. An increase in heterogeneity would lead to broader distribution curves of the heterogeneity and spatial metric. If the soil condition preferences, and thus the feedback quantification, would change is questionable.

An interesting difference in the model data is the number of events found per region. Using the CCLM data 16 to 20 % less events are detected compared to the INCA data. This may be the result of biases in the precipitation diurnal cycle of the CCLM (Figure 14). Precipitation intensity in the morning are overestimated, while precipitation areas are strongly underestimated in the afternoon. The combined effect results in less precipitation events detected in the afternoon and more events being excluded due to exceedance of the morning precipitation limit. The WRF data also show biases in the diurnal cycle. The precipitated intensity is also overestimated over the diurnal cycle, but precipitation occurrence on the other hand is strongly underestimated. These effects seem to cancel each other for the event classification. The higher number of events in WRF can be explained with the differences of the water bodies in the model domains, which reduces the area where precipitation events could be classified. In the southeastern region there are only a few water bodies and INCA and WRF data detect similar numbers of events. In the northern regions although there are differences. Because INCA resolves smaller water bodies, due to its higher resolution, less events can be found compared to the WRF data, resulting in 10 to 15 % more detected events in the northwestern and northeastern study region.

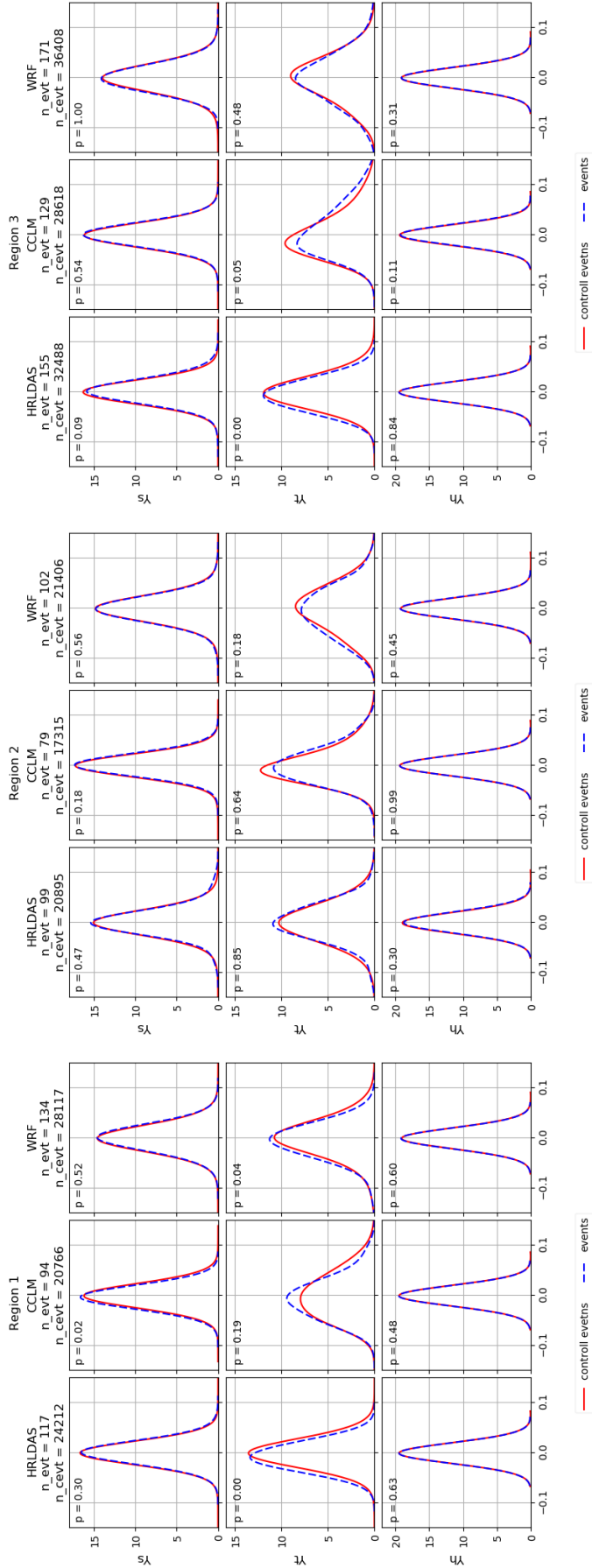


Figure 29 Probability density curves of the feedback metrics of the control event data (solid red line) and the event data (dashed blue line). The abscissa depicts the metric values, while the ordinate shows the probability density. The top row depicts the distributions of the spatial metric (Y^s), the middle row of the temporal metric (Y^t) and the lowest row of the heterogeneity metric (Y^h). The three left columns display results of Region 1 (northwestern region), the three middle columns of Region 2 (southeastern region) and the three right columns of Region 3 (northeastern region). Of the regional results, the left column displays the distributions of the HRLDAS data, the middle column of CCLM and the right column of WRF data. The number of events and control events found in the regions are depicted for every model at the top.

The small but significant differences of probability density in the northern regions for the spatial (CCLM Region 1) and temporal (HRLDAS Region 1 and 3, CCLM Region 3 and WRF Region 1) metric can have many different causes. For instance, sub regional differences may have an impact on the soil condition preferences. Areas with high ET dependence on soil moisture in the study region (east and southeast) may be influenced by the SMPF mechanisms and thus display more negative or positive feedback metrics. To evaluate these influences, the location of every precipitation event is plotted and colored depending on the spatial and temporal feedback metric strength. If events with negative or positive feedback metrics accumulate in certain areas, they could be further investigated in detail.

First, the events detected using the INCA data and feedback metric strength calculated with soil moisture from the HRLDAS are presented in Figure 30. An accumulation of events can be found in the Austrian part of the Bohemian Massif. This accumulation seems not to depend on spatial or temporal precipitation preference but affects all events. The Bohemian Massif in Austria reaches 800 to below 1000 m height. Thus, it is not excluded in the analysis. The strong orographic effect on precipitation is suspected to be the driving force behind the increased number of events. Important to mention are also the large areas in the eastern regions, which had to be excluded from the analysis due to Lake Neusiedl in Burgenland. Further, there seems to be no accumulation of events affected by a positive or negative SMPF. Even in southeastern region, where ET conditions are suitable for the feedback mechanisms to arise, there are no systematic patterns.

Similar analysis of the precipitation event location is done for the CCLM model (Figure 31). For this data, as aforementioned, 20 % less events are detected. Similarly, to the INCA data there are accumulations in the Bohemian Massif, but they seem not to favor drier or more humid soil conditions in neither the spatial, nor the temporal dimension. Aside from these patterns of orographic origin, no significant subregional accumulations can be found.

Lastly, the analysis of the WRF data event locations likewise do not show any areas with systematical soil condition preferences (Figure 32). The orographic effect in the Bohemian Massif is even stronger pronounced than in the other models, with strong accumulation of events, especially in the north of the mountain range.

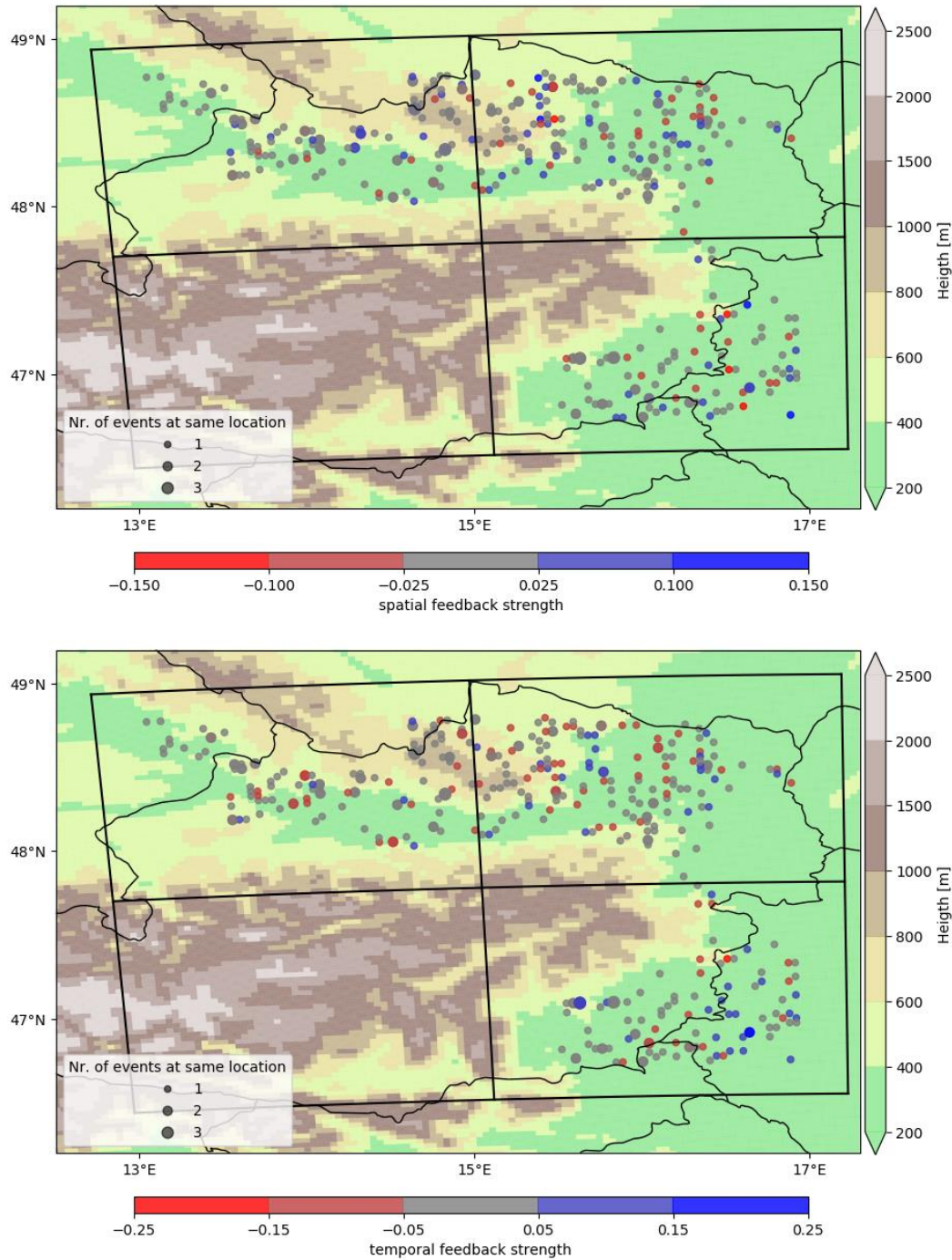


Figure 30 Topographic height in meters and location of all detected precipitation events from 2005 to 2014 using the INCA data (dots). The coloring indicates the spatial feedback metric (top) and the temporal feedback metric (bottom) for each event. Red indicates negative, blue positive and grey insignificant soil moisture feedback conditions. The size of the dots represents the number of events at the same location. In this case the color indicates the mean metric for the coinciding events.

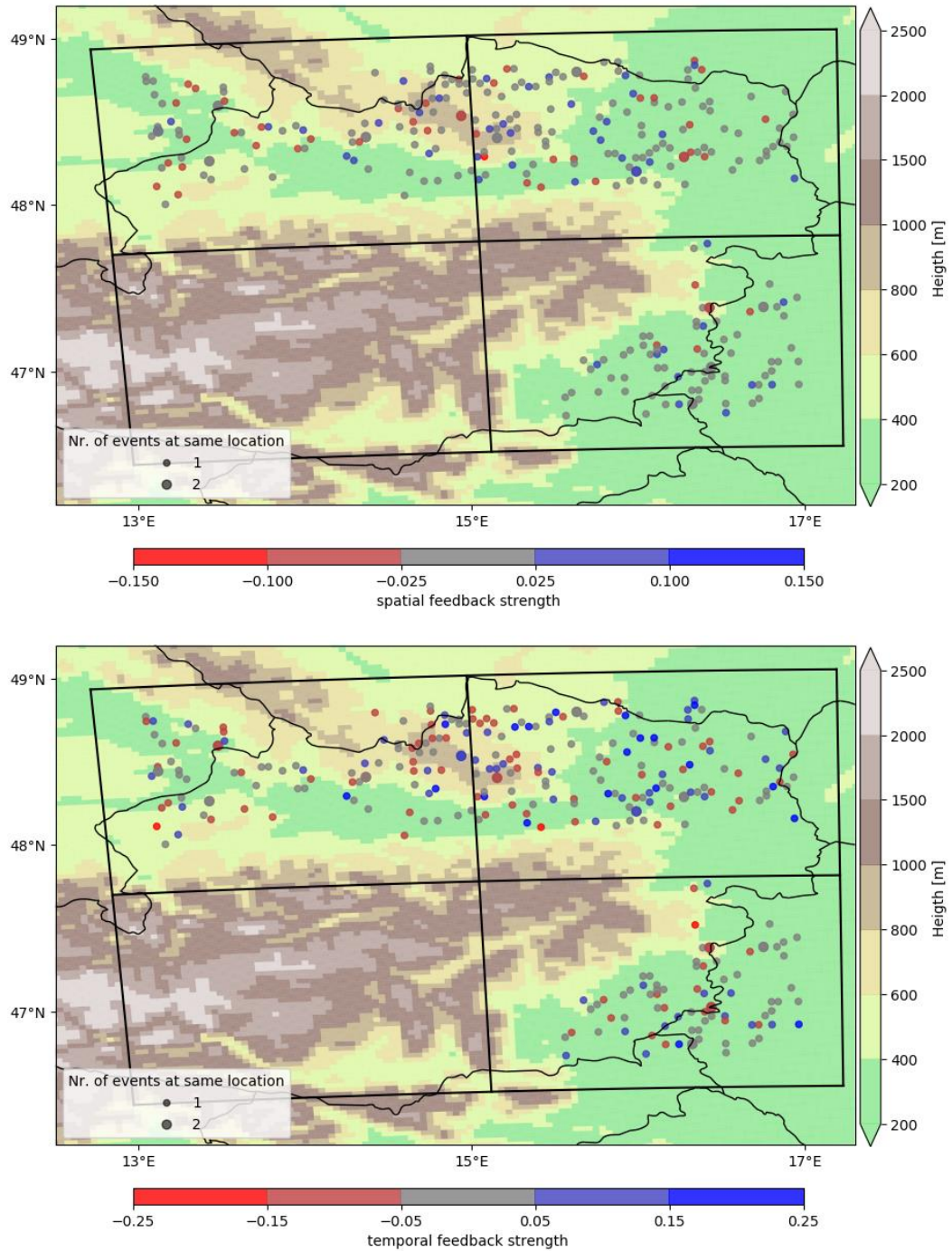


Figure 31 Topographic height in meters and location of all detected precipitation events from 2005 to 2014 using the CCLM data (dots). The coloring indicates the spatial feedback metric (top) and the temporal feedback metric (bottom) for each event. Red indicates negative, blue positive and grey insignificant soil moisture feedback conditions. The size of the dots represents the number of events at the same location. In this case the color indicates the mean metric for the coinciding events.

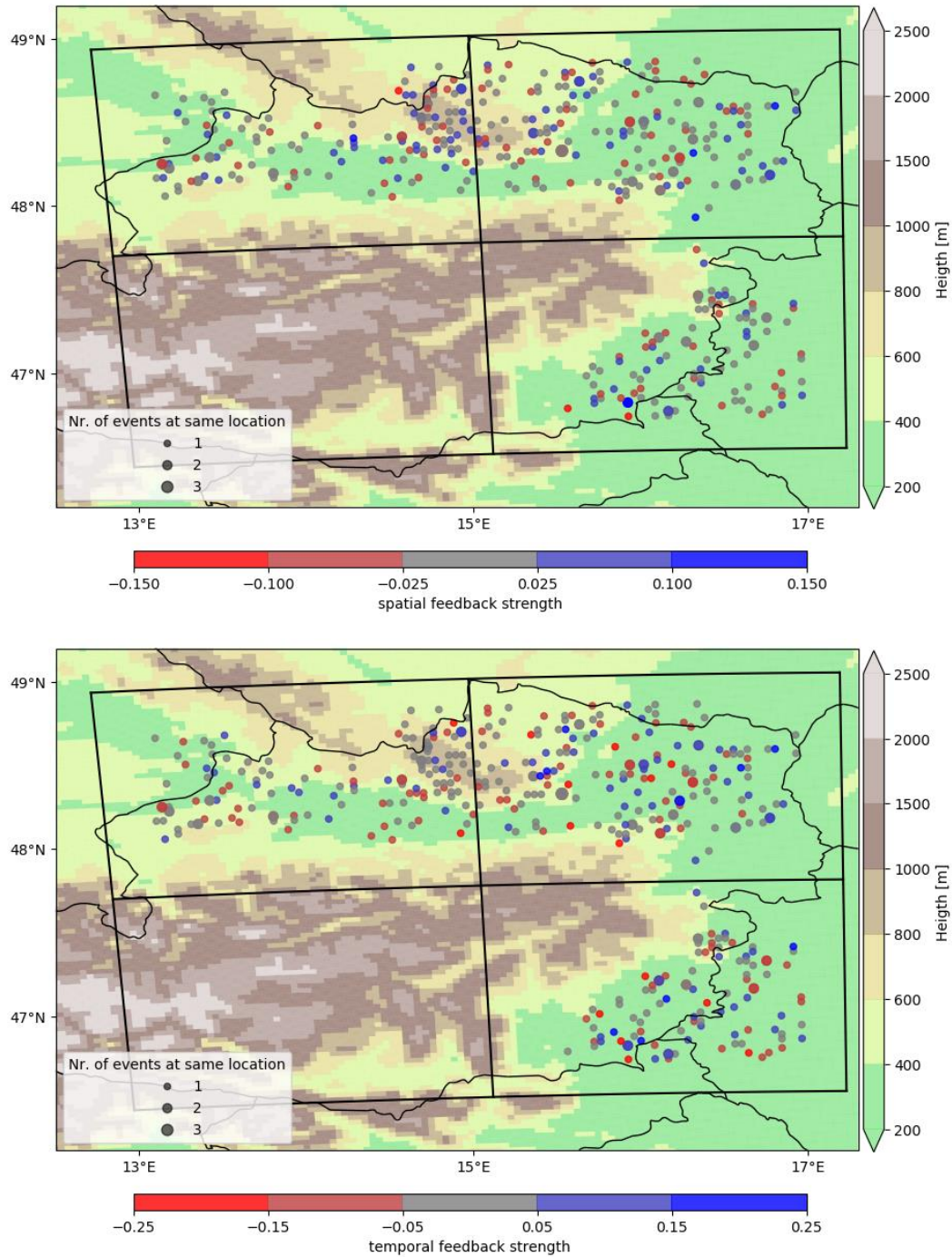


Figure 32 Topographic height in meters and location of all detected precipitation events from 2005 to 2014 using the WRF data (dots). The coloring indicates the spatial feedback metric (top) and the temporal feedback metric (bottom) for each event. Red indicates negative, blue positive and grey insignificant soil moisture feedback conditions. The size of the dots represents the number of events at the same location. In this case the color indicates the mean metric for the coinciding events.

Taking all results of the SMPF analysis and the analysis of the Bowen ratio and the ET regime into account it can be concluded that there is no systematic and significant influence of the soil moisture conditions on precipitation patterns in Austria. There is no substantial evidence that this feedback is present in any of the studied subregions. It is likely, that the differences in the feedback metrics of the events compared to the control events are the product of internal variability of the climate system or other factors. In Austria, and the entire Alpine region, synoptic and orographic effects and their influence on regional circulation seem to be the dominant driver on precipitation. Individual events may well be influenced by the prevailing soil conditions, affecting regional circulation, but a systematic feedback mechanism towards precipitation preferences over drier or more humid soil cannot be deducted. Similar results of the RCMs lead to the conclusion that no unrealistic mechanisms within the models affect the development of a SMPF.

Although the soil moisture anomalies, which is the critical soil parameter in this study, are well represented, the absolute soil moisture is poorly represented by these models. Especially the strong drying of the soil in the July, August and September, reaching levels close to the wilting point, of the CCLM and WRF reveals possible model deficits. This behavior may have substantial consequences on the land surface energy budget and the hydrological budget within the models. For instance, the negative soil moisture-temperature feedback in semi-arid regions may lead to an increase in near surface temperatures when soil moisture is unrealistically low. This would have consequences for regional climate projections when using these models. Here it is important to mention that the CCLM uses soil moisture values from the active soil layer, which reduces the effect of the drying. On the other hand, this also reduces the seasonal variation of soil moisture, potentially impacting seasonal hydrological processes. Moreover, soil moisture from the model data shows that heterogeneity is not well represented by the LSMs compared to the observations from the WegenerNet. This is in part due to the coarse resolution of land surface and soil parameters. This may affect land surface-atmosphere interactions in climate models, which are often driven by strong spatial soil moisture gradients (e.g. Chen & Avissar, 1994; Hohenegger & Stevens, 2018).

The method to analyze the SMPF adapted from Taylor et al. (2012), Guillod et al. (2015) and Moon et al. (2019) has weaknesses when investigating the SMPF on a regional level, with complex terrain, strong synoptic influence and homogeneous distribution of soil

moisture. First precipitation resulting from large- and meso-scale circulation may not be sufficiently filtered and interfere with the results. A more rigorous method to limit the analysis to atmospheric conditions, where regional circulation can shape precipitation patterns would deliver a clearer picture of the feedback. Further, due to the low spatial soil moisture variability in central Europe, increased by LSM deficits, the distribution of the feedback metrics, especially the spatial and heterogeneity metric, is very narrow. Evaluating the sign of the feedback based on the distribution of mean values obtained by sampling from the narrow spread can result in the false perception of a SMPF. Very small deviations of the feedback metrics of the precipitation events compared to the control events are classified as strong feedbacks. The decision to taking a closer look into the underlying distributions, thus was necessary to compare the results from the different regions and models. Another concept to improve the method is to focus the analysis on convective initiations, not accumulated afternoon precipitation (e.g. Taylor, 2015; Taylor et al., 2011). Prolonged precipitation events can be transported by background winds and thus change the location of maximal precipitation compared to the area where the convection initiates (Froidevaux et al., 2014). Because soil moisture and atmospheric conditions however are coupled via differences in surface energy fluxes and convective processes, the focus should be on the regional convection patterns. One approach would be to focus on the location where precipitation first set in and compare the prevailing soil conditions to the surrounding areas.

Another approach to investigate the influence of soil moisture on precipitation patterns, that may be more suitable for regional studies, would be to conduct simulations of single precipitation events. Assuming that an event is well represented by RCMs or an ensemble of models, the impact of the soil conditions could be evaluated by prescribing different moisture fields. Not only the influence of wetter or drier soil, but also of the moisture heterogeneity could be analyzed. From these analyses the conditionality of a SMPF and its impact, as well as regional changes in future soil conditions could be assessed.

6. Conclusions

Internal climate feedbacks are a major source of complexity within the climate system. Understanding the driving mechanisms will improve climate and weather projections, which is important to inform socioeconomic changes towards a more resilient and sustainable society. Among others, feedbacks involving land surface conditions shape the climate system and processes, especially on a regional scale. It has been shown, that the SMPF can have a significant influence on precipitation patterns via changes in the regional circulation, especially in semi-arid regions with strong soil moisture gradients (Hohenegger and Stevens, 2018; Taylor et al., 2013, 2011).

In this thesis the influence of soil moisture conditions on precipitation in Austria is evaluated, by utilizing and adapting the statistical method introduced by Taylor et al. (2012), Guillod et al. (2015) and Moon et al. (2019). Because of the lack of comprehensive observational soil moisture data, the HRLDAS is utilized to generate soil moisture data from atmospheric observations (INCA, ERA5). Further, the performance regarding the soil moisture-precipitation interaction of two convection permitting RCMs, CCLM and WRF, is analyzed. To validate the soil moisture data of these three models, they are compared to in-situ records of the WegenerNet.

All three models have deficits representing the soil moisture. The HRLDAS data shows substantial deviations from the observations, with up to 50 % less soil moisture in winter and about 15 % in summer. Further, the moisture heterogeneity is significantly lower than observed. This is important to note, because strong soil moisture heterogeneity is suspected to be a condition for a negative feedback to arise. Because the HRLDAS is driven with high quality observation data, there are two main reasons for these deficits. First, model initiation data, like the soil texture type, are only available on coarse resolutions, reducing especially regional differences. The low heterogeneity may in part be caused by the coarse resolution of this data. Secondly, deficits in the HRLDAS may also contribute to the poor performance. However, the soil moisture anomaly data, which is the crucial metric for the SMPF analysis, on the other hand shows good agreement with the observations. Therefore, the SMPF analysis is supposed to give realistic results. The performance of the RCMs shows even larger deficits. WRF produces similar soil moisture data to the HRLDAS in the winter months. This is due to the fact that both models have the same land surface model (Noah LSM) in its core. In summer although, soil moisture

drops to very low levels, resembling arid conditions. This may in part be due to a negative precipitation bias of WRF in the months of May to September. Similar biases are present in CCLM, which also produces very dry soil conditions in July, August and September. Further the soil model of CCLM (TERRA-ML), providing land surface conditions to the climate model, is conceptualized to take the soil water content from the surface down to deep layers into account. Thus, the upper most soil layers, which were available for this analysis, may not represent the soil conditions of the model. The upper most soil layer has the strongest seasonal variations, which are dampened in deeper soil layers. Thus, the effect of the drying soil in summer is likely less pronounced in the energy and hydrological fluxes in the model. Due to the seasonal stable soil moisture heterogeneity of WRF and CCLM, it can be concluded that the drying in late summer does not have significant influence on a theoretical SMPF. Other land surface-atmospheric interactions, like the soil moisture-temperature feedback, on the other hand may be triggered by these conditions and influence regional climate conditions. Similar to the HRLDAS, soil moisture anomaly of both RCMs has good agreement with the observational data.

Consequently, the analysis on precipitation preference over soil conditions to evaluate the SMPF is performed. In none of the three subregions a significant negative or positive feedback could be determined for the quasi observational data (HRLDAS). Neither the spatial nor the temporal feedback parameter of the precipitation events showed strong deviations from the background climatology. Although, the temporal feedback parameter distributions of the northern subregions differ significantly, this could have different causes than a land surface-atmospheric feedback. For instance, in areas where soil moisture conditions are relatively stable, with low horizontal gradients, like Austria in the summer months, the feedback parameters are narrowly distributed. In this case averaging of subsamples leads to an even narrower climatology. Very small deviations of the precipitation events may thus be classified as significant preferences. Further, the method used to evaluate the SMPF has some deficiencies when analyzing regions with strong orographic and synoptic influences. Though synoptic effects are reduced by focusing on the summer season and by excluding events with associated morning precipitation, there may still be a significant number of events resulting from frontal dynamics. Similarly, orographic impacts have been reduced by excluding areas of high elevation, but their effects can still impact precipitation far off from mountain ranges.

Subregional locations where precipitation occurs more preferably over drier or more humid soil could also not be found. Also, in the southeast of the study area, where the soil conditions indicated the theoretical possibility of a SMPF, preferences could not be observed. The analysis of RCM data gives comparable results, with no dominating influence of the SMPF being detected in any region or any subregional area.

From the HRLDAS output data land surface condition parameters could be evaluated. From the latent and sensible energy fluxes the Bowen ratio of the study region was derived. Most areas of the study region depict humid soil conditions in the warm season. Exceptions are mountainous and urban areas, as well as regions towards the southeast, indicating the increasingly arid climate of the European transition zone. Further, following the analysis of Teuling et al. (2009), the evapotranspiration (ET) regime was determined by computing its correlation with incoming radiation and soil moisture. Very strong dependence on radiation and neglectable or negative correlation on soil moisture imply that ET is limited by energy and not by the availability of water. The opposite can again be observed in the transition zone towards the southeast. Because the dependence of ET on soil moisture is required for the SMPF to arise (Koster et al., 2004), a systematic influence of soil moisture on precipitation patterns is unlikely. Though, it is important to mention that individual events may well be influenced by land surface conditions. To evaluate these impacts of soil moisture on individual events, different techniques would be required. If due to climate change and increased temperatures the extend of the European transition zone moves further north, the conditions in Austria could become suitable for the SMPF (Seneviratne et al., 2006).

Future investigations into the SMPF using this method should be designed to account for more interfering influences. By including analysis into the synoptic meteorological conditions like weather typing, influences could be further reduced. Greater distances from mountainous areas would also improve the quality of the analysis. Investigations concerning the effect of soil moisture onto precipitation patterns in Austria could be done by simulating individual events and prescribing drier or more humid soil conditions. For this purpose, improvements of RCMs and LSMs, especially of the representation of soil moisture, are necessary. From the resulting impacts conclusions could be made. Especially from investigations into the SMPF in future land surface conditions in the Alpine region, vital information about precipitation patterns could be derived.

Bibliography

- Atkinson, B.W., Wu Zhang, J., 1996. Mesoscale shallow convection in the atmosphere. *Rev. Geophys.* 34, 403–431. <https://doi.org/10.1029/96RG02623>
- Awan, N.K., Truhetz, H., Gobiet, A., 2011. Parameterization-Induced Error Characteristics of MM5 and WRF Operated in Climate Mode over the Alpine Region: An Ensemble-Based Analysis. *J. Clim.* 24, 3107–3123. <https://doi.org/10.1175/2011JCLI3674.1>
- Böhm, U., Kücken, M., Ahrens, W., Block, A., Hauffe, D., Keuler, K., Rockel, B., Will, A., 2006. CLM - The Climate Version of LM: Brief Description and Long-Term Applications. *COSMO Newsl.* 6, 225–235.
- Budyko, M.I., 1974. *Climate and life*. Academic Press, New York.
- Bundesforschungs- und Ausbildungszentrum für Wald, Naturgefahren und Landschaft (BFW), 2016. eBOD - die digitale Bodenkarte.
- Chen, F., Avissar, R., 1994. Impact of Land-Surface Moisture Variability on Local Shallow Convective Cumulus and Precipitation in Large-Scale Models. *J. Appl. Meteorol. Climatol.* 33, 1382–1401. [https://doi.org/10.1175/1520-0450\(1994\)033<1382:IOLSMV>2.0.CO;2](https://doi.org/10.1175/1520-0450(1994)033<1382:IOLSMV>2.0.CO;2)
- Chen, F., Dudhia, J., 2001. Coupling an Advanced Land Surface-Hydrology Model with the Penn State-NCAR MM5 Modeling System. Part I: Model Implementation and Sensitivity. *Mon. Weather Rev.* 129, 569–585. [https://doi.org/10.1175/1520-0493\(2001\)129<0569:CAALSH>2.0.CO;2](https://doi.org/10.1175/1520-0493(2001)129<0569:CAALSH>2.0.CO;2)
- Chen, F., Janjić, Z., Mitchell, K., 1997. Impact of Atmospheric Surface-layer Parameterizations in the new Land-surface Scheme of the NCEP Mesoscale Eta Model. *Bound.-Layer Meteorol.* 85, 391–421. <https://doi.org/10.1023/A:1000531001463>

- Chen, F., Manning, K.W., LeMone, M.A., Trier, S.B., Alfieri, J.G., Roberts, R., Tewari, M., Niyogi, D., Horst, T.W., Oncley, S.P., Basara, J.B., Blanken, P.D., 2007. Description and Evaluation of the Characteristics of the NCAR High-Resolution Land Data Assimilation System. *J. Appl. Meteorol. Climatol.* 46, 694–713. <https://doi.org/10.1175/JAM2463.1>
- Chen, F., Mitchell, K., Schaake, J., Xue, Y., Pan, H.-L., Koren, V., Duan, Q.Y., Ek, M., Betts, A., 1996. Modeling of land surface evaporation by four schemes and comparison with FIFE observations. *J. Geophys. Res. Atmospheres* 101, 7251–7268. <https://doi.org/10.1029/95JD02165>
- Coppola, E., Sobolowski, S., Pichelli, E., Raffaele, F., Ahrens, B., Anders, I., Ban, N., Bastin, S., Belda, M., Belusic, D., Caldas-Alvarez, A., Cardoso, R.M., Davolio, S., Dobler, A., Fernandez, J., Fita, L., Fumiere, Q., Giorgi, F., Goergen, K., Güttler, I., Halenka, T., Heinzeller, D., Hodnebrog, Ø., Jacob, D., Kartsios, S., Katragkou, E., Kendon, E., Khodayar, S., Kunstmann, H., Knist, S., Lavín-Gullón, A., Lind, P., Lorenz, T., Maraun, D., Marelle, L., van Meijgaard, E., Milovac, J., Myhre, G., Panitz, H.-J., Piazza, M., Raffa, M., Raub, T., Rockel, B., Schär, C., Sieck, K., Soares, P.M.M., Somot, S., Srnec, L., Stocchi, P., Tölle, M.H., Truhetz, H., Vautard, R., de Vries, H., Warrach-Sagi, K., 2020. A first-of-its-kind multi-model convection permitting ensemble for investigating convective phenomena over Europe and the Mediterranean. *Clim. Dyn.* 55, 3–34. <https://doi.org/10.1007/s00382-018-4521-8>
- Dee, D.P., Uppala, S.M., Simmons, A.J., Berrisford, P., Poli, P., Kobayashi, S., Andrae, U., Balmaseda, M.A., Balsamo, G., Bauer, P., Bechtold, P., Beljaars, A.C.M., van de Berg, L., Bidlot, J., Bormann, N., Delsol, C., Dragani, R., Fuentes, M., Geer, A.J., Haimberger, L., Healy, S.B., Hersbach, H., Hólm, E.V., Isaksen, L., Kållberg, P., Köhler, M., Matricardi, M., McNally, A.P., Monge-Sanz, B.M., Morcrette, J.-J., Park, B.-K., Peubey, C., de Rosnay, P., Tavolato, C., Thépaut, J.-N., Vitart, F., 2011. The ERA-Interim reanalysis: configuration and performance of the data assimilation system. *Q. J. R. Meteorol. Soc.* 137, 553–597. <https://doi.org/10.1002/qj.828>

- Doms, G., Förstner, J., Heise, E., Herzog, H.-J., Mironov, D., Raschendorfer, M., Renhardt, T., Ritter, B., Schrodin, R., Schulz, J.-P., Vogel, G., 2018. COSMO-Model Version 5.05: A Description of the Nonhydrostatic Regional COSMO-Model - Part II: Physical Parameterizations. https://doi.org/10.5676/DWD_PUB/NWV/COSMO-DOC_5.05_II
- Dy, C.Y., Fung, J.C.H., 2016. Updated global soil map for the Weather Research and Forecasting model and soil moisture initialization for the Noah land surface model: SOIL MAP AND SOIL MOISTURE. *J. Geophys. Res. Atmospheres* 121, 8777–8800. <https://doi.org/10.1002/2015JD024558>
- Ek, M.B., Mitchell, K.E., Lin, Y., Rogers, E., Grunmann, P., Koren, V., Gayno, G., Tarpley, J.D., 2003. Implementation of Noah land surface model advances in the National Centers for Environmental Prediction operational mesoscale Eta model. *J. Geophys. Res. Atmospheres* 108, 2002JD003296. <https://doi.org/10.1029/2002JD003296>
- FAO (Ed.), 1978. Soil map of the world: = Carte mondiale des sols. Vol. 10: Australasia. UNESCO, Paris.
- Fischer, E.M., Seneviratne, S.I., Lüthi, D., Schär, C., 2007. Contribution of land-atmosphere coupling to recent European summer heat waves. *Geophys. Res. Lett.* 34, L06707. <https://doi.org/10.1029/2006GL029068>
- Fisher, R.A., Koven, C.D., 2020. Perspectives on the Future of Land Surface Models and the Challenges of Representing Complex Terrestrial Systems. *J. Adv. Model. Earth Syst.* 12. <https://doi.org/10.1029/2018MS001453>
- Ford, T.W., Quiring, S.M., Frauenfeld, O.W., Rapp, A.D., 2015. Synoptic conditions related to soil moisture-atmosphere interactions and unorganized convection in Oklahoma: Synoptic Patterns Related to Convection. *J. Geophys. Res. Atmospheres* 120, 11,519-11,535. <https://doi.org/10.1002/2015JD023975>
- Froidevaux, P., Schlemmer, L., Schmidli, J., Langhans, W., Schär, C., 2014. Influence of the Background Wind on the Local Soil Moisture–Precipitation Feedback. *J. Atmospheric Sci.* 71, 782–799. <https://doi.org/10.1175/JAS-D-13-0180.1>

- Fuchsberger, J., Kirchengast, G., 2013. Deriving Soil Moisture from Matric Potential in the WegenerNet Climate Station Network. <https://doi.org/10.13140/RG.2.2.33461.68320>
- Fuchsberger, J., Kirchengast, G., Bichler, C., Leuprecht, A., Kabas, T., 2020. WegenerNet climate station network Level 2 data. <https://doi.org/10.25364/WEGC/WPS7.1:2020.1>
- Gabathuler, M., Marty, C.A., Hanselmann, K.W., 2001. PARAMETERIZATION OF INCOMING LONGWAVE RADIATION IN HIGH-MOUNTAIN ENVIRONMENTS. *Phys. Geogr.* 22, 99–114. <https://doi.org/10.1080/02723646.2001.10642732>
- Gobiet, A., Kotlarski, S., Beniston, M., Heinrich, G., Rajczak, J., Stoffel, M., 2014. 21st century climate change in the European Alps—A review. *Sci. Total Environ.* 493, 1138–1151. <https://doi.org/10.1016/j.scitotenv.2013.07.050>
- Goosse, H., 2015. Climate system dynamics and modeling. Cambridge University Press, New York, NY.
- Guillod, B.P., Orlowsky, B., Miralles, D.G., Teuling, A.J., Seneviratne, S.I., 2015. Reconciling spatial and temporal soil moisture effects on afternoon rainfall. *Nat. Commun.* 6, 6443. <https://doi.org/10.1038/ncomms7443>
- Haiden, T., 2009. Meteorologische Analyse des Niederschlags von 22.-25. Juni 2009 (Technical report). Zentralanstalt für Meteorologie und Geodynamik.
- Haiden, T., Kann, A., Wittmann, C., Pistotnik, G., Bica, B., Gruber, C., 2011. The Integrated Nowcasting through Comprehensive Analysis (INCA) System and Its Validation over the Eastern Alpine Region. *Weather Forecast.* 26, 166–183. <https://doi.org/10.1175/2010WAF2222451.1>
- Hartmann, D.L., 2016. Global physical climatology, Second edition. ed. Elsevier, Amsterdam; Boston.
- Hénin, R., Ramos, A.M., Schemm, S., Gouveia, C.M., Liberato, M.L.R., 2019. Assigning precipitation to mid-latitudes fronts on sub-daily scales in the North Atlantic and European sector: Climatology and trends. *Int. J. Climatol.* 39, 317–330. <https://doi.org/10.1002/joc.5808>

- Hersbach, H., Bell, B., Berrisford, P., Hirahara, S., Horányi, A., Muñoz-Sabater, J., Nicolas, J., Peubey, C., Radu, R., Schepers, D., Simmons, A., Soci, C., Abdalla, S., Abellan, X., Balsamo, G., Bechtold, P., Biavati, G., Bidlot, J., Bonavita, M., Chiara, G., Dahlgren, P., Dee, D., Diamantakis, M., Dragani, R., Flemming, J., Forbes, R., Fuentes, M., Geer, A., Haimberger, L., Healy, S., Hogan, R.J., Hólm, E., Janisková, M., Keeley, S., Laloyaux, P., Lopez, P., Lupu, C., Radnoti, G., Rosnay, P., Rozum, I., Vamborg, F., Villaume, S., Thépaut, J., 2020. The ERA5 global reanalysis. *Q. J. R. Meteorol. Soc.* 146, 1999–2049. <https://doi.org/10.1002/qj.3803>
- Hohenegger, C., Brockhaus, P., Bretherton, C.S., Schär, C., 2009. The Soil Moisture–Precipitation Feedback in Simulations with Explicit and Parameterized Convection. *J. Clim.* 22, 5003–5020. <https://doi.org/10.1175/2009JCLI2604.1>
- Hohenegger, C., Stevens, B., 2018. The role of the permanent wilting point in controlling the spatial distribution of precipitation. *Proc. Natl. Acad. Sci.* 115, 5692–5697. <https://doi.org/10.1073/pnas.1718842115>
- Holgate, C.M., Van Dijk, A.I.J.M., Evans, J.P., Pitman, A.J., 2019. The Importance of the One-Dimensional Assumption in Soil Moisture - Rainfall Depth Correlation at Varying Spatial Scales. *J. Geophys. Res. Atmospheres* 124, 2964–2975. <https://doi.org/10.1029/2018JD029762>
- Hong, S.-Y., Jang, J., 2018. Impacts of Shallow Convection Processes on a Simulated Boreal Summer Climatology in a Global Atmospheric Model. *Asia-Pac. J. Atmospheric Sci.* 54, 361–370. <https://doi.org/10.1007/s13143-018-0013-3>
- Imamovic, A., Schlemmer, L., Schär, C., 2017. Collective Impacts of Orography and Soil Moisture on the Soil Moisture-Precipitation Feedback. *Geophys. Res. Lett.* 44, 11,682-11,691. <https://doi.org/10.1002/2017GL075657>
- IPCC. (2001). *Climate change 2001: The scientific basis: contribution of Working Group I to the third assessment report of the Intergovernmental Panel on Climate Change* [Houghton, J.T., Ding, Y., Griggs, D.J., Noguer, M., van der Linden, P.J., Dai, X., Maskell, K., & Johnson, C.A. (eds.)]. Cambridge University Press, Cambridge, United Kingdom and New York, NY, USA, 881 pp.

- IPCC. (2007). *Climate change 2007: The physical science basis: contribution of Working Group I to the Fourth Assessment Report of the Intergovernmental Panel on Climate Change* [Solomon, S., Qin, D., Manning, M., Chen, Z., Marquis, M., Averyt, K.B., Tignor, M. & Miller, H.L. (eds.)]. Cambridge University Press, Cambridge, United Kingdom and New York, NY, USA, 996 pp.
- IPCC. (2013). *Climate change 2013: The physical science basis: Working Group I contribution to the Fifth assessment report of the Intergovernmental Panel on Climate Change* [Stocker, T.F., Qin, D., Plattner, G.-K., Tignor, M., Allen, S.K., Boschung, J., Nauels, A., Xia, Y., Bex, V. & Midgley, P.M. (eds.)]. Cambridge University Press Cambridge, United Kingdom and New York, NY, USA, 1535 pp.
- Jacob, D., Petersen, J., Eggert, B., Alias, A., Christensen, O.B., Bouwer, L.M., Braun, A., Colette, A., Déqué, M., Georgievski, G., Georgopoulou, E., Gobiet, A., Menut, L., Nikulin, G., Haensler, A., Hempelmann, N., Jones, C., Keuler, K., Kovats, S., Kröner, N., Kotlarski, S., Kriegsmann, A., Martin, E., van Meijgaard, E., Moseley, C., Pfeifer, S., Preuschmann, S., Radermacher, C., Radtke, K., Rechid, D., Rounsevell, M., Samuelsson, P., Somot, S., Soussana, J.-F., Teichmann, C., Valentini, R., Vautard, R., Weber, B., Yiou, P., 2014. EURO-CORDEX: new high-resolution climate change projections for European impact research. *Reg. Environ. Change* 14, 563–578. <https://doi.org/10.1007/s10113-013-0499-2>
- Jenkner, J., Sprenger, M., Schwenk, I., Schwierz, C., Dierer, S., Leuenberger, D., 2009. Detection and climatology of fronts in a high-resolution model reanalysis over the Alps. *Meteorol. Appl.* 17, 1–18. <https://doi.org/10.1002/met.142>
- Keil, C., Baur, F., Bachmann, K., Rasp, S., Schneider, L., Barthlott, C., 2019. Relative contribution of soil moisture, boundary-layer and microphysical perturbations on convective predictability in different weather regimes. *Q. J. R. Meteorol. Soc.* 145, 3102–3115. <https://doi.org/10.1002/qj.3607>
- Kida, H., Koide, T., Sasaki, H., Chiba, M., 1991. A New Approach for Coupling a Limited Area Model to a GCM for Regional Climate Simulations. *J. Meteorol. Soc. Jpn. Ser II* 69, 723–728. https://doi.org/10.2151/jmsj1965.69.6_723

- Koster, R.D., Dirmeyer, P.A., Guo, Z., Bonan, G., Chan, E., Cox, P., Gordon, C.T., Kanae, S., Kowalczyk, E., Lawrence, D., Liu, P., Lu, C.-H., Malyshev, S., McAvaney, B., Mitchell, K., Mocko, D., Oki, T., Oleson, K., Pitman, A., Sud, Y.C., Taylor, C.M., Verseghy, D., Vasic, R., Xue, Y., Yamada, T., 2004. Regions of Strong Coupling Between Soil Moisture and Precipitation. *Science* 305, 1138–1140. <https://doi.org/10.1126/science.1100217>
- Malberg, H., 2007. *Meteorologie und Klimatologie: Eine Einführung*. Springer-Verlag Berlin Heidelberg, Berlin, Heidelberg.
- Maraun, D., 2013. When will trends in European mean and heavy daily precipitation emerge? *Environ. Res. Lett.* 8.
- Miller, S.T.K., Keim, B.D., Talbot, R.W., Mao, 2003. Sea breeze: Structure, forecasting, and impacts. *Rev. Geophys.* 41, 1011. <https://doi.org/10.1029/2003RG000124>
- Monteith, J.L., Unsworth, M.H., 2013. *Principles of environmental physics: plants, animals, and the atmosphere*, 4th ed. ed. Elsevier/Academic Press, Amsterdam; Boston.
- Moon, H., Guillod, B.P., Gudmundsson, L., Seneviratne, S.I., 2019. Soil Moisture Effects on Afternoon Precipitation Occurrence in Current Climate Models. *Geophys. Res. Lett.* 46, 1861–1869. <https://doi.org/10.1029/2018GL080879>
- Niu, G.-Y., Yang, Z.-L., Mitchell, K.E., Chen, F., Ek, M.B., Barlage, M., Kumar, A., Manning, K., Niyogi, D., Rosero, E., Tewari, M., Xia, Y., 2011. The community Noah land surface model with multiparameterization options (Noah-MP): 1. Model description and evaluation with local-scale measurements. *J. Geophys. Res.* 116, D12109. <https://doi.org/10.1029/2010JD015139>
- Oki, T., Kanae, S., 2006. Global Hydrological Cycles and World Water Resources. *Science* 313, 1068–1072. <https://doi.org/10.1126/science.1128845>
- Piazza, M., Prein, A.F., Truhetz, H., Csaki, A., 2019. On the sensitivity of precipitation in convection-permitting climate simulations in the Eastern Alpine region. *Meteorol. Z.* 28, 323–346. <https://doi.org/10.1127/metz/2019/0941>

- Powers, J.G., Klemp, J.B., Skamarock, W.C., Davis, C.A., Dudhia, J., Gill, D.O., Coen, J.L., Gochis, D.J., Ahmadov, R., Peckham, S.E., Grell, G.A., Michalakes, J., Trahan, S., Benjamin, S.G., Alexander, C.R., Dimego, G.J., Wang, W., Schwartz, C.S., Romine, G.S., Liu, Z., Snyder, C., Chen, F., Barlage, M.J., Yu, W., Duda, M.G., 2017. The Weather Research and Forecasting Model: Overview, System Efforts, and Future Directions. *Bull. Am. Meteorol. Soc.* 98, 1717–1737. <https://doi.org/10.1175/BAMS-D-15-00308.1>
- Seneviratne, S.I., Corti, T., Davin, E.L., Hirschi, M., Jaeger, E.B., Lehner, I., Orlowsky, B., Teuling, A.J., 2010. Investigating soil moisture–climate interactions in a changing climate: A review. *Earth-Sci. Rev.* 99, 125–161. <https://doi.org/10.1016/j.earscirev.2010.02.004>
- Seneviratne, S.I., Lüthi, D., Litschi, M., Schär, C., 2006. Land–atmosphere coupling and climate change in Europe. *Nature* 443, 205–209. <https://doi.org/10.1038/nature05095>
- Seneviratne, S.I., Stöckli, R., 2008. The Role of Land-Atmosphere Interactions for Climate Variability in Europe, in: Brönnimann, S., Luterbacher, J., Ewen, T., Diaz, H.F., Stolarski, R.S., Neu, U. (Eds.), *Climate Variability and Extremes during the Past 100 Years*. Springer Netherlands, Dordrecht, pp. 179–193. https://doi.org/10.1007/978-1-4020-6766-2_12
- Shepherd, T.G., 2014. Atmospheric circulation as a source of uncertainty in climate change projections. *Nat. Geosci.* 7, 703–708. <https://doi.org/10.1038/ngeo2253>
- Skamarock, W., Klemp, J., Dudhia, J., Gill, D., Barker, D., Wang, W., Huang, X.-Y., Duda, M., 2008. A Description of the Advanced Research WRF Version 3. UCAR/NCAR. <https://doi.org/10.5065/D68S4MVH>
- Suklitsch, M., Gobiet, A., Leuprecht, A., Frei, C., 2008. High Resolution Sensitivity Studies with the Regional Climate Model CCLM in the Alpine Region. *Meteorol. Z.* 17, 467–476. <https://doi.org/10.1127/0941-2948/2008/0308>
- Taylor, C.M., 2015. Detecting soil moisture impacts on convective initiation in Europe. *Geophys. Res. Lett.* 42, 4631–4638. <https://doi.org/10.1002/2015GL064030>

- Taylor, C.M., Birch, C.E., Parker, D.J., Dixon, N., Guichard, F., Nikulin, G., Lister, G.M.S., 2013. Modeling soil moisture-precipitation feedback in the Sahel: Importance of spatial scale versus convective parameterization: SOIL MOISTURE FEEDBACK IN MODELS. *Geophys. Res. Lett.* 40, 6213–6218. <https://doi.org/10.1002/2013GL058511>
- Taylor, C.M., de Jeu, R.A.M., Guichard, F., Harris, P.P., Dorigo, W.A., 2012. Afternoon rain more likely over drier soils. *Nature* 489, 423–426. <https://doi.org/10.1038/nature11377>
- Taylor, C.M., Gounou, A., Guichard, F., Harris, P.P., Ellis, R.J., Couvreux, F., De Kauwe, M., 2011. Frequency of Sahelian storm initiation enhanced over mesoscale soil-moisture patterns. *Nat. Geosci.* 4, 430–433. <https://doi.org/10.1038/ngeo1173>
- Teuling, A.J., Hirschi, M., Ohmura, A., Wild, M., Reichstein, M., Ciais, P., Buchmann, N., Ammann, C., Montagnani, L., Richardson, A.D., Wohlfahrt, G., Seneviratne, S.I., 2009. A regional perspective on trends in continental evaporation: EVAPORATION TRENDS. *Geophys. Res. Lett.* 36. <https://doi.org/10.1029/2008GL036584>
- Truhetz, H., Goergen, K., 2019. Effects of a shallow convection scheme in perennial convection permitting CORDEX-FPS WRF simulations.
- Vargas Zeppetello, L.R., Battisti, D.S., Baker, M.B., 2019. The Origin of Soil Moisture Evaporation “Regimes.” *J. Clim.* 32, 6939–6960. <https://doi.org/10.1175/JCLI-D-19-0209.1>
- Weigand, C., 2019. Statistik mit und ohne Zufall: Eine anwendungsorientierte Einführung.
- Whan, K., Zscheischler, J., Orth, R., Shongwe, M., Rahimi, M., Asare, E.O., Seneviratne, S.I., 2015. Impact of soil moisture on extreme maximum temperatures in Europe. *Weather Clim. Extrem.* 9, 57–67. <https://doi.org/10.1016/j.wace.2015.05.001>

List of Figures

Figure 1 Components of the climate system and their interactions	5
Figure 2 Characteristic soil moisture levels and units	8
Figure 3 Schematic of land surface-atmosphere interactions	9
Figure 4 Global and annual average energy fluxes.....	11
Figure 5 Definition of the soil moisture regimes and the corresponding ET regimes....	12
Figure 6 Global correlation of ET and radiation and ET with precipitation.....	13
Figure 7 Schematic of the soil moisture-temperature and -precipitation feedback	14
Figure 8 Global soil moisture-temperature coupling strength of the periods 1970 – 1989 and 2080 - 2099	15
Figure 9 Conceptual scheme of regional circulation with and without background wind	17
Figure 10 Global precipitation preference over soil moisture anomalies.....	19
Figure 11 WegenerNet Feldbach region	24
Figure 12 Schematic representation of the Noah LSM in coupled mode.....	26
Figure 13 EURO-CORDEX and CORDEX-FPS domain	28
Figure 14 Diurnal cycle of hourly mean precipitation, fraction of precipitated areas and precipitation intensity of INCA, CCLM and WRF.....	30
Figure 15 Study of this thesis domain with the four subregions	38
Figure 16 Exemplary classification of precipitation events in the SMPF analysis	40
Figure 17 Daily mean absolute soil moisture and anomalies of one WegenerNet station and three different soil types.....	45
Figure 18 Daily mean absolute soil moisture and anomalies of four different runoff schemes and three soil types compared to one WegenerNet station	47
Figure 19 Exemplary HRLDAS soil moisture field for the 21.06.2009.....	48
Figure 20 HRLDAS soil texture types in the study domain.....	49

Figure 21 Soil moisture anomaly for the 21.06.2009.....	50
Figure 22 High resolution soil texture type map over Austria.....	51
Figure 23 Comparision of the WegenerNet, HRLDAS, CCLM and WRF daily mean soil moisture data from 2013 - 2015	52
Figure 24 Multiyear daily mean precipitation of INCA, CCLM and WRF.....	53
Figure 25 Comparison of the daily mean soil moisture anomaly of the WegenerNet, HRLDAS, CCLM and WRF.	54
Figure 26 Mean Bowen ratio in the study region for May to September.....	56
Figure 27 Mean correlation coefficient of ET with radiation and ET with soil moisture in the study region for May to September	59
Figure 28 Spatial, temporal and heterogeneity SMPF metric of the study subregions ...	61
Figure 29 Probability density curves of the feedback metrics of the control event and the event data.....	64
Figure 30 Location, spatial and temporal feedback metric of all detected precipitation events using the INCA data.....	66
Figure 31 Location, spatial and temporal feedback metric of all detected precipitation events using the CCLM data	67
Figure 32 Location, spatial and temporal feedback metric of all detected precipitation events using the WRF data.....	68
Figure 33 Event number analysis results.....	85
Figure 34 Seasonal mean Bowen ratios of the study area	86
Figure 35 Seasonal mean correlations of ET with radiation	87
Figure 36 Seasonal mean correlations of ET with soil moisture.....	87

Appendix

A. Event size and precipitation limit tests

At the start of the SMPF analysis the event location size had to be set with the impact on the number of detected events in mind. Thus, the INCA data was used to evaluate the number of events that could be found, dependent on the event location size. Five different sizes of 15, 33, 45, 63 and 75 km, corresponding to 5, 11, 15, 21 and 25 grid cells respectively, were tested. The minimal number of events was chosen to be 100. Consequently, the event size was chosen to be 45 km.

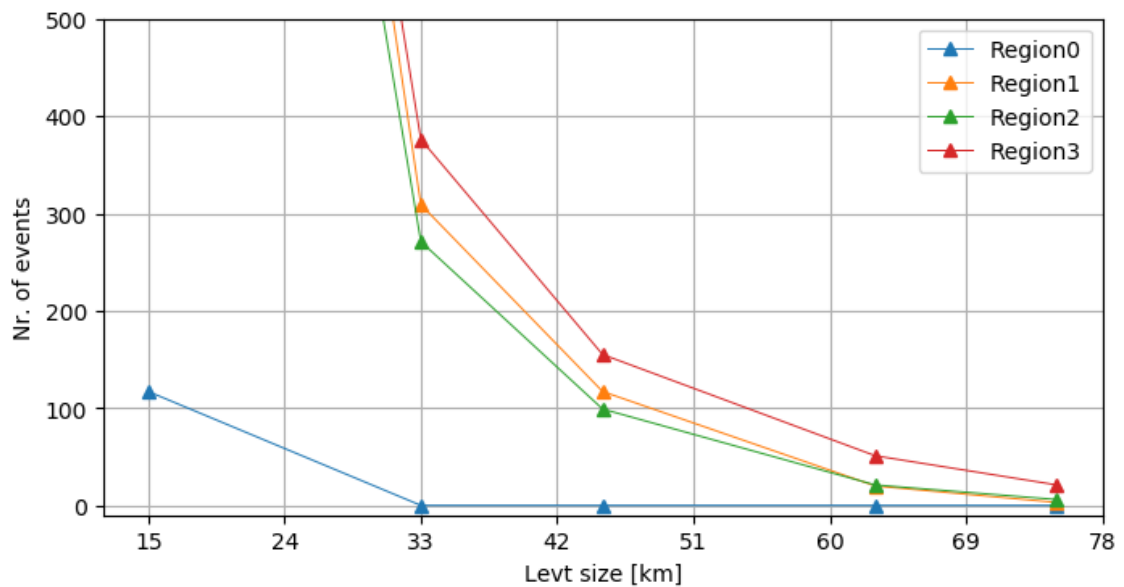


Figure A.1 Number of events detected in all four study subregions (Region0 = southwest, Region1 = northwest, Region2 = southeast, Region3 = northeast) in the INCA data, depended on the size of the event area (Levt). The number of events found for the event size of 15 km is close to 2000 for Region1 to 3.

B. Seasonal land surface conditions

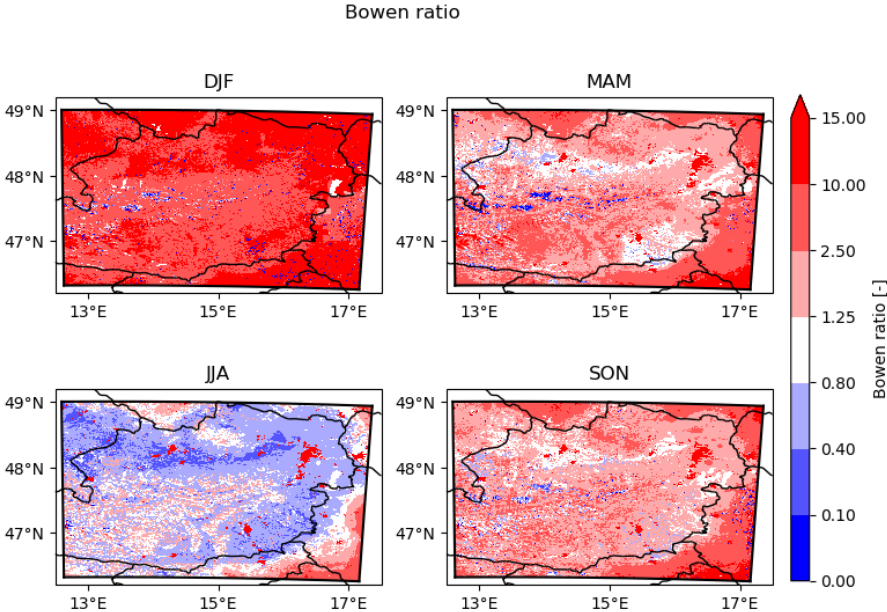


Figure B.1 Seasonal Bowen ratio computed from HRLDAS output data of the period 2005 to 2014, for the months of December, January and February (DJF, top left), March, April and May (MAM, top right), June, July and August (JJA, bottom left) and September, October and November (SON, bottom right).

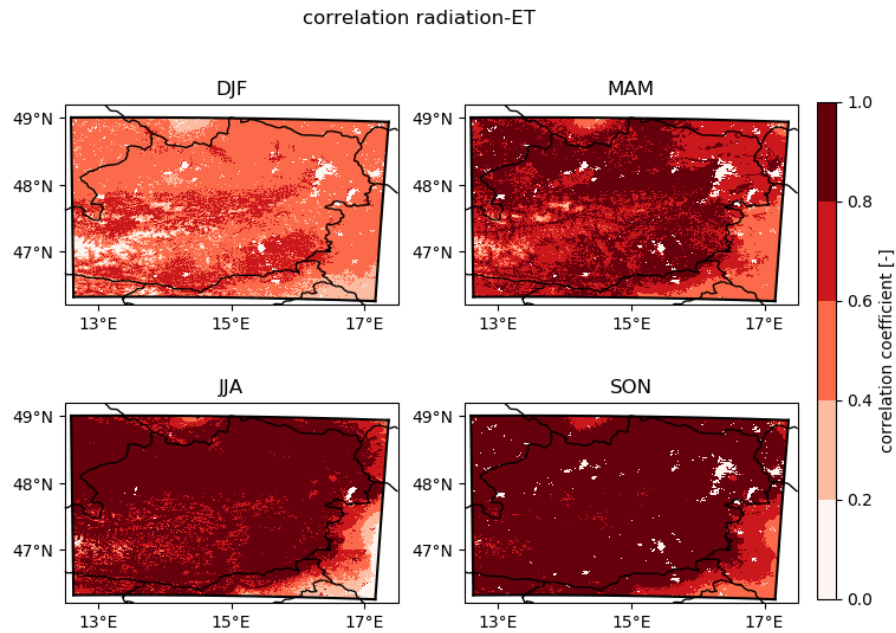


Figure B.2 Correlation of incoming radiation and ET computed from HRLDAS output data of the period 2005 to 2014, for the months of December, January and February (DJF, top left), March, April and May (MAM, top right), June, July and August (JJA, bottom left) and September, October and November (SON, bottom right).

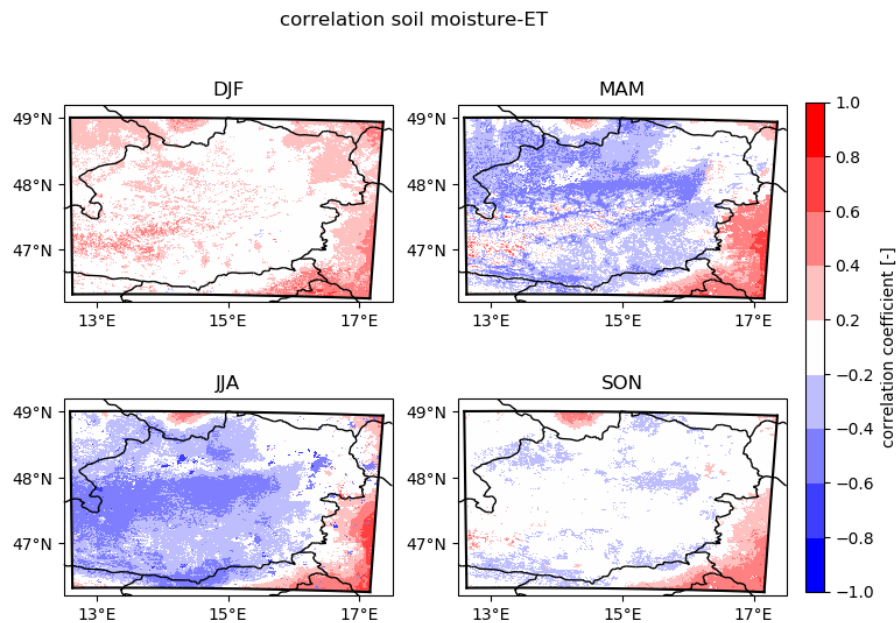


Figure B.3 Correlation of soil moisture and ET computed from HRLDAS output data of the period 2005 to 2014, for the months of December, January and February (DJF, top left), March, April and May (MAM, top right), June, July and August (JJA, bottom left) and September, October and November (SON, bottom right).